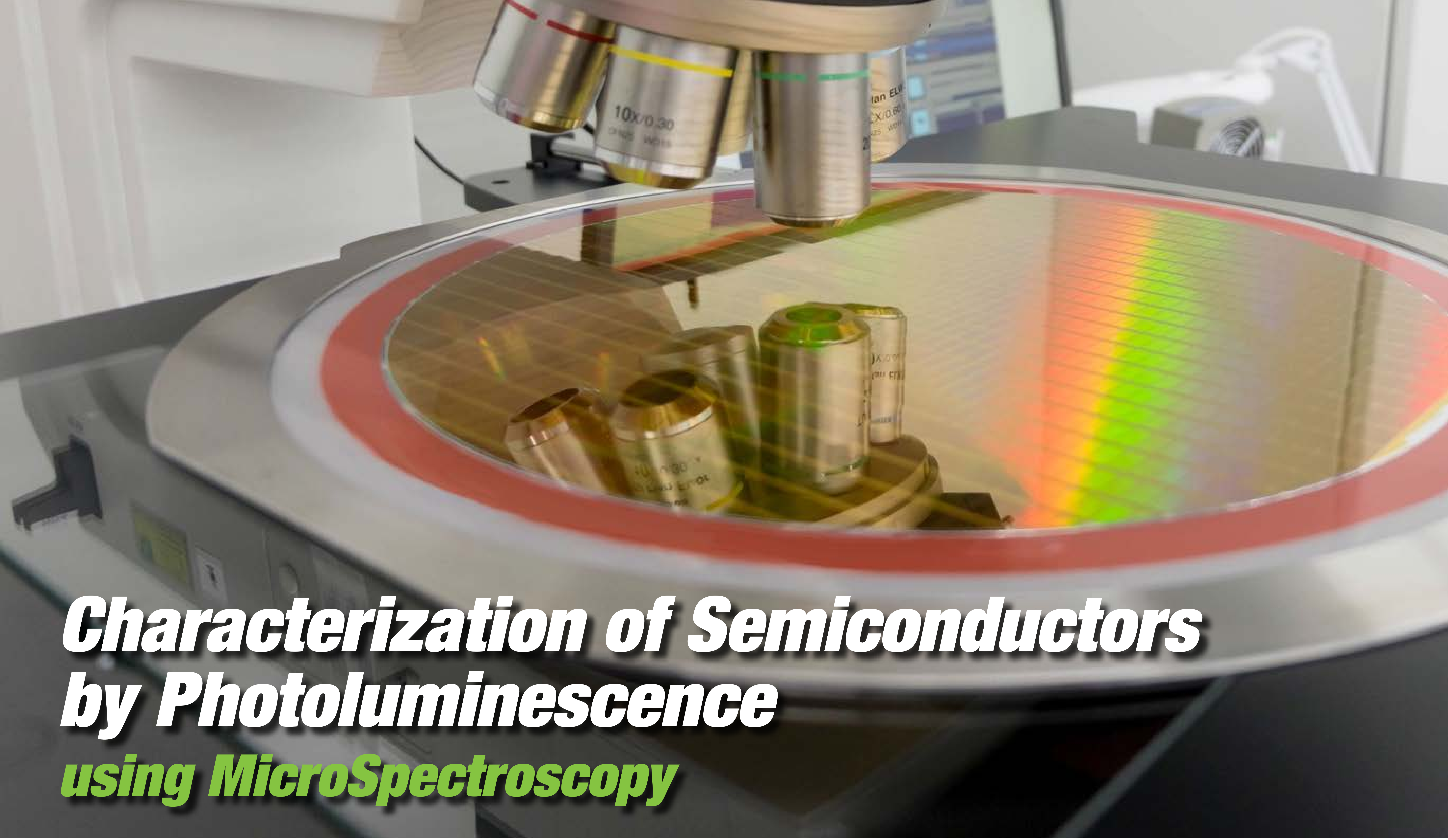

Characterization of Semiconductors by Photoluminescence

using MicroSpectroscopy

HORIBA Scientific

You couldn't live without semiconductors these days.

Semiconductor characterization depends on photoluminescence

You couldn't live without semiconductors these days. They are the engine that drives LED lights, computer displays and other technologies. Most electronics employ semiconductors, most notably computer chips.

Photoluminescence (PL) is a powerful tool for semiconductor characterization in the various stages in its life cycle. That includes development, testing, quality control, and failure analysis. Most modern semiconductor devices are engineered materials made from multi-layered structures fabricated on wafers. These are then diced up into individual devices. The process of engineering the base material, fabricating the wafers and characterizing the devices made from these wafers all depend on techniques like PL.

Photoluminescence

Photoluminescence phenomena result from materials absorbing excitation light photons and getting raised into an excited state. In the case of semiconductors, these levels are typically above the bandgap of the material. When the excited species relax, it releases this excess energy in the form of luminescence, or emission of photons. The emitted light is often characteristic of either the material or its surrounding environment, and can even provide information about local dynamics around emitting species.

PL is entirely a photon, mediated process, so it is a non-contact and non-destructive method of probing materials. Therefore, manufacturers can integrate PL into the production process without destroying or contaminating the tested sample.

NEXT »

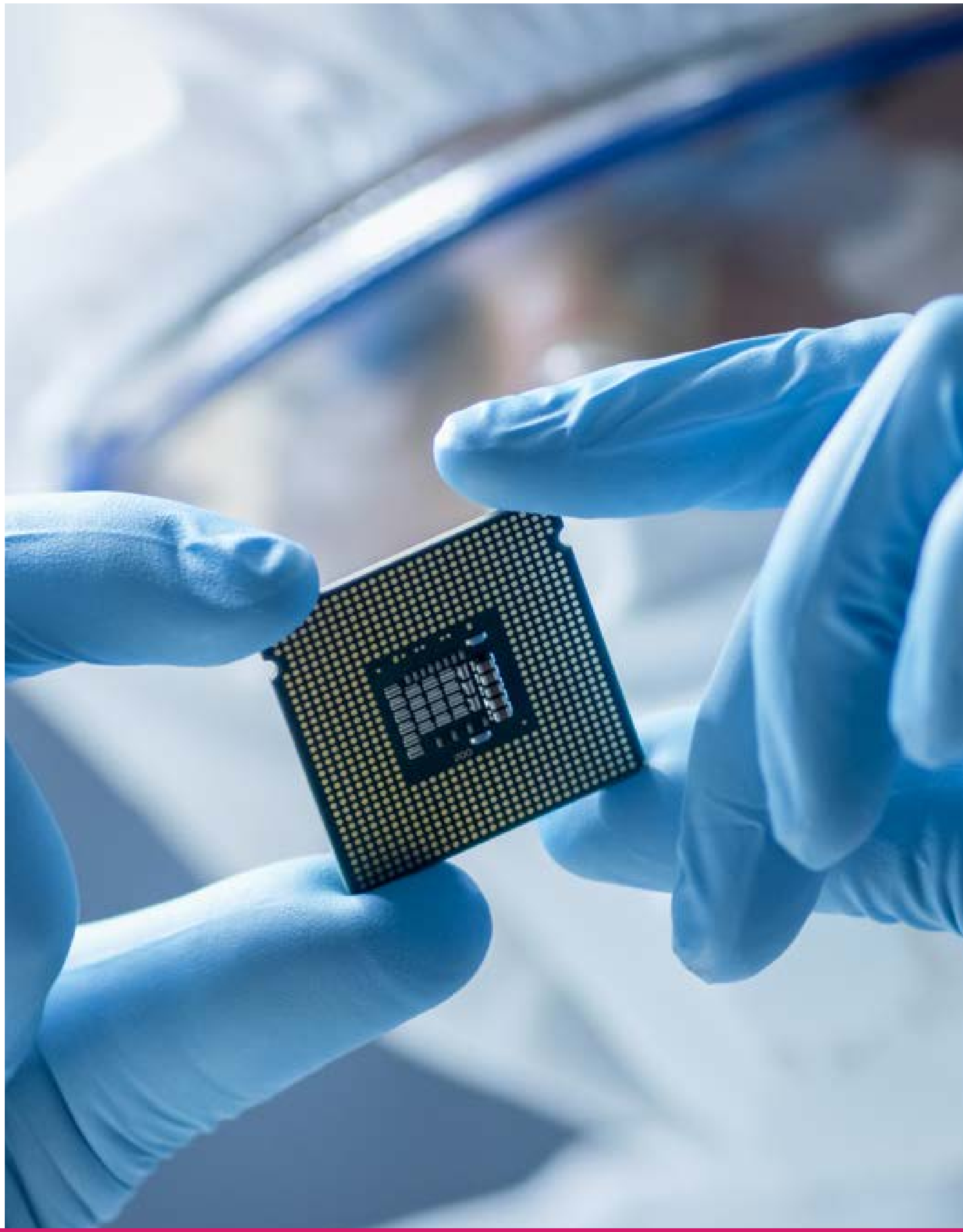

HORIBA Scientific

Semiconductor characterization depends on photoluminescence, cont.

Photoluminescence investigations

Modern semiconductors are highly engineered materials designed to exhibit certain defined behaviors. These materials are usually made on various substrates by epitaxial processes that stack different material layers one over another. Engineers build semiconductors from stacks of various atoms. This process has very tight tolerances, and PL is a tool that can be used to verify what is being made will perform as expected. The way you stack up the atoms, and which atoms you stack up, determines the function of what you ultimately get, from solar cells to LEDs.

For example, the LED lights in a home supply store have different colors. Some are bright white, and others have a yellowish tint. That is all materials engineering, and PL helps determine which parts of the wafer are fit for the various light sources.

PL offers unique signatures, providing operators with information on quality and other characteristics. It allows device designers and manufacturers to determine, prior to the manufacturing process, which parts of the wafer meet the functional requirements of the intended device before they are actually made. Once made, failure of a device to meet performance expectations can be very costly – so it is a lot cheaper to determine and weed out non-performing devices early on in the process. PL is a key technique for doing this.

Photoluminescence is also widely used for defect analysis in semiconductor analysis. Defects are usually foreign dopants that are embedded into a host material matrix – by design or accident, or, they can be structural deformations of the material itself. In either case, these defects affect the band structure of the material in which they occur. Since PL is really a measure of the band structure of the material, it therefore serves as a useful tool for defect analysis both in material engineering and device fabrication and quality control...

"Many of our industrial and research customers use our PL mappers such as (HORIBA's) MicOS mainly in the process of determining wafer homogeneity and in other cases for defect analysis"

-HORIBA Scientific Optical Spectroscopy Division Product Line Manager Francis Ndi, Ph.D.

« PREVIOUS

NEXT »

Semiconductor characterization depends on photoluminescence, cont.

A typical PL mapper, such as the HORIBA MicOS PL mapper, works by scanning a focused excitation laser beam over a wafer or device and collecting the full PL spectrum at thousands to millions of points across the structure. Various parameters of the PL emission can be displayed, as shown in Figure 1.

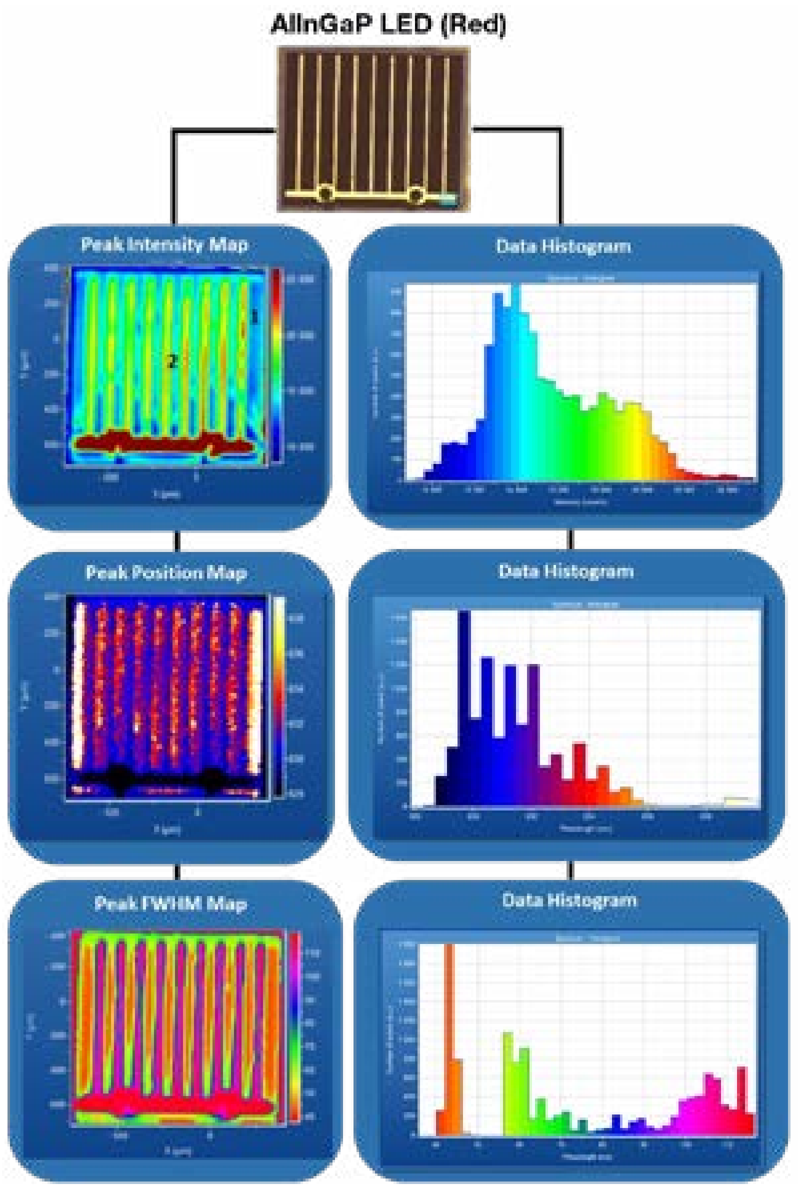

Figure 1

Photoluminescence at various fabrication stages

Foundational to any semiconductor device endeavor is the material engineering effort, to ensure that the materials used in the device exhibit the right properties that support the expected device performance. This work often boils down to band structure engineering, so PL is obviously a key analytical technique at this stage.

At the pre-production level, manufacturers use PL to fine tune the actual wafer fabrication process by characterizing such considerations as the homogeneity of the deposition process, or presence and location of defects introduced intentionally or otherwise.

Technicians use PL at the end stage to do quality control to ensure that device performance is consistent across different fabrication batches. PL is also used to check and maintain the stability and robustness of the fabrication process itself – a tool to monitor and ensure the often tight tolerances required for correct device fabrication is maintained.

Finally, PL is also key in the analysis of failed devices, still part of quality control. A device may fail in the field. A section of your monitor might not appear correctly. It could happen on an industrial level, or even for an agency like NASA, where device failure can be very expensive. Researchers use PL to understand why the component failed, so they can correct it in the development or manufacturing stages.

HORIBA offers the **MicOS** Microscope Optical Spectrometer, part of its **Standard Microscope Spectroscopy Solutions (SMS)**, to carry out these and other analyses. It is a modular, versatile and cost effective microspectrometer platform for steady state and lifetime photoluminescence.

The MicOS combines a custom high throughput microscope head with a high-performance, triple grating, imaging spectrometer that can accommodate up to three different detectors. HORIBA can customize the MicOS with various light sources and detectors to meet the requirements of the research at hand. The MicOS merges microscopy and photoluminescence spectroscopy, to provide optimal coupling from the sample, all the way to the detector.

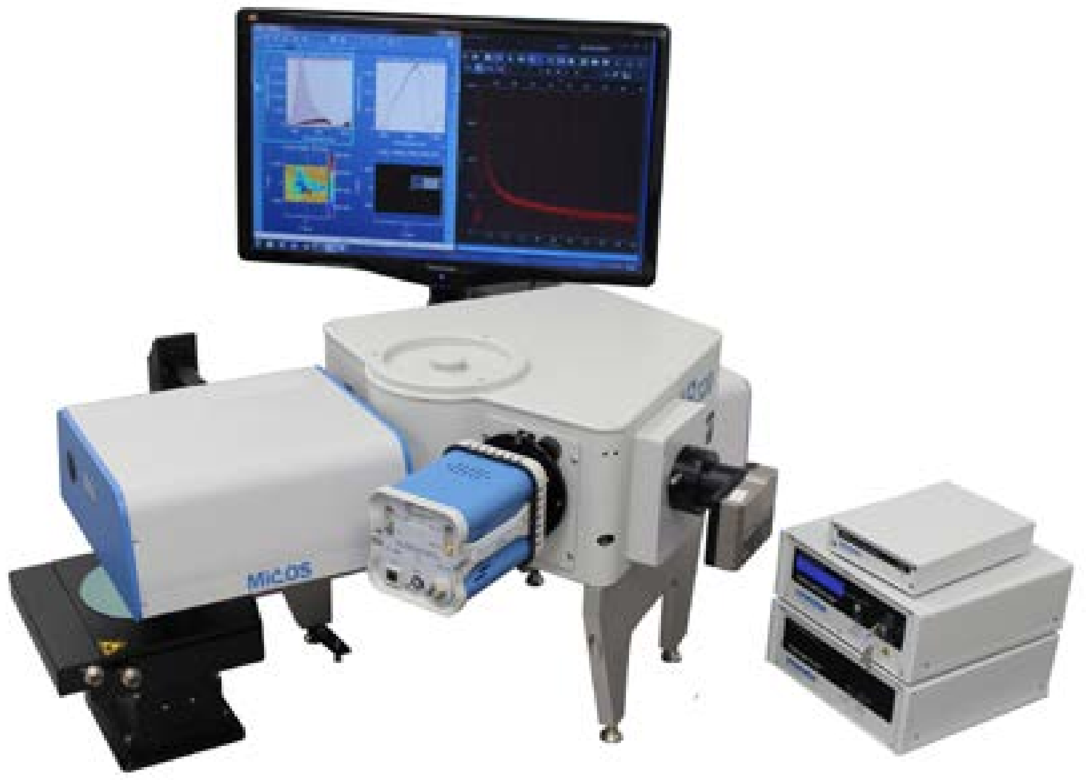

« PREVIOUS

Nanoscale materials are promising, low-cost light absorbers for solar energy conversion into chemical fuels or electricity...

Nanotechnology: A pathway to efficient solar energy

A Colorado group is tackling one of the largest issues facing us with some of the smallest materials known to mankind

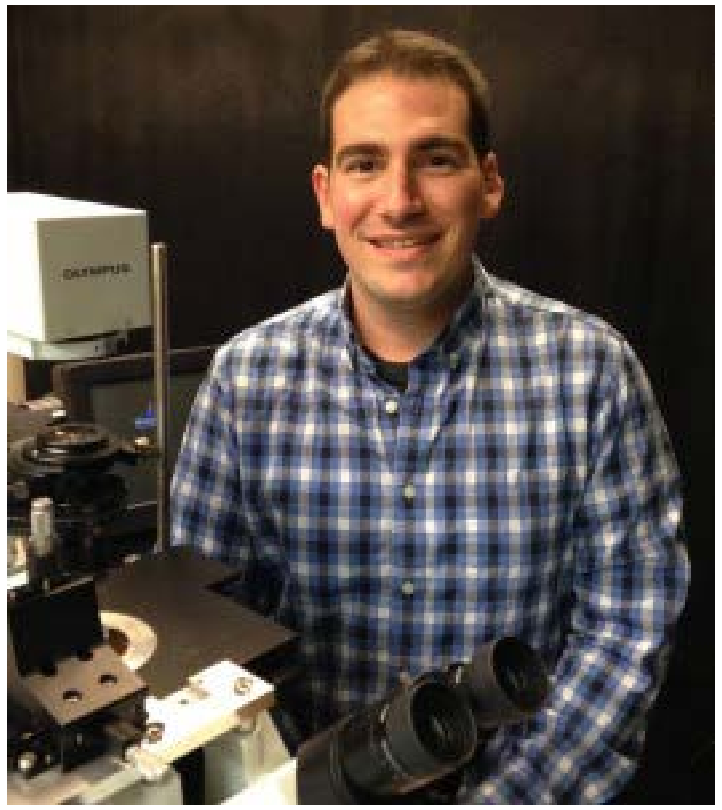

Justin Sambur

Justin Sambur, Ph.D. is an Assistant Professor of Chemistry with the College of Natural Sciences at Colorado State University. He uses nanotechnology to investigate how to convert light into electricity and ultimately provide low-cost energy to the planet, and beyond.

The 34-year old researcher focuses on the need to develop massively-scalable renewable energy technologies. Nanoscale materials are promising, low-cost light absorbers for solar energy conversion into chemical fuels or electricity, he said. But it is unclear how the chemical, electronic, and physical properties of individual nanomaterials affect their collective function.

That's where his research begins.

Nanoscale solar power

His group develops new analytical tools to visualize device function on the nanoscale level and use this information to guide the development of high-efficiency devices.

Sambur uses a custom made HORIBA SMS system – which is a standard Olympus IX-73 inverted microscope customized with multiple spectroscopy capabilities - to study ultra-thin semiconductor materials. These are two-dimensional graphene materials like MoS_2 and $MoSe_2$ (molybdenum disulfide and molybdenum diselenide).

"They're interesting for a lot of ultra-thin optoelectronic applications, things like LEDs, solar cells, and transistors," he said. "When you make them, they're quite heterogeneous. They sometimes have different shapes, sizes and thicknesses. My group is really interested in understanding structure and function relationships between the materials themselves and their performance."

Sambur and his team developed some techniques with their HORIBA system to correlate the effects of exciting materials in various layer thicknesses. How does that scale, and how do the physical properties scale with the energy conversion efficiency? After all, the end game is the generation of large amounts of energy.

"We study them down to the mono-layer or three atoms thick, and we find very interesting, nonlinear relationships between thickness and energy conversion efficiency," he said.

The researchers consist of undergraduate, graduate and post-doctoral students. They believe the efficiencies have something to do with the electrical contacts that these ultra-thin materials make with the current collector of the substrate that it sits on.

The materials are so thin, the environment around it can have a huge impact on its properties. The group is beginning to change the materials in the electrical contacts because of the impact of the substrates, or conducting electrodes.

Sambur and his group are doing basic research, which hopefully will be studied by other scientists and eventually be commercialized.

"We're working with model systems, and trying to understand some basic key structure-function relationships that could be useful for solar energy conversion," Sambur said.

NEXT »

Nanotechnology: A pathway to efficient solar energy, cont.

They measure power conversion efficiency, which is in the neighborhood of 1 percent in these nanomaterials.

“But you could fix this in the future by making them somehow nanostructured, putting them on very high surface area materials,” he said.

That might take shape in the form of covering a building or a mountainside.

Since the light absorbing material is so thin, it has some properties that are different from the bulk material. In some cases, materials exhibit efficient carrier multiplication, where a cell that is excited with one photon produces two electrons. In effect, you get double the current in a cell.

“If we can begin to understand these materials and harness those type of physics, then you can have a next generation ultra-thin device,” Sambur said.

"If it could be optimized, the ultra-thin materials could be flexible and lightweight devices for niche applications,"he aaid. It has advantages, like if you were to wrap it around a pole, or in space applications. In fact, Sambur is funded by the U.S. Air Force because they're interested in very lightweight photovoltaics in space. “We hope to reveal structure, function, and relationships for these devices that are going to either dictate how they're engineered, and also develop new materials,” he said. “If we find some scaling relationships that are useful with thickness as well as the chemistry of the material, we hope that it's going to inspire the way we design and synthesize new materials for solar energy conversion applications.”

« PREVIOUS

TOM and Jerry

Sambur’s lab has two optical microscope setups. The researchers refer to them as TOM and Jerry. Jerry is a custom-built HORIBA Scientific multi-functional spectroscopy system. TOM to refers to The Other Microscope that is mainly used for single molecule imaging studies.

Jerry is a beast. It has multitasking capabilities, with multiple light sources, detectors and an optical microscope sprouting from its core. It features dedicated systems for spectroscopy and wide field imaging. The standard microscope spectroscopy (SMS) system is a platform allowing several types of analytical techniques, including Raman spectroscopy, photoluminescence, reflectance and photocurrent to be added to a any standard microscope, according to HORIBA Scientific Product Line Manager, Francis Ndi. “What makes it so great is we can really see our samples on our imaging camera and then we can do all sorts of spectroscopy measurements on specific areas on interest,” Sambur said. “We can switch between imaging and spectroscopy modes really quickly.”

TOM and Jerry sit in a microscope room in the Colorado State University chemistry facility on two eight by five-foot tables. The HORIBA microscope takes up an entire table.

Why the customization?

“We wanted to be able to excite our samples multiple different ways,” Sambur said. “Jerry is set up to do single molecule fluorescence microscopy, where we excite the sample from above. It's also set up to do mapping experiments, where we send the laser through the back of the microscope to excite a tiny spot on the sample and measure light emission or photo-current generation from that tiny spot.”

The design team for the instrument layered additional functionality, which is made possible by the openness of the system.
The confocal microscope and spectrometer was made by HORIBA’s Optical Spectroscopy Division, a systems integrator. It built the system as an open platform.

As Sambur’s team becomes familiar with Jerry, their own efficiency grows.

“All that flexibility, we're really leveraging it now,” he said.

HORIBA Scientific’s LabSpec 6 Spectroscopy software suite has been a critical component for Sambur’s researchers. He notes the software’s ease of use, and its triggering capability, where it can talk to other instruments.

“At any one time, our microscope is talking to five different instruments, and that's been really useful for us to do the things that we do,” he said.

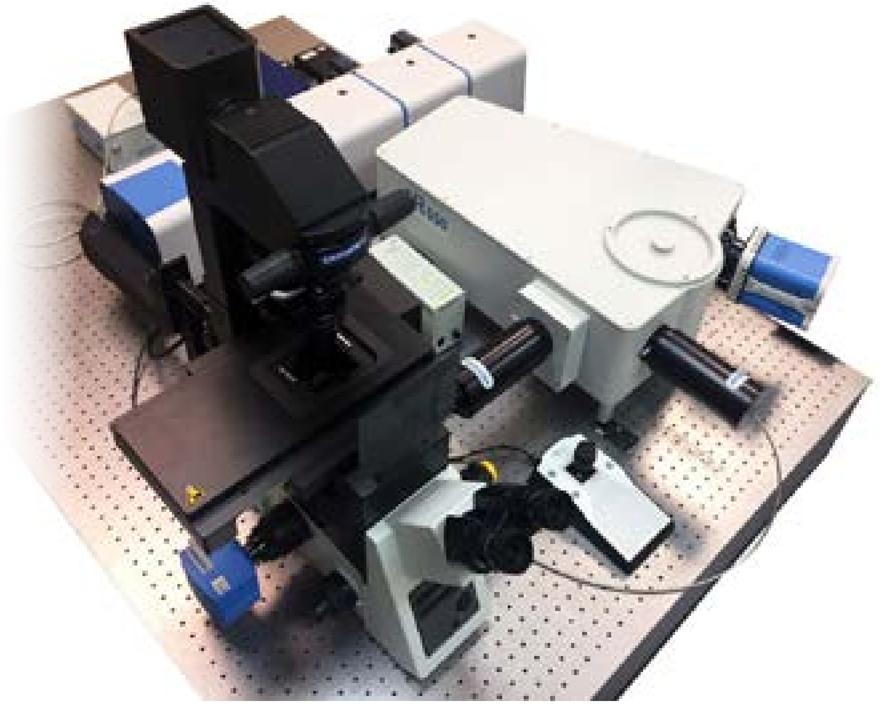

My computer always seems to run slow.

Using low temperature probes

My computer always seems to run slow. No matter how souped-up it is, I still seem to waste time waiting for applications and documents to open.

Imagine if these devices ran 100 times faster?

Our computers and other electronic devices are, at its essence, made of microcircuits, highly miniaturized integrated circuits. These devices cram hundreds, thousands, millions, or even billions of electronic components onto tiny chips of silicon no bigger than a fingernail. At its core, it is a vehicle for electrical conduction and transport.

So the speed electricity travels through these microcircuits partially determines the speeds that your electronic devices function.

The fields of research look into fundamental properties of better materials for these devices and environments in which these microcircuits operate. That's the focus of Rui He's work.

He is a Ph.D. in applied physics and an Associate Professor in Electrical and Computer Engineering at Texas Tech University in Lubbock, Texas. The dry, flat, sandstorm prone city is home to research that takes a different approach to exploring physical properties of the best materials to use in devices.

Rui He, Ph.D., Associate Professor in Electrical and Computer Engineering at Texas Tech University

"People strive to make devices faster and more energy efficient," she said. "If we can study the fundamental properties and see if proposed materials would be suitable for these types of applications, it can help people design or make devices."

Using low temperature probes, cont.

Freezing temperatures

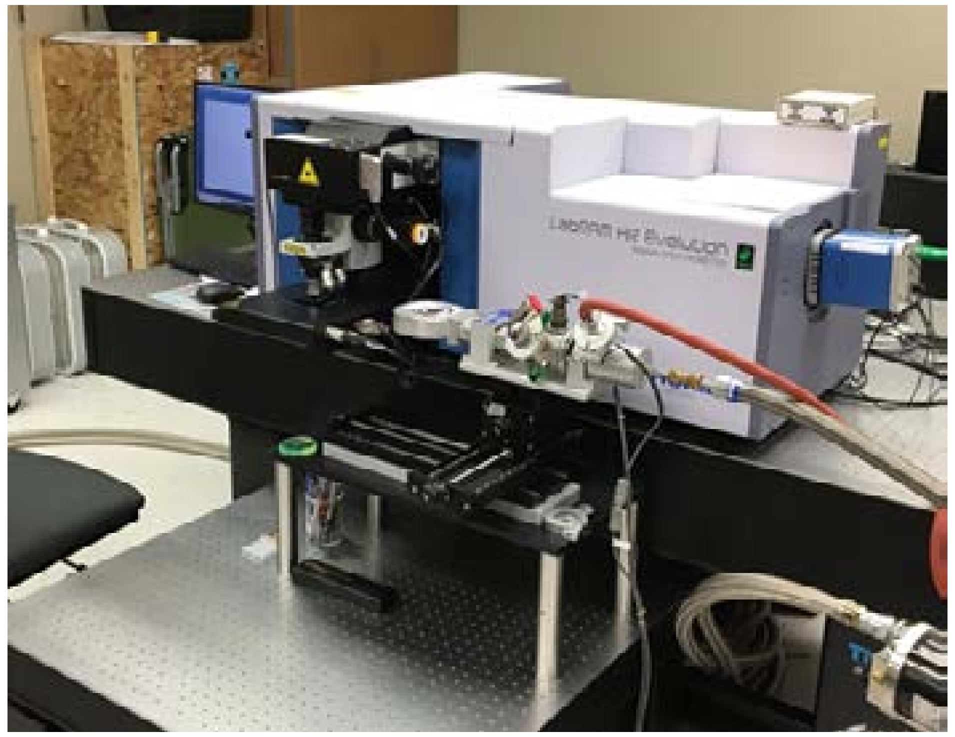

A HORIBA LabRAM HR Evolution Raman Spectrometer in Rui He's research lab.

He studies the vibrational, electronic, and magnetic properties of various materials at low temperatures: About 10 degrees Kelvin, which is equal to -263.15 Celsius or -441.67 Fahrenheit. That's close to absolute zero.

Why test the materials at such low temperatures?

"Physical properties of materials may change significantly as a function of temperature," she said. "For instance, lattice structures may change due to a structural phase transition, and some materials exhibit magnetic properties at low temperatures even under a zero external magnetic field. One of the examples is chromium triiodide which becomes magnetic at temperatures below about 45 Kelvin. In order to probe these materials' physical properties, we need to cool the samples down to a low temperature."

But why study the materials at such low temperatures, when most of the actual devices will have to function at room temperature? "Right now, we are still at the beginning," he said. "These properties may only exist at low temperatures, but with the rapid advance of fabrication techniques, characterization, and fundamental studies of materials, we hope to see materials that can exhibit desired electronic and magnetic properties at higher temperatures."

He works with 2D materials. Those are layered materials whose atoms within the layers are strongly bonded, whereas the interactions between each layer are much weaker. By controlling the number of atomic layers, you could tune the optical and electronic properties. She studies traditional 2D materials like graphene and molybdenum disulfide. Recently she expands her studies to novel 2D magnetic materials like chromium triiodide. It has magnetic properties below a critical temperature.

He, in collaboration with her colleagues, Dr. Liuyan Zhao of University of Michigan and Dr. Adam Tsen of University of Waterloo, Canada, recently had their research findings published in Nature Communications, a multidisciplinary journal.

"The research we published is to report our recent study on magnetic excitations in a ferromagnetic – a substance with high magnetic permeability – 2D material chromium triiodide," He said. "We discovered terahertz frequency spin waves, which are much higher in frequency than those in conventional ferromagnetic materials."

This, He said, will open up new opportunities for making ultrafast spintronic devices – devices that use electrons' spins for realizing spin currents that are much faster than gigahertz spintronic devices and much more energy efficient than electronics currently on the market.

"Computers run with gigahertz processors, so if we can use the technology based on the new 2D ferromagnetic materials, then we may bring the processing up to run 100 times faster or even more," He said. "Spintronics could also help reduce the heat from these devices and lower the power consumption."

He uses Raman spectroscopy to study the physical properties of her samples. She has a HORIBA LabRAM HR Evolution; a confocal Raman microscope ideally suited for both micro and macro measurements. It also offers advanced confocal imaging capabilities in 2D and 3D.

"Raman allows us to study a broad range of material properties and it's a nondestructive technique," He said. "That makes it very important for characterization and fundamental studies of materials. With the ultra-low frequency features that we have, we can probe ultra-low frequency excitations in the material and study diverse properties of materials from interlay interactions to electronic and magnetic excitations."

It might be years before the principles He is uncovering will go into practical use. She is working at a very basic science level, doing fundamental research.

"And then there are engineers who use these properties and try to build better devices," she said.

A material unfamiliar to the masses may provide a huge leap in solar energy technology over the next few years. It's called perovskite...

Low cost solar power on the horizon

A material unfamiliar to the masses may provide a huge leap in solar energy technology over the next few years.

It's called perovskite, a naturally occurring crystal structure that, when grown in the lab, has the capacity to convert solar energy to electricity by absorbing light and separating electrical charges in the material. Unlike its more mature cousin, the silicon semiconductor in solar cell applications, perovskite is more flexible and cheaper to manufacture. It just hasn't met the test of longevity – yet.

Silicon solar cells, made from silicon wafers, have a useful life of 20 years, meaning they degrade by 5 percent a year. Perovskites are spin-coated on a surface, analogous to painting it on the surface – but they degrade more quickly. For now.

That's according to Principal Scientist, Alex Siemiarczuk, Ph.D. of HORIBA Scientific's Fluorescence Division. He helps researchers understand HORIBA's technology in spectrophotometry and, in this case, how it applies to making a more efficient perovskite solar cell.

The efficiencies of perovskite solar cells have gone from single digits to a certified 22.1 percent in a few years' time, according to a 2017 story published in Science Magazine. That is quickly approaching the efficiencies of traditional crystalline silicon solar cells.

It's a "promising way to offset carbon emissions and meet increasing demand in energy consumption," according to the story.

Perovskite can be applied in a liquid form. It can be painted onto objects, like buildings, clothing and even windows.

Researchers have been experimenting with hybrid perovskites, mimicking the physical chemical structure of perovskites, but introducing new elements into its formation to increase efficiencies and resilience.

NEXT »

HORIBA Scientific

Low cost solar power on the horizon, cont.

“Perovskites are essentially crystals,” Siemiarczuk said. “The original perovskite mineral was composed of two metals and three atoms of oxygen,” Siemiarczuk said. “Depending on the application, you will have different groups used, for example, methylammonium, lead and three halide atoms. That's what is commonly used in photovoltaics.”

In energy applications of solar cells, the perovskite layer is the light harvesting layer. The light is absorbed by the light harvesting layer, and there is charge separation, transport, and charge collection. As a result, some voltage is generated between the electrodes of the solar cell.

« PREVIOUS

To better understand those critical processes, and to improve the efficiency and stability of perovskite solar cells, some researchers employ HORIBA’s hybrid fluorometers QuantaMaster™, Fluorolog and FluoroMax®, combined with HORIBA-IBH lifetime components for both fluorescence steady state and lifetime measurements, according to Ben Yang, Ph.D., an Applications Scientist for the fluorescence division of HORIBA Scientific. These are used by basic research labs trying to discover the photo-physical properties of hybrid perovskites, and applied research labs where scientists are trying to monetize the perovskite technology.

“The efficiency of this largely depends on how far those charge carriers can diffuse, and how long the electrons and holes can stay separated before recombination. One technology used often is fluorescence lifetime, which can be used to measure carrier separation lifetime. We offer both hybrid fluorometers, and dedicated lifetime instruments like DeltaFlex and DeltaPro, manufactured in our Scottish facility, HORIBA-IBH. We come with our equipment so we can actually assess the efficiency of this light harvesting process. Photoluminescence allows you to assess the function and efficiency of your device,” Yang said. Jinsong Huang, Ph.D., and Professor in the Department of Applied Physical Sciences at the University of North Carolina is working on providing solutions to industry to commercialize perovskite solar cells. His team provides scientific support to overcome the major technology barriers so that perovskite solar cells can be manufactured at a competitive price in large scale, by addressing issues related to stability, efficiency, and large scale and fast fabrication. He also conducts research to understand the unique properties of hybrid perovskites to find out why they are so good at photovoltaics.

He is also investigating other uses of perovskites.

“In addition to solar cells, we do research to find applications that perovskites not only fit, but also are much better than existing materials, such as sensitive ultrafast perovskite photodetectors, and perovskite X-ray detectors, which are more than 1,000 times more sensitive than commercial X-ray detectors in medical imaging devices,” he said.

Huang employs HORIBA Scientific’s DeltaFlex turnkey TCSPC florescence lifetime spectrofluorometer. He uses it to measure the recombination rate in detecting their efficiencies.

“It’s a parameter we need to know,” he said.

Due to their nonlinear optical properties, perovskites are also used in laser technology to enhance frequency doubling of the coherent light source and generate laser output at shorter wavelengths.

Like your phone, all electronics get hot, and the device's lifetime consequently decreases.

How to measure temperature with light

Satellite communications, military radar systems and those 5-G networks you will soon depend on have something in common. Scientists base these systems on microelectronics – the design, manufacture, and use of integrated circuits.

One bottleneck in the integrated circuits is self-heating. These devices get hot because of the Joule heating that occurs in it. Like your phone, all electronics get hot, and the device's lifetime consequently decreases.

It is therefore necessary to measure the temperature these devices and circuits generate to understand the component mean-time-to-failure.

The problem is the devices exist on a sub-micron level. Engineers have shrunk these devices below the limits of physical thermometers and thermocouples that are used to measure temperatures at larger scales.

They have to find a way to measure that temperature on a small scale.

An innovative approach

Sukwon Choi, Ph.D., and Assistant Professor of Mechanical Engineering at Penn State University, has found a way.

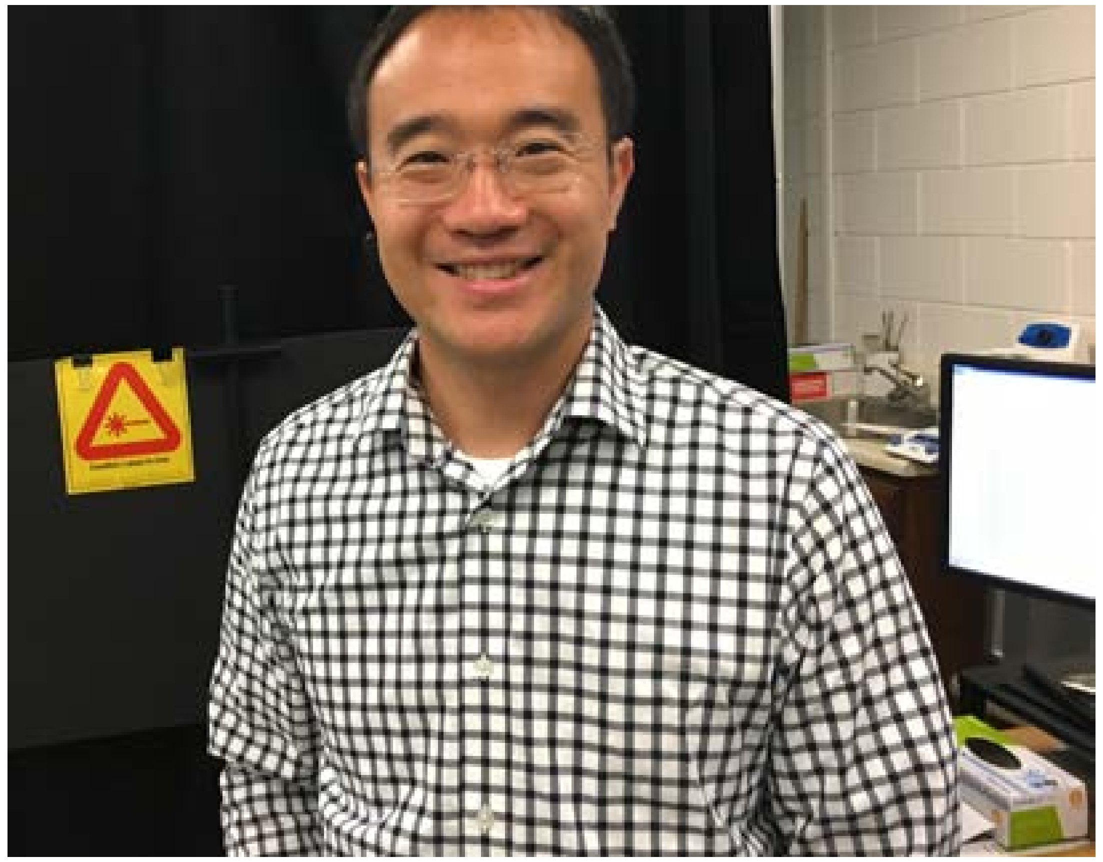

"Failure is a local phenomenon," Choi said. "Like our car, if the tire breaks, the whole car breaks. If you get a weak spot in the circuit and that spot fails, then the whole system fails. Similarly, with these transistors, if you have a hotspot and failure occurs at that local hotspot, then the transistor doesn't work anymore."

Those thermal hotspots are on the submicron scale in length.

"These microelectronic devices are prone to overheating," Choi said. "You have to be able to measure that temperature in order to design cooling systems, or to assess or predict the component lifetime."

Local peak temperature and device lifetime are directly correlated. Thus, scientists need to know the temperature to estimate the mean-time-to-failure or component lifetime.

Physical thermometers are too large to measure the local temperature in a circuit. These next generation devices, based on microcircuits for power conversion and wireless communications, operate under high voltage and high current conditions. You can't touch a device for safety reasons. Physical contact will also interfere with the device's operation.

Choi uses light to measure temperature.

"We want a high spatial resolution, noncontact and noninvasive thermography or thermometry technique," he said. "And we can do that with light using micro-Raman spectroscopy. You're basically inventing an optical thermometer. We're leveraging Raman's capabilities for optical thermography."

NEXT »

How to measure temperature with light, cont.

Raman as an optical thermometer

How does that work?

Raman spectroscopy looks into the frequency or energy of phonons, or quantized lattice vibrations. A phonon is a discrete unit or quantum of vibrational energy, just as a photon is a quantum of electromagnetic or light energy. Phonons and electrons are the two main types of elementary particles, or excitations, in solids.

“They're looking into phonon frequency - the frequency of the atoms that oscillate within a crystal or amorphous solid. That oscillation frequency is directly related to energy. Raman spectroscopy measures that frequency, or energy,” he said.

Raman spectroscopy looks into a phonon frequency or energy. Researchers ordinarily use that capability to study the structure of materials. Yet lattice vibrations or phonons are related to thermal transport in solids, and thus temperature. Heat conduction in a solid happens in the form of vibrational waves, according to Choi.

“For conventional electronics, transistors and diodes going into all of these consumer electronics are based on silicon,” he said. “But for applications that demand higher power, higher current, higher voltage operation, silicon has its own limits regarding its material properties. One important thing is the electronic band gap.”

For these high frequency, high power electronics, microelectronics researchers have been seeking materials with wider band gaps for higher frequency, high voltage and higher power operation. These researchers have been pursuing gallium nitride and silicon carbide for the past 10 years.

“Researchers have had huge successes in terms of applications like electric vehicles or wireless communications, satellite communications and military applications. We mainly focus on gallium nitride.”

The next step

Now scientists are looking into what they refer to as ultra-wide band gap semiconductors as the next generation for these high power electronic devices. That includes materials like aluminum gallium nitride and gallium oxide.

Larger band gap materials conduct more energy that permits the operation of devices under higher voltage conditions. Wider band gap translates into a larger critical electric field of the material, which means for a given thickness, it can tolerate higher voltage without burning out.

That opens the door for many favorable aspects, such as development of smaller and lighter systems with higher efficiency, Choi said.

For things like electric cars, researchers want to make smaller power converters that consume less battery power.

“However, a major bottleneck to the commercial success of wide band gap and ultra-wide band gap semiconductors is overheating,” he said.

The lab

LabRAM HR Evolution Confocal Raman Microscope examines a silicon wafer

Choi uses a HORIBA LabRAM HR Evolution Confocal Raman Microscope with an ultra-low frequency (ULF) filter and customized pulsed laser source. The filter allows him to capture Stokes and anti-Stokes Raman scattering, giving him more accurate temperature readings. Choi uses the ULF filter measurements with other methods to get the most precise readings possible.

How to measure temperature with light, cont.

"You can go down to low wave numbers and you can see more peaks that can be leveraged to measure temperature and study sub-continuum-scale thermal transport," he said.

The genteel, soft-spoken professor gestures with his hands, drawing imaginary waves on a graph against a black curtain. Black barriers surround the instrument to eliminate ambient light for more accurate measurements.

"The LabRAM has a longer focal length compared to other Raman systems, which translates into higher spectral resolution, which in turn gives us a higher temperature resolution. It also has very good mapping capabilities," Choi said.

His research uses Raman spectroscopy as a unique solution to study thermal problems in micro/nanosystems.

"We're leveraging the Raman capability for temperature measurement instead of structural characterization that all others do, so we can understand the self-heating or overheating behavior of next generation microelectronic devices," he said. "It's usually based on wide band gap semiconductors, like gallium nitride or beyond that are going to be used in high power, high frequency applications, like power conversion for electric vehicles, renewable energy sources, and RF power amplifiers for wireless communication applications."

LabRAM HR Evolution Confocal Raman/PL microscope

« PREVIOUS

Photoluminescence spectroscopy (PL) is a powerful optical method used for characterizing materials.

Photoluminescence of semiconductors

Introduction

Photoluminescence spectroscopy (PL) is a powerful optical method used for characterizing materials. PL can be used to find impurities and defects in silicon and group III-V element semiconductors, and to determine semiconductor band-gaps. A material absorbs light, creating an electron-hole air; an electron from the valence jumps to the conduction band leaving a hole. The photon emitted upon re-combination corresponds to the energy-difference between the valence and conduction bands, and is hence lower in energy than the excitation photon.

Features

- 500 to 2000 nm operation
- Integrated sample optics and viewer
- Precision xy sample positioning
- Specifically designed for use with cryostat
- Integrated data collection and analysis

Benefits

- Unique system for continuous monitoring from visible to IR without realignment
- Optimizes collected signal and accurately targets sample
- Automated mapping facility
- Ambient and low temperature capabilities
- Completely automated PL system

Experimental setup

In order to measure photoluminescence of semiconductors, there are various requirements: (a) A stable, powerful mono-chromatic light source; (b) optics to focus light on the sample; (c) sample holder; (d) collection optics; e) monochromator; and (f) detector for spectral analysis. Actual sample excitation and collection optics used depend on the type of samples and experimental conditions required. For some samples, excitation and collection are optimal at 90°. In some cases it is also important to map an entire semiconductor wafer to analyze impurities found in different areas of the sample. Computerized mapping can be done with a precision x-y stage, and here, usually the optics are positioned at zero degrees to the sample.

Various experimental parameters derived from the spectra, such as peak symmetry, FWHM of the peak, center position of the peak, and fine structure, can give information about the structure and composition of doped semiconductors. This type of analysis can also be used to evaluate growth methods using different input gas mixtures.

Figure 1 shows the optical and mechanical arrangement of the photoluminescence system for analysis and mapping of a semiconductor sample. The sample is placed on the MapMax x-y translational stage and fixed in position in the sample holder.

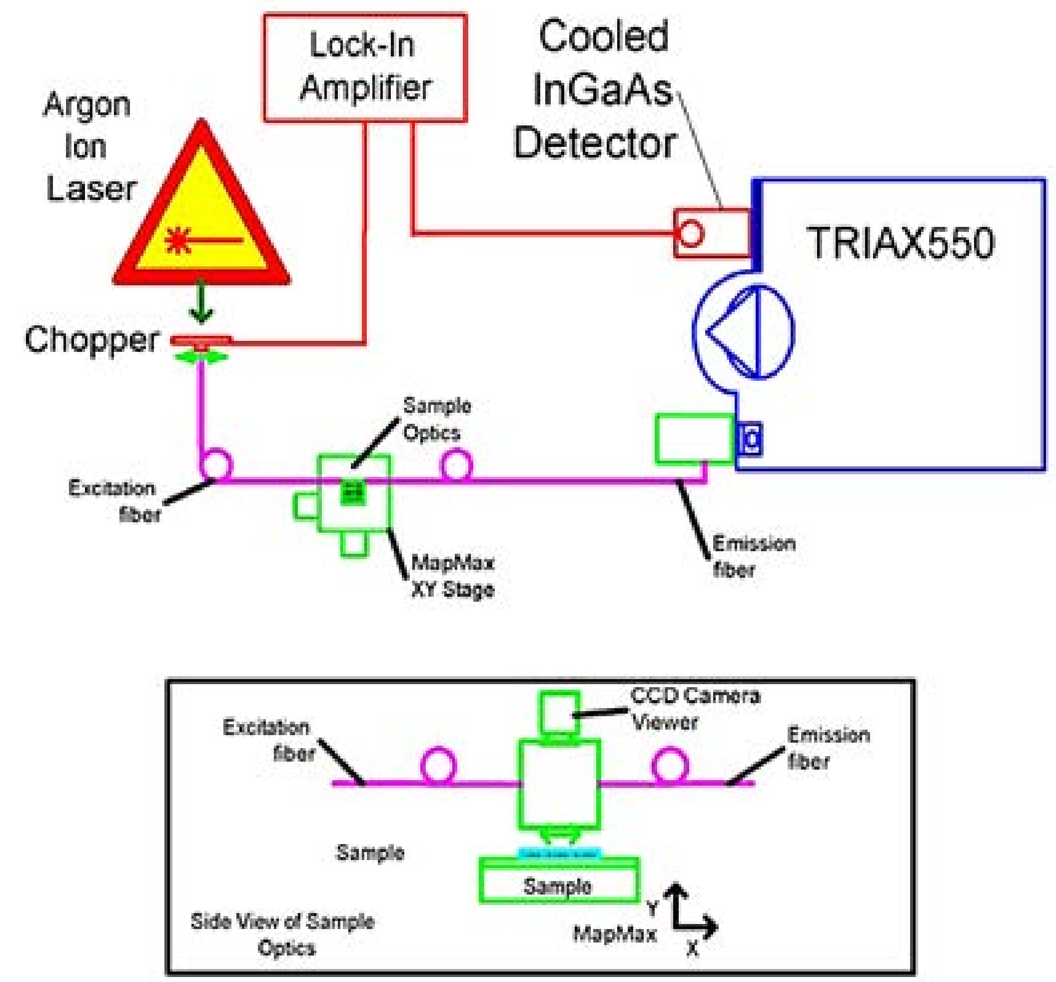

Figure 1

NEXT »

Photoluminescence of semiconductors, cont.

The HORIBA Scientific Macro Illuminator allows light to be focused on the sample while the image is displayed on the monitor. An Ar laser is used as the excitation source. Light from the laser is focused into a fiber, which goes into the input channel of the HORIBA Scientific Macro Illuminator. The photoluminescence from the sample is collected, goes through the output channel of the HORIBA Scientific Macro Illuminator, into a fiber, and finally into the TRIAX550 monochromator for analysis. The excitation light is chopped, so that a lock-in amplifier can be used with an InGaAs detector for data acquisition. After the initial system alignment is fixed, the experiment itself is controlled by computer using SpectraMax for Windows® spectroscopy software.

Results

An example of a typical doped semiconductor photoluminescence spectrum obtained with a HORIBA Scientific system is shown in Figure 2. Here, a liquid-nitrogen-cooled InGaAs detector was used, for optimal sensitivity and low noise. The entire experiment is controlled by SpectraMax for Windows® software, which provides easy data acquisition and analysis.

Conclusions

A complete, nearly turnkey system for photoluminescence measurements from HORIBA Scientific is shown to produce spectra with high signal-to-noise ratio, for diagnostic testing of semiconductors and other materials. A HORIBA Scientific photoluminescence system provides a comprehensive solution for characterization of semiconductor materials.

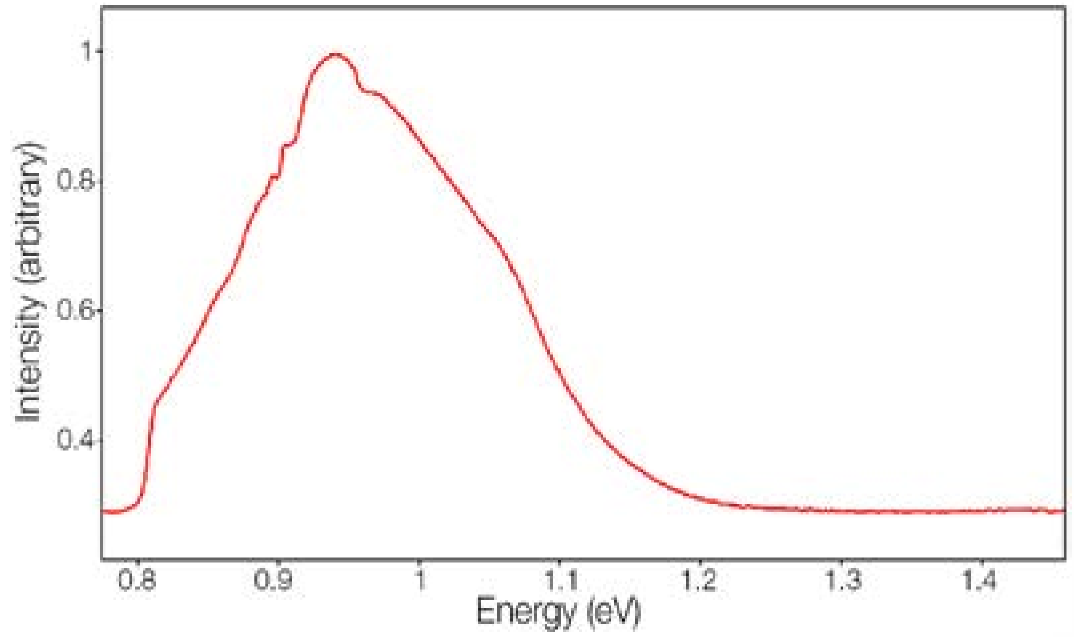

Figure 2: Photoluminescence spectrum of doped GaAs.

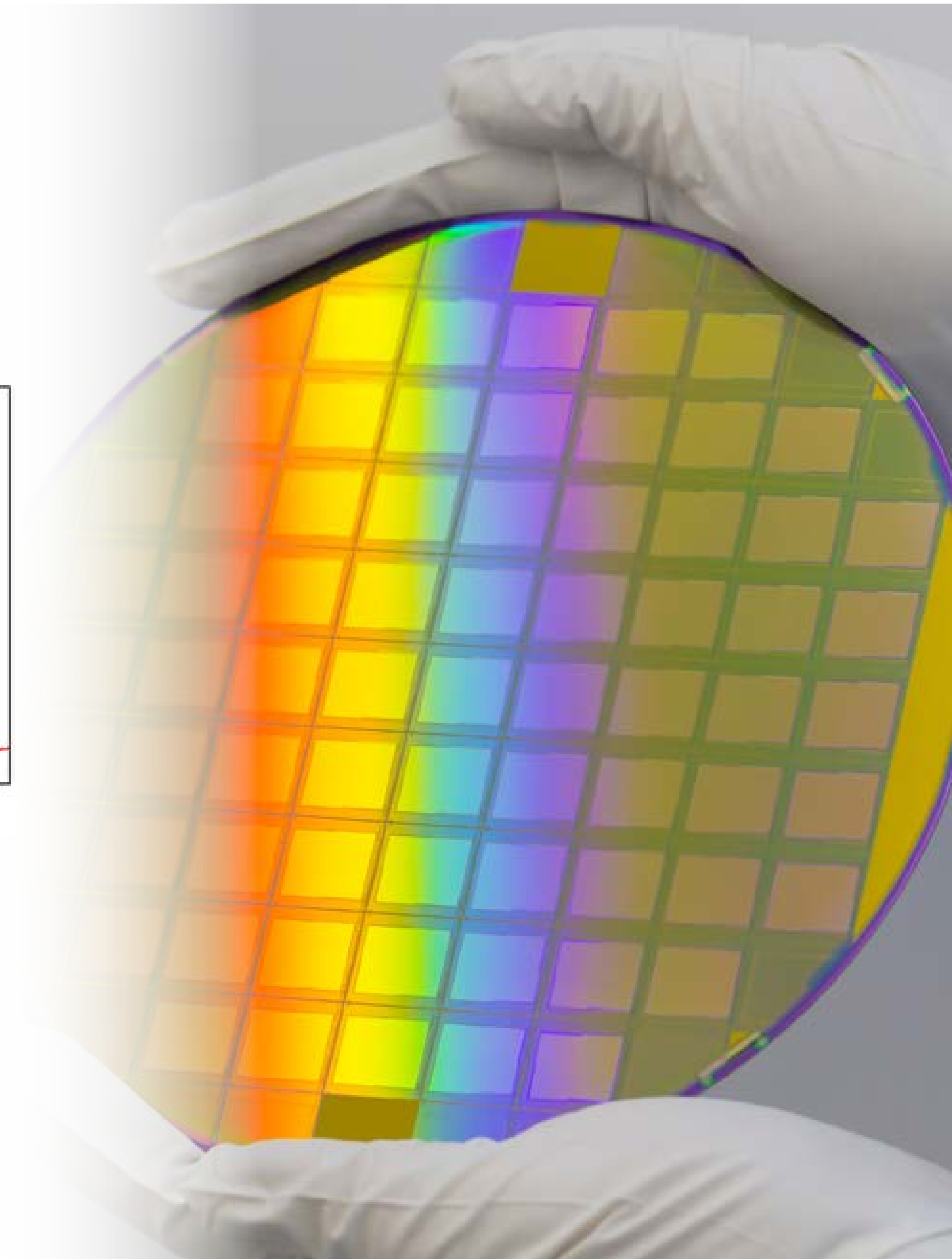

« PREVIOUS

HORIBA Scientific

Photoluminescence is the optical emission obtained by photon excitation.

Characterization of semiconductors with photoluminscence measurement system

Introduction

Photoluminescence is the optical emission obtained by photon excitation (usually a laser) and is commonly observed with III-V semiconductor materials. This type of analysis allows non-destructive characterization of semiconductors (material composition, qualitative investigations, etc.).

Description

An argon laser beam is focused on the sample which is located in the center of the sample compartment. If the energy of photons coming from the laser source is greater than the energy gap of the semiconductor, the sample emits photons. These are collected and analyzed with a dual flat field spectrograph. Two detectors are used, a CCD and an InGaAs array. This system allows investigations from 0.75 to 2.4 eV.

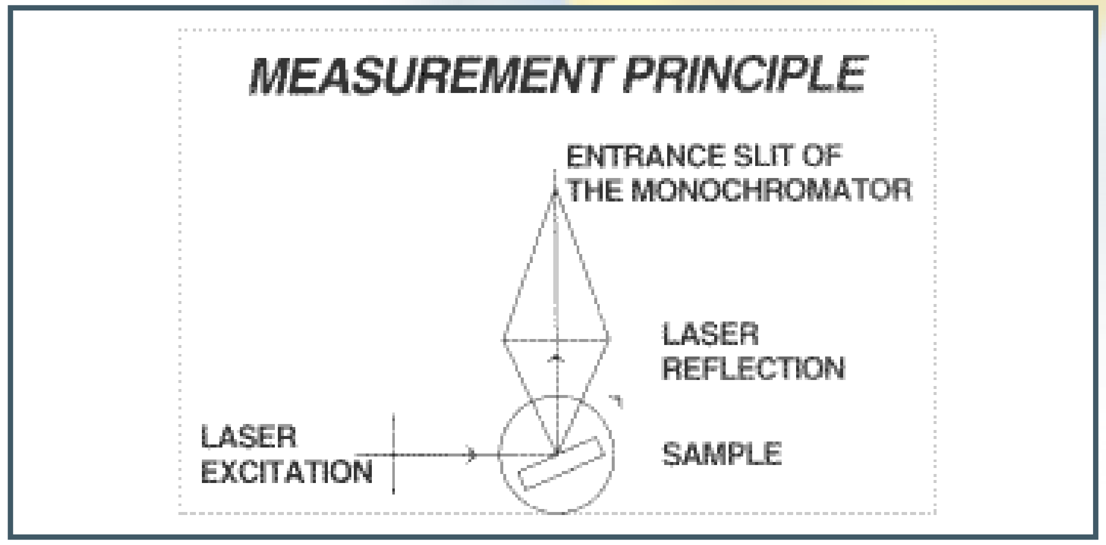

Measurement Procedure

We identify the position of one or several photoluminescence lines, and with the help of mathematical models, determine the composition of the material. Example: GaAlAs sample. The following expression gives the AlAs composition as a function of the photoluminescence line position (*):

E(x) = 1.424 + 1.247 x (at T = 300K)
with
E(x): line position (in eV units) x: AlAs composition
Measured line position: 1.643 eV
then x = 0.18 (18% of AlAs)

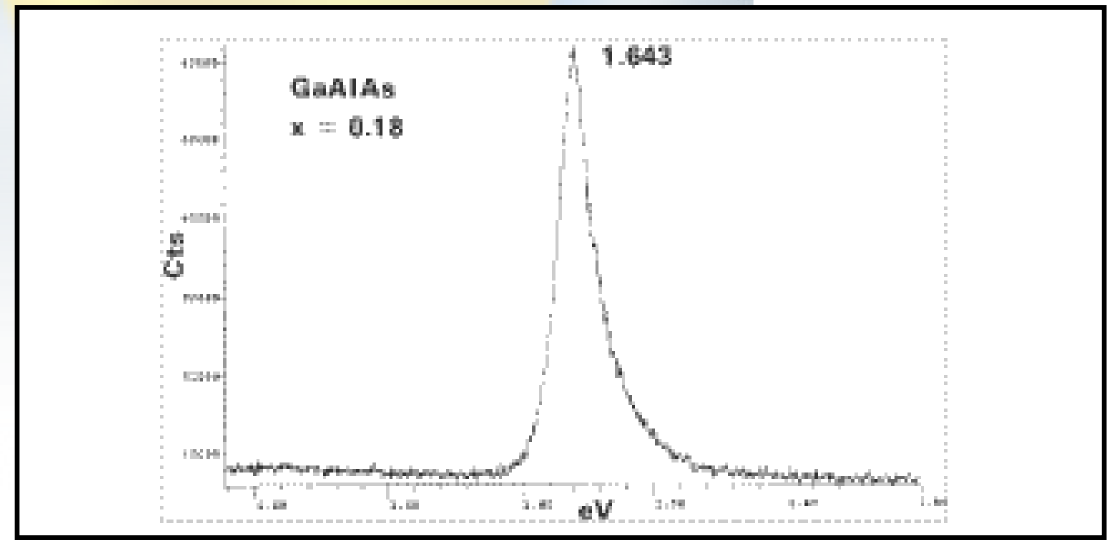

Applications

- Qualitative investigations for semiconductors.
- Fast determination of alloy composition in ternary compounds (GaAlAs, GaInAs, AlInAs...)

System Advantages

The two array detectors, CCD and InGaAs, offer high sensitivity and speed. They can both be mounted simultaneously on a Dual Flat Field Spectrograph allowing full characterization of the sample with ease.

Microstructures GaN and related alloys are important materials used to build short-wavelength light sources.

Photoluminescence characterization of GaN alloys and other semiconductor microstructures

MicOS characterizes III-V semiconductor

Microstructures GaN and related alloys are important materials used to build short-wavelength light sources (lasers and LEDs). Room- and low-temperature photoluminescence (PL) are used to characterize these materials, as well as device performance. Parameters such as IQE of quantum wells (QW) can be measured for patterned structures using selective optical excitation of microstructures made from these materials. Selective excitation means fine control of the laser-excitation beam size and positioning, and visualization of the sample under measurement.[1]

In many such measurements, important electronic structure information can only be revealed at low temperatures. Therefore, the PL measurement system also must be compatible with a cryostat. Figure 1 shows a typical configuration of a HORIBA MicOS measurement system, and Figure 2, the resultant PL spectra.[2] Our MicOS (Figure 3) also has the flexibility to accommodate different user-selectable excitation laser wavelengths for III-V material excitation, and includes vision so that the user can readily see excitation position and areas of interest on the sample (Figure 3).

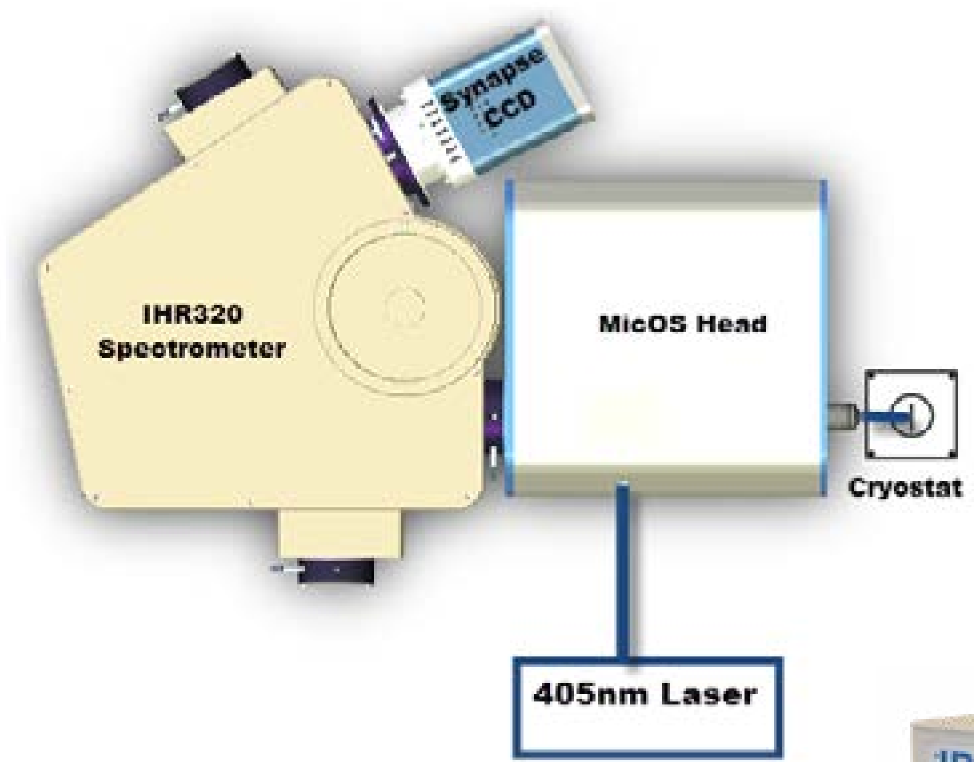

Figure 1: Typical low-temperature, direct-coupled micro-PL setup. Direct coupling of the microscope's front end increases throughput to the spectrometer (for low-light samples). System also has flexibility to measure sample via the side window of an upright cryostat or in a down-looking configuration.

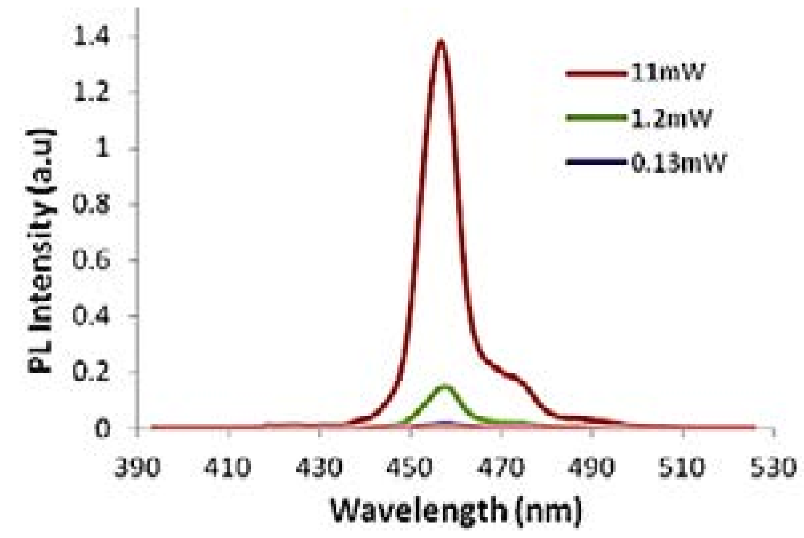

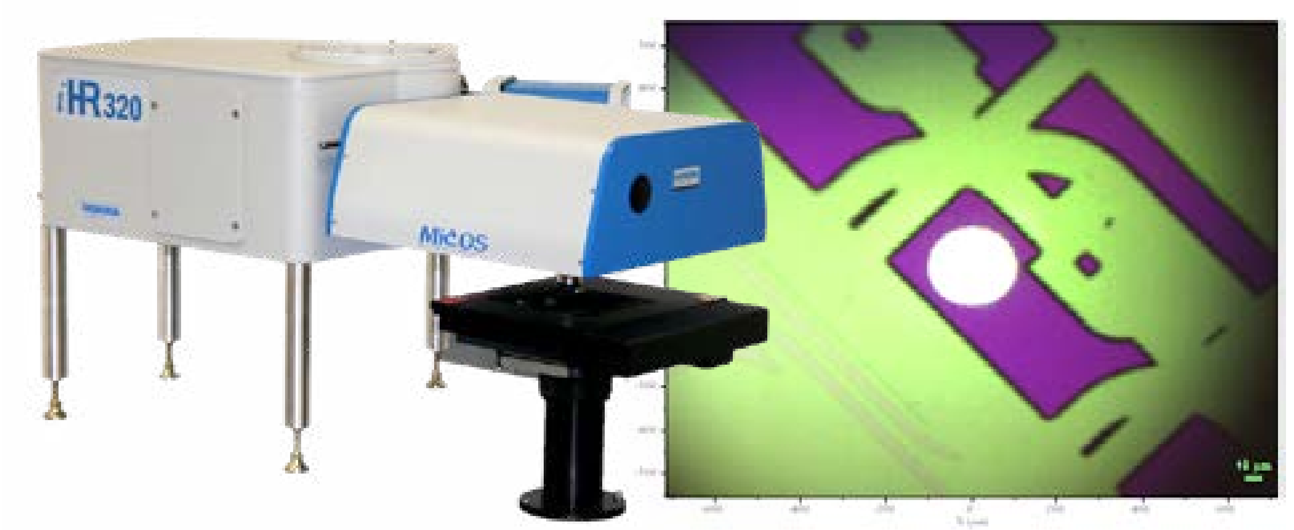

Figure 3: (Top) Down-looking version of HORIBA MicOS with mapping stage. (Right) Representative image of a patterned sample showing laser excitation on a region of interest.

References: 1. J. Korean Phys. Soc., 58(6) June 2011, 1660–1663. 2. Proprietary—semiconductor manufacturer.

Temperature-dependent photoluminescence(PL) spectroscopy is a powerful optical method for characterizing materials.

High resolution low-temperature photoluminescence of semiconductors

Introduction

Temperature-dependent photoluminescence (PL) spectroscopy is a powerful optical method for characterizing materials. PL can be used to identify defects and impurities in Si and III-V semiconductors, as well as determine semiconductor bandgaps. At room temperature, PL emission is usually broad—up to 100 nm in width. When samples are cooled, structural details may be resolved; a small spectral shift between two samples may represent a difference in structure. For cooling, two types of cryostat typically are used: A cryostat using liquid N_2 or liquid He, or a closed-cycle cryostat in which cryogenic liquid is included as part of the cooling system. The cooled sample is excited by a laser, and the PL is coupled to a spectrometer via an optical interface. In this technical note, sample data are shown from a high-resolution PL system.

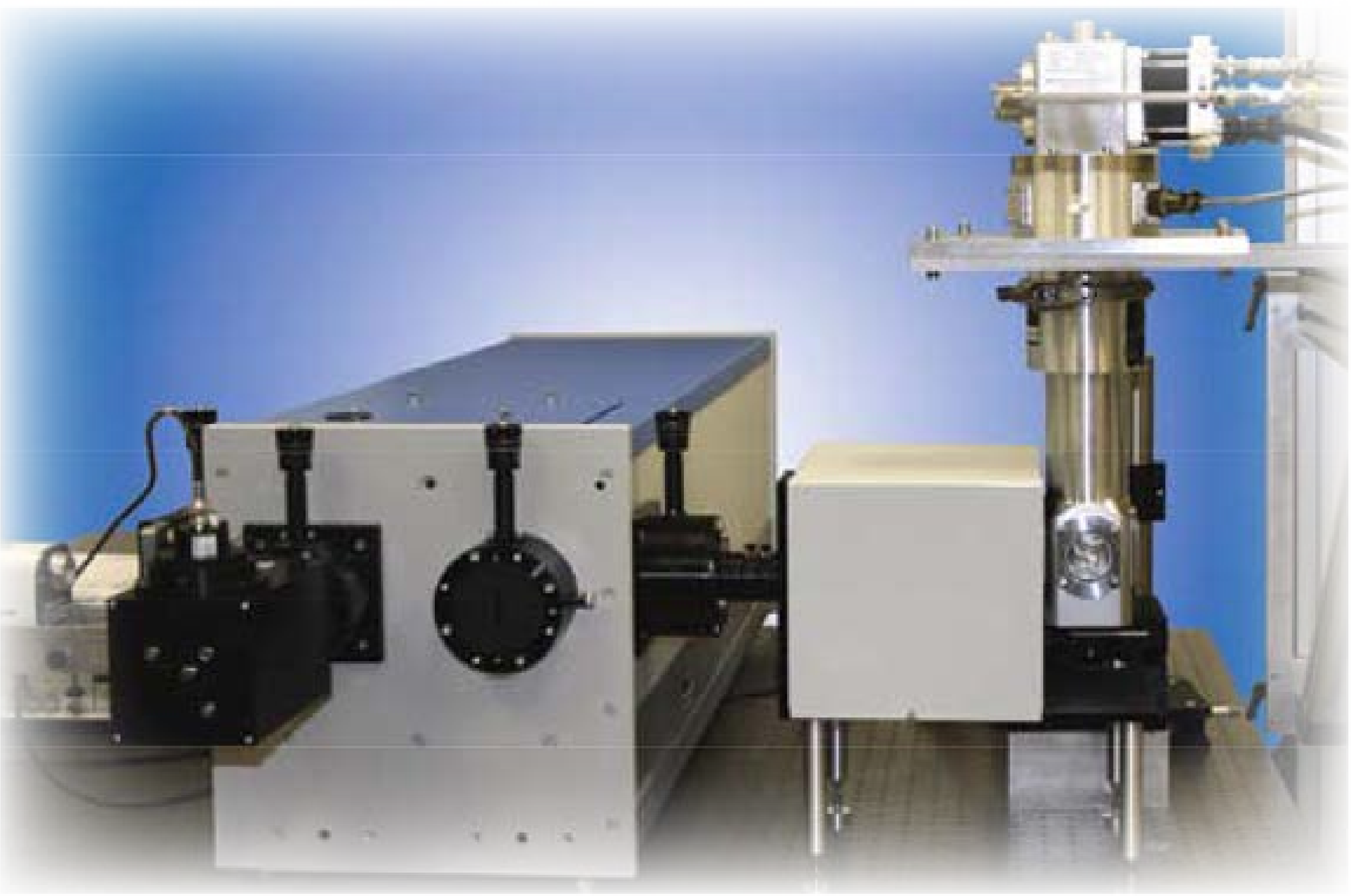

Experimental setup

A 1 m focal-length monochromator (1000M Series II, 600 gr/mm grating) scanned from 800–1650 nm. The detection system was a thermoelectrically cooled InGaAs detector with chopper and lock-in amplifier. Semiconductor samples were mounted in a closed cycle cryostat mounted above the optical table, and cooled to 4.5 K. A HORIBA Scientific Low Temperature Cryostat Interface optimized the optical coupling into the monochromator. The excitation source was a 10 mW HeNe laser (λ= 632.8 nm). Figure 1 shows the experimental apparatus.

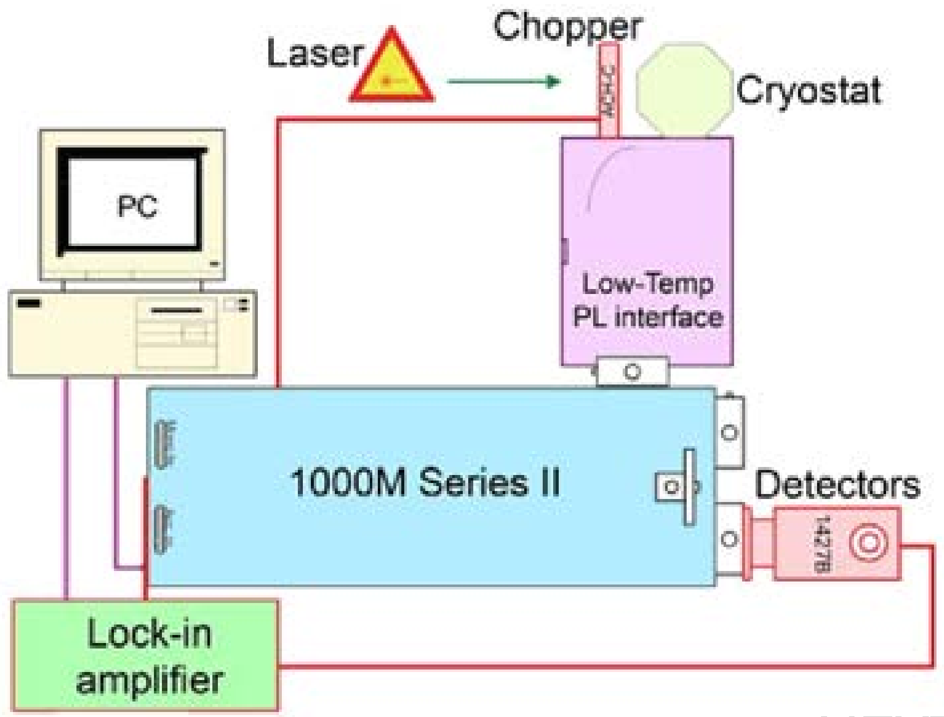

Figure 1: Experimental system.

NEXT »

High resolution low-temperature photoluminescence of semiconductors, cont.

Results

Figure 2 shows spectra of the same sample measured at room temperature, and at 4.5 K. In PL spectroscopy, a material absorbs light, creating an electron-hole pair. An electron from the valence band jumps to the conduction band, leaving a hole in the valence band. The photon emitted upon recombination corresponds to the energy difference between the valence and conduction bands (band gap), and is hence lower in energy than the excitation photon, so that the emission is red-shifted with respect to the excitation light. At low temperatures, a PL peak is quite sharp. As the temperature increases, the peak broadens and shifts to lower energy. This red-shift is typical of the function of temperature. The decrease in peak intensity indicates that electrons escape via non-radiative processes.

Figure 3 compares PL spectra from a sample of Nd:YAG laser-glass, using the 1000M Series II (1 m focal length) and the iHR320 (0.32 m focal length) spectrometers. Note the sharper peaks recorded with the 1000M system.

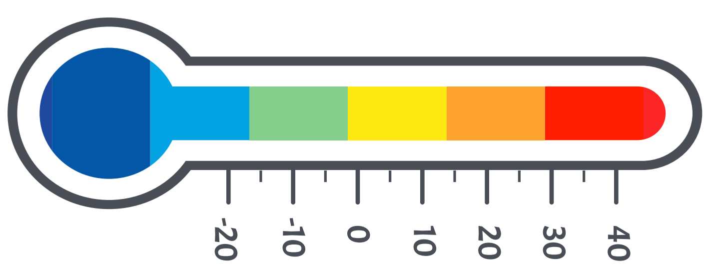

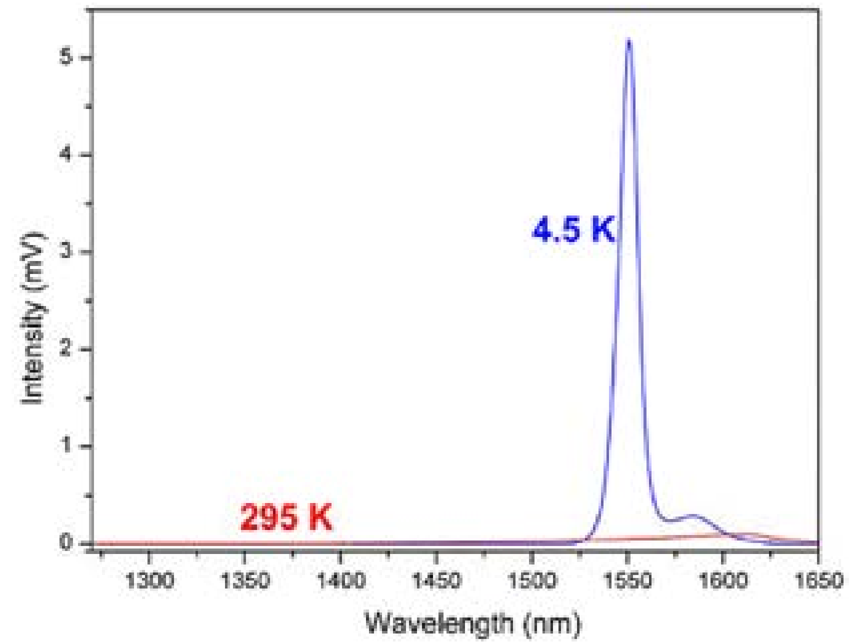

Figure 2: PL from typical semiconductor sample at room temperature, and also cooled to 4.5 K.

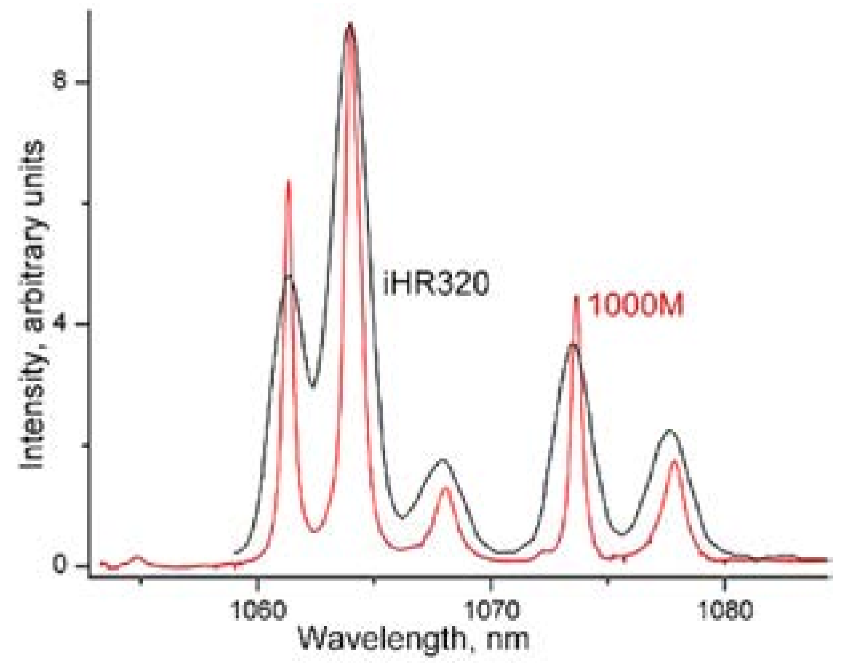

Figure 3: PL spectra of Nd:YAG laser-glass, taken with (black) iHR320 spectrometer and (red) 1000M spectrometer.

System components

In order to measure photoluminescence of semiconductors, the following are needed: A stable, powerful monochromatic light source, optics to focus light on the sample, a sample holder, collection optics, a spectrometer, and a detector for spectral analysis. The low temperature PL optical Interface from HORIBA Scientific provides a stable collection-optics system to collect the maximum amount of light from the sample inside either type of cryostat, and couples it efficiently into the spectrometer.

Benefits include:

- Reflective optics for maximum light collection
- Compatible with M-Series, iHR320/550, and FHR640/1000z
- Mounts directly on the spectrometer entrance slit
- Compatible with most cryostats with 90 mm dia. bodies
- Input f/1.5, output f/7.5
- Filter-holder included [standard 1 inch (2.5 cm) filter]

HORIBA Scientific component	Part number
Low temperature PL optical interface	ACC-CRYO-1000M
1000M Series II, 2 entrance and 1 exit slits	1000M II
Optical chopper	ACH-C
Lock-in amplifier	SR810
Solid-state detector interface	1427C
Thermoelectrically cooled InGaAs photodiode	DSS-IGA020T
SynerJY® spectroscopy software	CSW-SYNERJY
Closed-cycle He cryostat	Contact us
Cryostat-mounting hardware	Contact us

« PREVIOUS

Applications

III-V semiconductors are important to the fabrication of active photonic devices, such as light sources and detectors.

III-V wafer characterization through photoluminescence mapping

MicOS for mapping semiconductor wafers

III-V semiconductors are important to the fabrication of active photonic devices, such as light sources and detectors. Successful fabrication of such devices relies on the high quality of the underlying materials and precise deposition of intended geometries on a wafer substrate.[1] Defective materials and imperfections in geometries adversely affect yield, and usually increase cost and development times. The cost and delay penalties are further compounded when such defects in either material or device-geometry are not caught early enough in the cycle.

Photoluminescence (PL) spectroscopy is a robust, non-contact, non-destructive optical technique for determining material quality and geometrical accuracy for many III-V semiconductor-based components. Quality of the material is often obtained by measuring point PL on the bulk material, but geometrical accuracy of the device requires mapping PL over the entire device—or at least a region of interest on the device. Figure 1 shows a typical PL emission near-IR spectrum of a III-V semiconductor measured at a point on a wafer, using the HORIBA MicOS PL wafer-mapper (Figure 2).

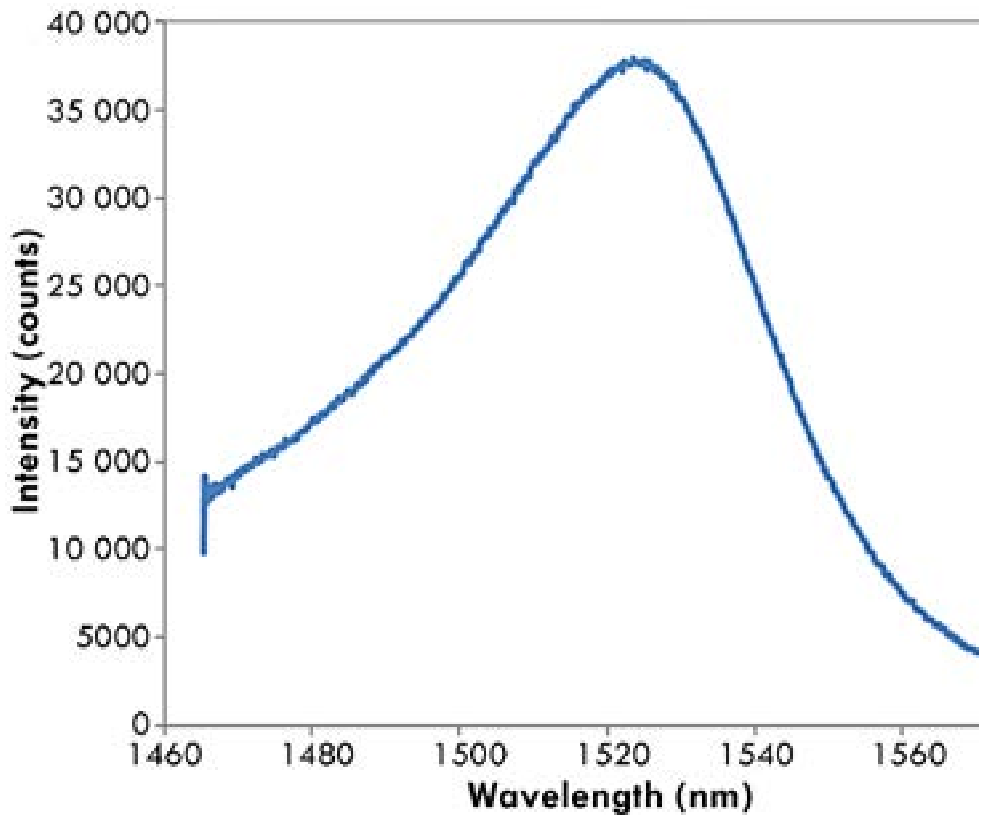

Figure 1: Typical room-temperature PL spectrum of a III-V semiconductor in the near-IR region of the spectrum following laser excitation at 532 nm. This measurement was carried out on the HORIBA MicOS system (Figure 2, see right).

Figure 2: Down-looking version of HORIBA MicOS with mapping stage.

References
A. Wójcik-Jedlińska, et al., "Photoluminescence characterization of AlGaAs/GaAs test superlattices used for optimization of quantum cascade laser technology," Optica Applicata, 39(4), 2009.

HORIBA Scientific

III-V wafer characterization through photoluminescence mapping, cont.

The versatile HORIBA MicOS PL wafer-mapper micro-PL system includes a vision camera so the user always sees the region of the wafer under excitation, useful when the wafer has patterned structures. The MicOS head is directly coupled to a triple-grating spectrometer, ensuring the highest throughput and wide spectral coverage (200–1600 nm). The MicOS can also use different excitation-laser wavelengths, and includes an assortment of motorized xyz stages for mapping wafers up to 300 mm. It can measure in a down-looking configuration for standard wafers, or side-looking configuration for facet-emitting samples.

Included with the MicOS wafer-mapper is LabSpec 6 software, which not only automates data collection, but offers an array of analytical tools for data processing and interpretation. LabSpec offers a data collection mode called SWIFT, in which the stage serves as the controller, and triggers detector-acquisition, bypassing the computer. This mode can collect data at high speed so that 2500 spectra can be collected over a two-inch wafer in under three minutes. LabSpec also offers an array of analytical and display tools, including peak identification and fitting, background subtraction, and multivariate analysis.

Figure 3 displays various PL parameters for wafers (peak intensity, peak wavelength, and FWHM of the emission), all of which can be correlated to material properties of the wafer. The PL measurements above are critical, and their implementation spans product design to fabrication and manufacturing quality control, including failure-mode analysis for field failures. In quality control, where time is critical, performing the mapping measurement quickly is important in order to create a statistically valid sample set, and thus increase the confidence level of the inferences drawn from the measurement.

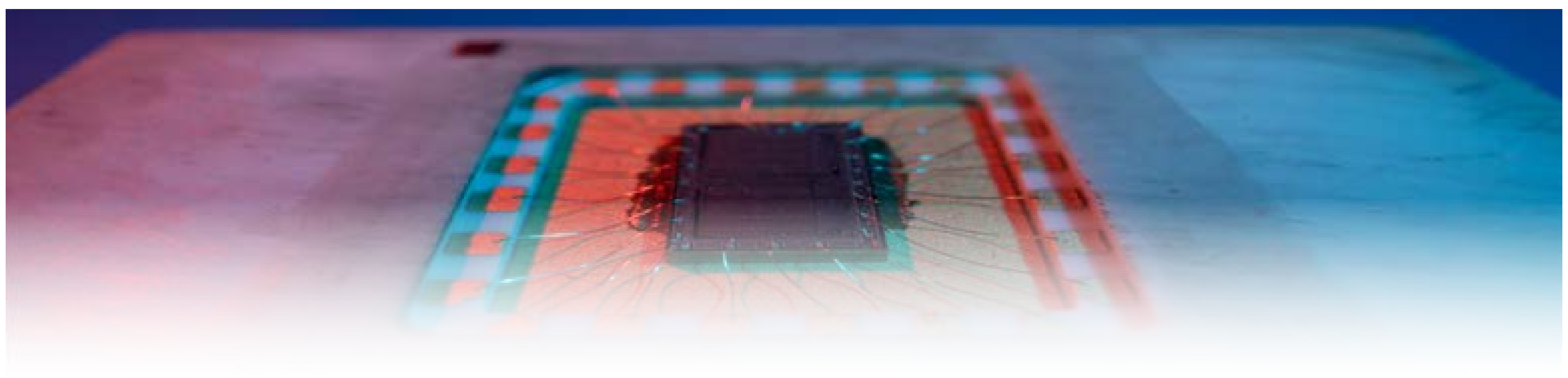

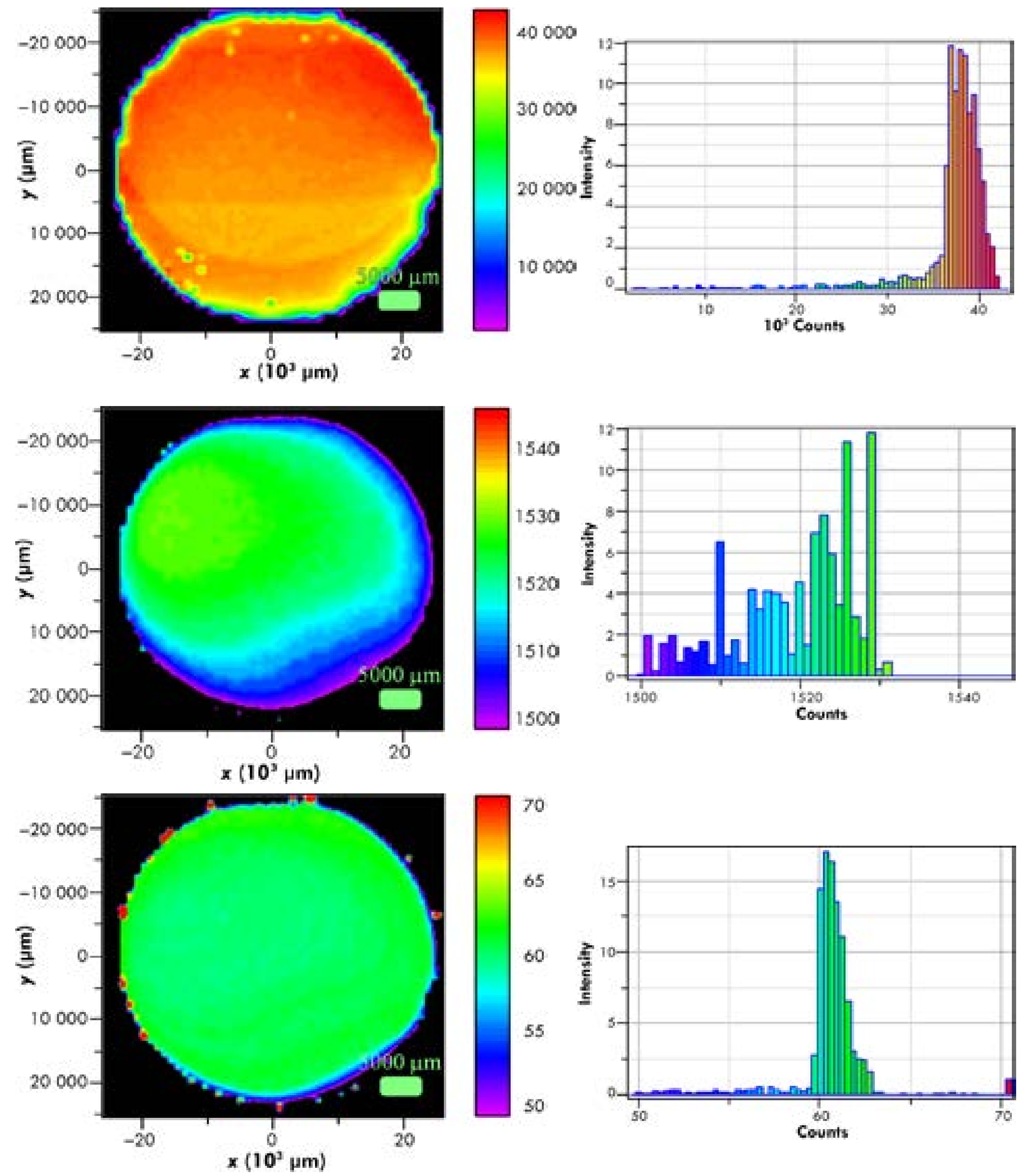

Figure 3: PL-spectrum parameters. Top to bottom: Distribution of PL peak position, peak wavelength, and FWHM of emission over wafer.

« PREVIOUS

Monolithic integration of optical components on CMOS platforms is ongoing in the optical communications industry.

Room-temperature micro-electroluminescent characterization of Ge-based IR sources

MicOS characterizes Ge-based micro-LEDs

Monolithic integration of optical components on CMOS platforms is ongoing in the optical communications industry. CMOS offers a mature and robust platform, and therefore is logical for building optical-interconnect modules. These modules include light sources, modulators, multiplexers, and detectors on a single substrate. Silicon is the foundational material for CMOS technology, but as a material with an indirect band gap, it poses a serious obstacle to building light sources via CMOS-based integrated photonics.

There is particular interest in integrated sources from 1300–1600 nm. Germanium has a band gap exactly within this range. Like Si, Ge is a group IV element, so it is a likely candidate for integration on a CMOS device. Yet Ge is also an indirect-band gap material, but with an adjacent (higher-energy) well in the conduction band capable of direct transitions. Various mechanisms have been developed to engineer population of this direct-bandgap path in SiGe alloys leading to integrated light sources.[1,2]

One class of such SiGe light sources uses an electrical bias to populate the direct band gap path. Electroluminescence (EL) is an appealing method for characterizing such devices. Figures 1 and 2 show the EL spectra of one such device (Figure 3, left) measured using the HORIBA MicOS microscope spectrometer (Figure 3, right).[3]

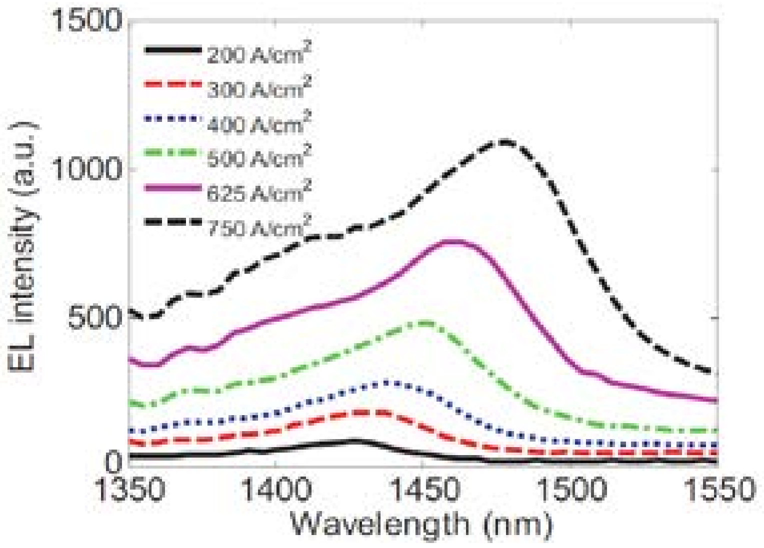

Figure 1: Electroluminescence spectra of a Si-Ge quantum well as a function of (left) bias current, and (right) temperature.

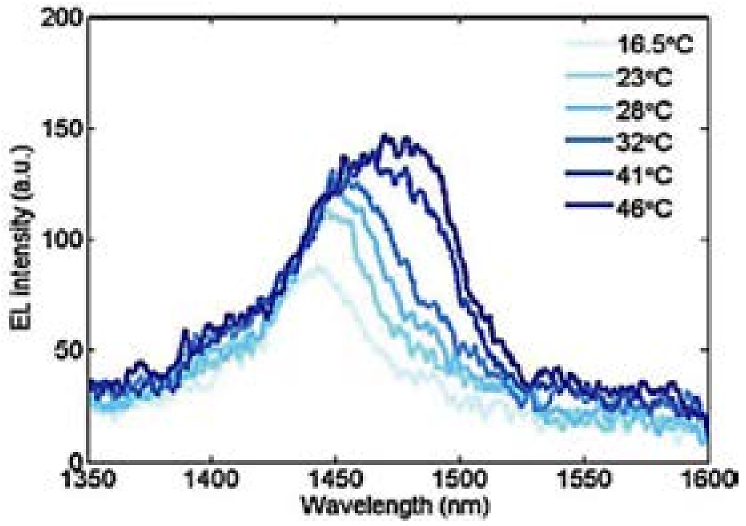

Figure 2: Electroluminescence spectra of a Si-Ge quantum well as a function of temperature.

Figure 3 (left). Representative image of EL from a micro-LED.
(Right) Down-looking version of HORIBA MicOS with mapping stage.

References
1. S. Cho, et al., Optics Express, 20(14), 14921 (July 2012).
2. S. Chen, et al., Optics Express, 17(12), 10019 (June 2009).
3. E. Fei, et al., Proc. IEEE Conf. on Group IV Photonics (2012), http://ieeexplore.ieee.org/xpl/abstractAuthors.jsp?reload=true&arnumber=6324112

The high spectral resolution of a Raman spectrometer can effectively perform PL spectroscopy of solid-state materials, particularly when the emission spectra consist of narrow bands or even lines.

Introduction to using a Raman spectrometer for PL

Why use a Raman instrument to perform photoluminescence studies?

Photoluminescence (PL), a non-contact, non-destructive method of probing the electronic structure of materials, produces information about the composition and solid-state makeup of a sample.

Light directed onto a material is absorbed and photo-excitation can occur. This causes the sample to jump to a higher electronic state, and release energy as photons, as the material relaxes and returns to a lower energy level. The emission of light, or luminescence, through this process is called PL.

A PL microscope is a laser or lamp-based instrument that measures optical luminescent emission excited on a microscopic sample when the excitation energy is above the band gap. PL provides information on electrical and optical properties of semiconductor materials, including band gap, emission wavelength, crystallinity, crystal structure, and defects.

Researchers and production labs use PL-optimized spectrometers for wide-ranging measurements, including compositional analysis of an epitaxial layer of compound semiconductors, defect evaluation of light-emitting materials, non-destructive evaluation of integrated optical circuits, quantitative analysis of impurities, and evaluation of various Laser Diodes and LEDs, ranging from GaN to InP.

Because a Raman spectrometer provides high spectral resolution, it can effectively perform PL spectroscopy of solid-state materials, particularly when the emission spectra consists of narrow bands or lines at low temperatures.

Here's why. When a sample is illuminated by a laser, both Raman scattering and PL can occur. PL can be many times stronger than the Raman scattering. In fact, the most frequent reason for failing to acquire a Raman spectrum is because of a strong and broad fluorescent background. The detector noise generated by the fluorescence overwhelms the Raman signal.

The high spectral resolution of a Raman spectrometer can detect broad PL emission, as well as resolve bands that are narrow and closely spaced.

So, a Raman microscope is also a high spectral resolution PL instrument, ideal for performing high-sensitivity, laser-excited PL, particularly on substances that have exceedingly narrow emissions.

By design, a Raman microscope is a high-performing PL microscope, and adjusting excitation wavelengths can allow Raman scattering measurements that don't get lost in the PL background noise.

There are advantages to performing PL and Raman spectroscopies simultaneously with the same instrument. This is especially true when studying two-dimensional (2D) semiconductors.

C.V. Raman

NEXT »

Introduction to using a Raman spectrometer for PL, cont.

The combination of both Raman and PL techniques on a single instrument provides more information and a better understanding of the sample's characteristics.

And since the sample doesn't have to be moved to a new instrument, both measurements are made at the same exact location on the sample for complete and precise analysis. So, when used to perform PL spectroscopy, a Raman spectrometer becomes, in essence, two instruments in one.

Many of our confocal Raman microscopes, depending on each one's specific configuration, are capable of measuring PL and Raman spectra from deep UV (~200nm) to infrared (up to several microns) using multiple detectors.

How do you use a Ramanspectrometer to measure PL?

When you perform Raman spectroscopy, PL is a problem when it occurs at the same wavelengths as the Raman scattering. To avoid the luminescence, you can choose excitation wavelengths that do not excite luminescence in the vicinity of the Raman signal. The traditional approach is to change to a longer excitation wavelength, where the photoluminescence is much weaker, producing less of a background. By selecting an excitation wavelength that generates little or no photoluminescence, the signal-to-noise of the Raman spectrum can be greatly improved. By selecting an excitation wavelength that generates little or no photoluminescence, the signal-to-noise of the Raman spectrum can be greatly improved.

Raman scattering is associated with vibrational transitions in which its creation causes an energy shift of the scattered light relative to the energy of the laser beam light source. It usually uses visible excitation, but many materials, when excited with visible excitation, will absorb and emit a luminescence. But with clever manipulation of the excitation wavelengths and the proper measurement scale, PL can be observed at the high-resolution that a Raman spectrometer provides.

« PREVIOUS

Note that the photoluminescence emission and bandwidth depend upon the material and the nature of the electronic transition, and not the spectrometer. The value of the high spectral resolution of the Raman spectrometer is only realized when the emissions themselves are spectrally narrow.

Here, in Figure 1a, at the 633 nanometer excitation, two peaks, labeled as PL, appear. The bands at the same Raman shift (in wave numbers) for either 532 or 633, are Raman bands.

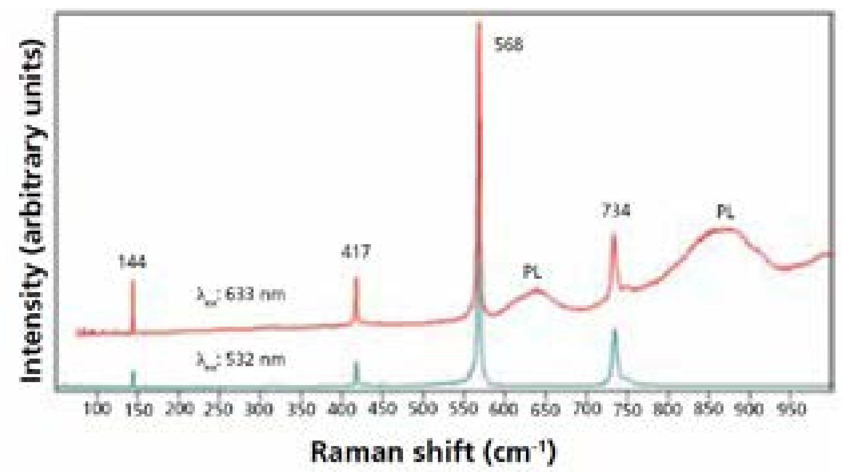

Figure 1a: Raman spectra acquired from the same location of single-crystal of $A_{l2}O_3$ using excitation wavelengths of 532 nm (green spectrum) and 633 nm (red spectrum). The bands marked PL are caused by photoluminescence.
Courtesy of Spectroscopy®

These must be Raman bands because these occur at the same Raman shift, at different absolute wavelengths.

But photoluminescence will occur at a specific absolute wavelength independent of the laser wavelength. If we were to plot the lowerspectrum at 532 out to a much greater Raman shift, we would see these two PL peaks right above it (see Figure 1b).

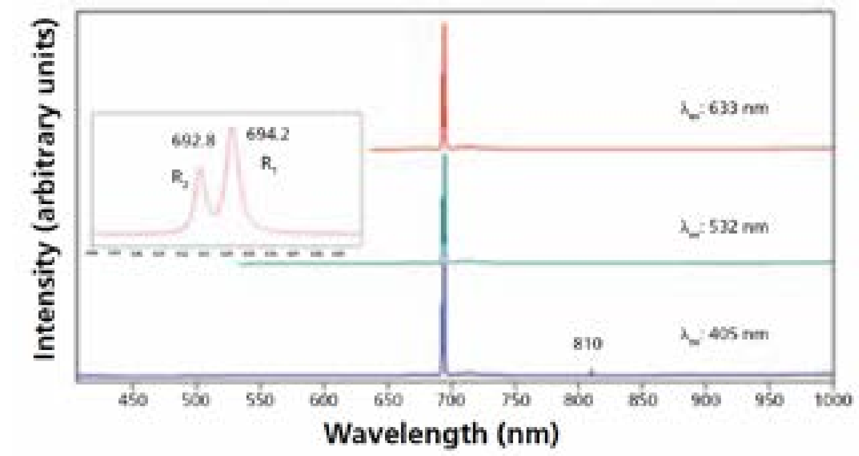

Figure 1b: The PL peaks align concisely when the data is displayed in nm scale.
Courtesy of Spectroscopy®

Photoluminescence is indicated because the emission occurs at a particular wavelength. PL generally does not occur when using longer excitation wavelengths because the light does not have the energy sufficient to excite an electronic transition. If no absorption of an incident photon takes place, then photoluminescence cannot take place. ***The fact that PL appears at the same absolute wavelength when excited with different excitation wavelengths confirms that it is photoluminescence.***

Vibrational energy transitions are generally not this broad. An exception to that appears in the Raman spectra of amorphous materials.

Some photoluminescence peaks are narrow. This is where a Raman spectrometer is so valuable. The real benefit of measuring PL with Raman is the high spectral resolution.

Raman spectroscopies simultaneously with the same instrument is advantageous, especially when studying two-dimensional (2D) crystals.

Photoluminescence spectroscopy using a Raman spectrometer

Photoluminescence can provide information about the composition and solid-state structure of a material. The high spectral resolution of a Raman spectrometer can be useful in performing photoluminescence spectroscopy of solid-state materials, particularly when the emission spectra consist of narrow bands or even lines. Having the capability to perform photoluminescence and Raman spectroscopies simultaneously with the same instrument is advantageous, especially when studying two-dimensional (2D) crystals. When used to perform photoluminescence spectroscopy, the Raman spectrometer becomes two instruments in one.

Raman scattering is a weak phenomenon and that is sometimes the reason for being unable to acquire a Raman spectrum, particularly at a low concentration or with a limited amount of sample. However, the most frequent reason for not being able to acquire a Raman spectrum is because a strong fluorescent background the detector noise generated by it overwhelms the Raman signal. Therefore, it should be self-evident that a Raman spectrometer is ideal for performing laser-excited photoluminescence. In a recent installment of “Molecular Spectroscopy Workbench,” we examined the choice of excitation wavelength to avoid photoluminescence (1). Here we discuss the use of a Raman spectrometer with the express purpose of performing photoluminescence spectroscopy.

The light illuminating a sample must be in resonance with an electronic transition of the material for photoluminescence to occur. More specifically, the sample must absorb a photon of the incoming light to promote an electron from the ground electronic state in a molecule, or valence band in a solid to the first excited molecular electronic state or conduction band in a solid, respectively. After the electron is in the excited electronic state or conduction band, it can undergo either radiationless decay or a photon can be emitted as the electron returns to the ground state or valence band. The latter emission process is called photoluminescence because the excited state was reached through the absorption of a photon. In contrast, had the electron been promoted from the valence to the conduction band through the application of a voltage and the passage of current, the subsequent emission would be more properly described as electroluminescence. Photoluminescence occurs in many bulk materials that are direct band gap semi-conductors and also because of impurities that absorb and emit light in an otherwise transparent medium. We discuss examples of both situations in this installment.

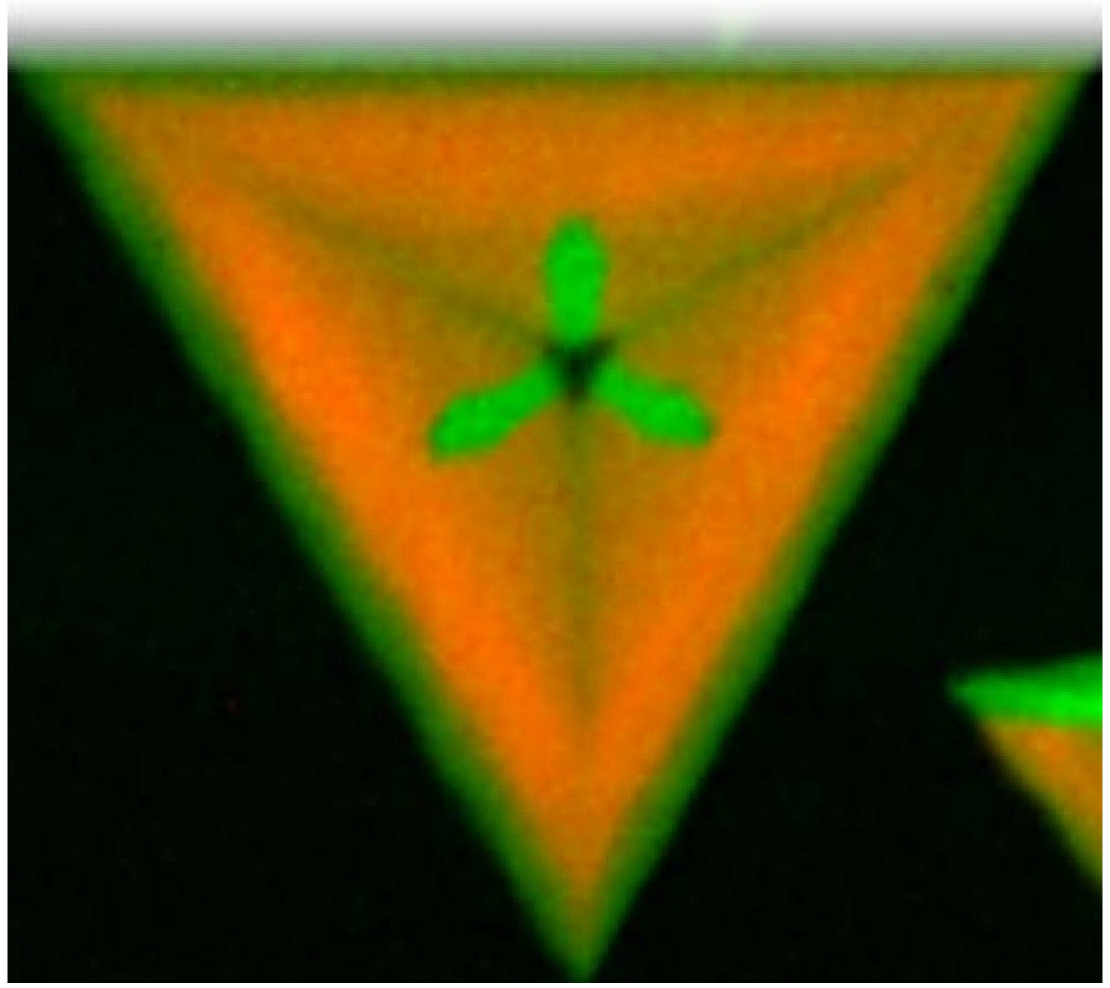

Raman Scattering (Green) and PL (Red) of 2D WS_2

NEXT »

HORIBA Scientific

Photoluminescence spectroscopy using a Raman spectrometer, cont.

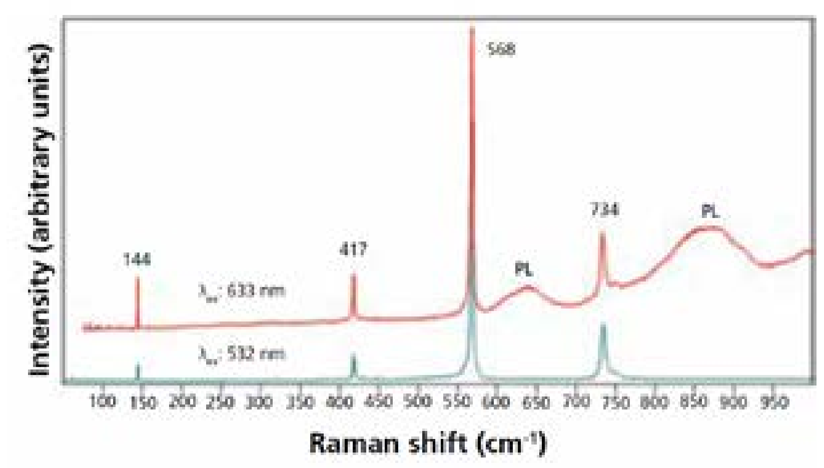

Figure 1a: Raman spectra acquired from the same location of a single-crystal of A_2O_3 using excitation wavelengths of 532 nm (green spectrum) and 633 nm (red spectrum). The bands marked PL are caused by photoluminescence.
Courtesy of Spectroscopy®

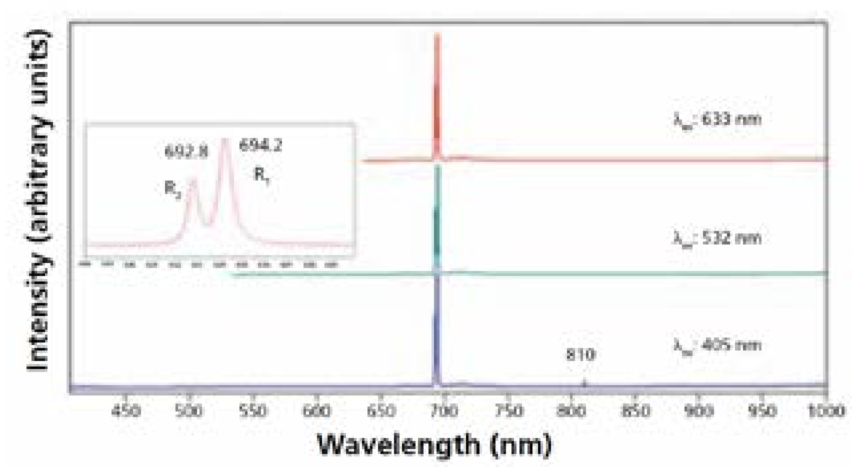

Figure 1b: The PL peaks align concisely when the data is displayed in nm scale.
Courtesy of Spectroscopy®

« PREVIOUS

Chromium Impurities in Aluminum Oxide

The aluminum oxide alumina (Al_2O_3) is known as corundum in its single crystal form. Within corundum the Al-O bond is approximately 60% ionic and 40% covalent with an Al atom at the center surrounded by six O atoms to form distorted octahedron (2). Therefore, the aluminum atoms in the crystal can be assigned a formal oxidation state of +3 with the surrounding O atoms each with a -2 formal oxidation state. Pure corundum is colorless; however, Al_2O_3 is often tinted or even deeply colored because of transition metal impurities in the crystal. Their presence at even less than 1% in the Al_2O_3 host lattice leads to the beautiful colors seen in gemstones such as ruby and sapphire. The presence of Cr^{3+} in Al_2O_3 is what gives ruby its red color, whereas sapphire, also a host crystal of corundum Al_2O_3, obtains its color from titanium impurities. The electron configuration of the Cr atom is [Ar] $3d^5$ $4s^1$. When occupying an Al site in the corundum crystal lattice, however, the electron configuration of Cr^{3+} is [Ar] $3d^3$ thereby allowing t_{2g}—e_g absorption and emission electronic transitions in the 3d orbitals. These electronic transitions are affected by the crystal field of the host lattice, which are then manifest in the absorption and emission spectra.

The combination of Raman and photoluminescence spectroscopies allows one to characterize the host crystal and the transition metal impurities, respectively. Raman spectra acquired from the same location of an Al_2O_3 crystal using 532 nm and 633 nm excitation are shown in Figure 1. Both spectra consist of Raman bands from the Al_2O_3 crystal at 144, 417, 568, and 734 cm^{-1}. However, the spectrum excited with 532 nm light has no background, whereas that excited at 633 nm manifests a steadily increasing background beginning at approximately 150 cm^{-1}. Furthermore, distinct broad peaks (relative to the Raman bands) appear at approximately 640 and 870 cm^{-1}. The appearance of these two broad peaks in the 633 nm excited spectrum and their absence in the 532 nm excited spectrum is confirmation that they are due to photoluminescence, and not Raman scattering. The use of different excitation wavelengths with the same sample is one of the best ways to differentiate photoluminescence from Raman scattering. Raman bands appear at the same position, independent of the excitation wavelength, when plotted on a Raman shift scale. However, if the bands appear at different Raman shifts, they are likely caused by photoluminescence. Now plot these same spectra on an absolute wavelength scale. If the bands appear at the same position when plotted on an absolute wavelength scale, their assignment as photoluminescent bands is confirmed.

The peaks at 640 and 870 cm^{-1} (659.5 and 669.7 nm, respectively) of the Raman spectrum are not the only, or even primary, emissions from this crystal of Al_2O_3. The photoluminescence spectra shown in Figure 2 were acquired using 405, 532, and 633 nm excitation. All of the spectra shown in this and other figures were acquired using a HORIBA LabRAM HR Evolution spectrometer with an 800 mm focal length and 1800 gr/mm gratings. Peaks appear at 692.8 nm and 694.2 nm for all excitation wavelengths when plotted on an absolute wavelength scale. The peak at 810 nm in the spectrum excited at 405 nm is from the grating's second-order diffraction of the 405 nm laser light. The inset plot with expanded scale of the spectrum excited at 532 nm shows how well resolved the peaks are, even though they are separated by only 1.4 nm. The high spectral resolution of a Raman spectrometer allows one to resolve these narrow and closely spaced missions. This particular pair of strong emissions is quite familiar and arises from Cr3+ impurities commonly found in Al_2O_3. In fact, if you take almost any piece of Al_2O_3 optical flat or window, and illuminate it with visible laser light, you are likely to observe these same two emissions, confirming that it is actually Al_2O_3:Cr^{3+}.

NEXT »

Photoluminescence spectroscopy using a Raman spectrometer, cont.

Without sufficient spectral resolution, the emission from Al_2O_3:Cr^{3+} can sometimes appear as a single line, known as the R line fluorescence of ruby, in a transition from the excited ^2E energy level to the $^4A_2$ level. However, the ^2E level distortions of the octahedral symmetry thereby produce two closely spaced emissions. These two Al_2O_3:Cr^{3+} peaks are well known as R1 (1.788 eV, 693.5 nm) and R2 (1.791 eV, 692.3 nm) and their peak positions have been used to determine the surrounding lattice strain (2). A stress can be applied to the crystal and the induced strain can be determined by the shift in the R1 and R2 emissions (3,4). This phenomenon of peak shifting as a result of applied stress is known as the piezo spectroscopic effect. Of course, the strain in the Al_2O_3 crystal induced by the applied stress can also be determined by the shifts in the Raman bands (5,6). Of the two techniques, photoluminescence may be the preferred method for determining strain in Al_2O_3:Cr^{3+} because of its much greater signal-to-noise ratio. There are several important points to take away from viewing the spectra plotted in Figure 2. The first is the high spectral resolution offered by using a spectrometer designed to resolve bands arising from vibrational modes and separated by wave-numbers (cm^{-1}). Such spectral resolution may not be necessary for typical molecular fluorescence work; however, spectral resolution can be extremely important depending upon the type of electronic transitions under study when working with solid state materials. Secondly, note that using a Raman spectrometer with a charge-coupled device (CCD) detector allows a free spectral range for detection of photoluminescence covering 400 nm to 1000 nm. Depending on the type of spectroscopic or materials science work that you do, having a Raman spectrometer can be like having two spectrometers in one.

4f-4f Orbital Transitions in Erbium Oxide

The lanthanide element erbium has a ground-state electron configuration of [Xe] $4f^{12}$ $6s^2$. With its oxidation to form the oxide Er_2O_3 the formal oxidation state of each Er atom is +3 and its electron configuration becomes [Xe] $4f^{11}$.Thus, the highest occupied molecular orbitals of Er^{3+} are the 4f orbitals, and they are partially filled. The 4f orbitals are non-bonding and are shielded from chemical interactions with surrounding O atoms; therefore, they do not couple strongly to the crystal lattice. The 4f-5d electronic transitions are allowed by parity selection rules. Such transitions, either absorption or emission, appear broad because of the coupling of the 5d orbital to the surrounding crystal lattice. In contrast, 4f-4f orbital transitions are forbidden by parity selection rules. However, the parity selection rule in Er_2O_3 is relaxed because the Er atom occupies a site lacking inversion symmetry. Under these conditions, the 4f orbitals can undergo some mixing with opposite parity orbitals such as 5d. This phenomenon is sometimes described as the forbidden 4f-4f transition, stealing intensity from the allowed 4f-5d transition. Consequently, 4f-4f electronic orbital transitions, absorption, and emission, are weakly allowed. Also, because the 4f orbitals are non-bonding and shielded from the surrounding O atoms, the absorption and emission bands appear quite sharp and narrow, similar to those of atomic transitions.

Photoluminescence spectra of Er_2O_3 excited with 405, 532, and 633 nm laser light are shown in Figure 3. The emission spectra consist of five clusters of narrow bands within the range from 405 to 1000 nm. The sharp peak at 810 nm in the spectrum excited with 405 nm light is from the grating's second- order diffraction of the 405 nm laser light. The sharpness of the bands is an indication that they can all be attributed to 4f-4f orbital transitions. Also, the distribution of the emission into multiple and discrete wavelength regions is why the lanthanides are important materials in lighting and display applications (7). Note that the clusters as individual entities vary in relative intensity depending on the excitation wavelength. That variation demonstrates how the use of different excitation wavelengths allows one to generate an excitation profile depending on how closely spaced the available exciting laser lines are. Within each cluster there appear many closely spaced emission bands. A magnified plot of the spectra between 535 nm and 720 nm is shown in Figure 4.

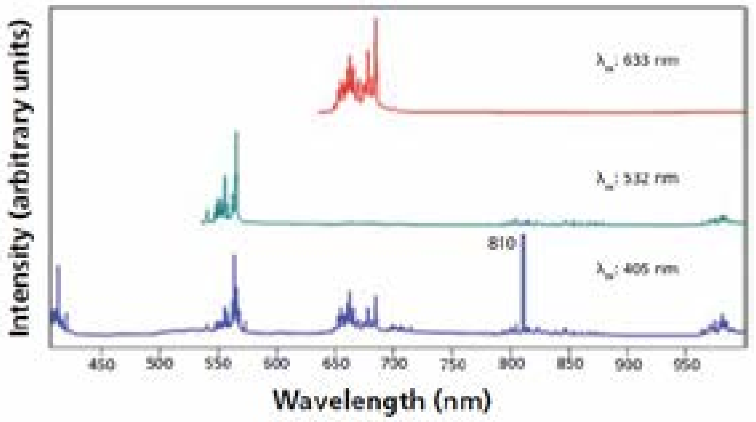

Figure 3: Photoluminescence spectra acquired from Er_2O_3 using excitation wavelengths of 405 nm (blue spectrum), 532 nm (green spectrum), and 633 nm (red spectrum).

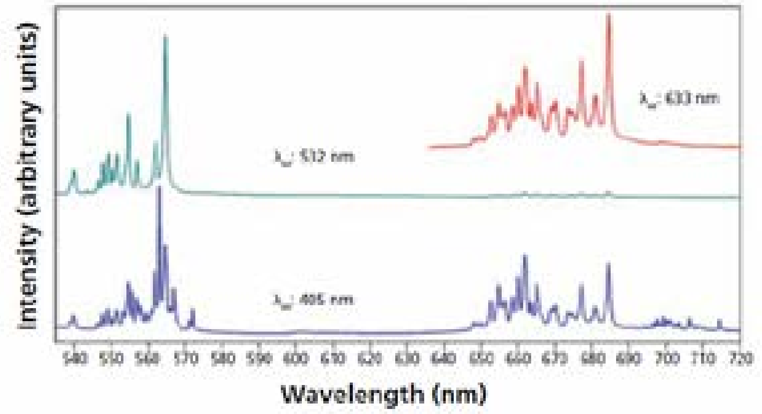

Figure 4: Photoluminescence spectra acquired from Er_2O_3 using excitation wavelengths of 405 nm (blue spectrum), 532 nm (green spectrum), and 633 nm (red spectrum).

Photoluminescence spectroscopy using a Raman spectrometer, cont.

Note how the relative intensities of the closely spaced bands within each cluster vary with excitation wavelength. These narrow bands can be resolved because of the high spectral resolution of the Raman spectrometer.

Photoluminescence in Nd-Doped Glass

Another lanthanide that should be quite familiar to spectroscopists is neodymium. The element Nd has a ground-state electron configuration of [Xe] $4f^4$ $6s^2$. The Nd:YAG crystal is the source of the 1064 nm laser line that functions as the excitation in Fourier Transform (FT) Raman spectroscopy. Frequency doubling the 1064 nm line produces the 532 nm laser line that is so commonly used now with dispersive Raman spectrometers. Of course, there are many other electronic transitions reported for Nd, and those transitions can be narrow or broad depending on the electronic orbitals involved in the transitions, and the degree to which they couple to the surrounding environment (8).

The electronic transitions of Nd have been well characterized and so glass doped with Nd is often used as a standard for spectral calibration. The Nd doped glass can appear faint to dark violet, depending on the thickness of the glass and therefore its optical density. The violet color of the glass indicates that the Nd is very likely in the +3 oxidation state because Nd_2O_3 has the same faint violet color (9). When Nd is oxidized to form Nd_2O_3, the formal oxidation state of the neodymium atom becomes +3 and its electron configuration is now [Xe] $4f^3$. Consequently, $4f^3$ becomes the highest occupied molecular orbital of Nd^{3+}. Photoluminescence spectra of Nd doped glass excited with 405, 532 and 633 nm laser light are shown in Figure 5. The spectra appear quite barren in contrast to those of Er_2O_3 in Figures 3 and 4. The Nd-doped glass spectra are quite similar for all excitation wavelengths consisting of a weak peak at approximately 800 nm, and a cluster of three partially resolved bands in the region from approximately 850 to 920 nm. The sharp peak at 810 nm in the spectrum excited with 405 nm light is from the grating's second-order diffraction of the 405 nm laser light. We can infer from the widths of these bands that the electronic transitions involved are highly coupled to the surrounding oxide environment. That is, the chemical interactions with the surrounding glass are probably similar to those of Nd_2O_3. That interpretation would certainly be consistent with the violet color of the glass. It is likely that these transitions involve 4f-5d orbitals of Nd^{3+} with strong coupling of the 5d orbital to the SiO_2 glass.

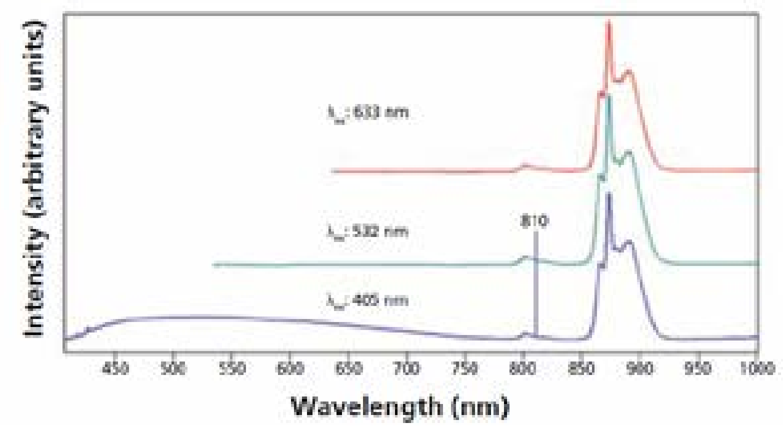

Figure 5: Photoluminescence spectra acquired from Nd-doped glass using excitation wavelengths of 405 nm (blue spectrum), 532 nm (green spectrum), and 633 nm (red spectrum).

Raman Spectroscopy and Photoluminescence of 2D MoS_2

The interest in two dimensional (2D) transition metal dichalcogenides (TMD) in general, and MoS_2 in particular, is that a single layer of MoS_2 atoms is a direct band gap semiconductor, whereas the bulk form is an indirect band gap semiconductor. Thus, single layer MoS_2 emits light when illuminated with light whose energy is above the band gap. This property holds the promise of being able to fabricate electro-optic devices from single-layer MoS_2 or other TMDs and has therefore been the subject of intense research and development over the past few years.

The crystalline structure of $2HMoS_2$ belongs to the D6h crystal class, and factor group analysis predicts one A_{1g}, one E_{1g}, and two E_{2g} Raman active modes (10–16). The symmetry assignments and corresponding Raman band positions for bulk hexagonal MoS_2 are E_{1g} (286 cm-1), E^1_{2g} (383 cm^{-1}), A_{1g} (408 cm^{-1}), and E^2_{2g} (32 cm^{-1}). Furthermore, it is important to remember that some visible wavelengths of the laser light used to excite Raman scattering correspond to energies of MoS_2 electronic transitions. The absorption spectrum of MoS_2 reflects the band gap of 1.7 eV, but it also manifests fine structure with narrow absorption peaks at 1.9 eV (653 nm) and 2.1 eV (590 nm) related to d-to-d orbital transitions split by spin-orbit coupling and designated A1 and B1 excitons, respectively (10,17). Consequently, one can observe an excitation wavelength dependence of the first-order Raman band intensities, as well as the appearance of Raman bands assigned to harmonic and combination modes when the laser excitation is of a wavelength that couples into these excitonic transitions (10,14,16,17).
i

Photoluminescence spectroscopy using a Raman spectrometer, cont.

Exfoliated few-layer flakes of MoS_2 are typically heterogeneous, and so the Raman and photoluminescence spectra tend to spatially vary on the flake. The effect of excitation wavelength on the photoluminescence spectra of few-layer MoS_2 flakes can be seen in the spectra shown in Figure 6.

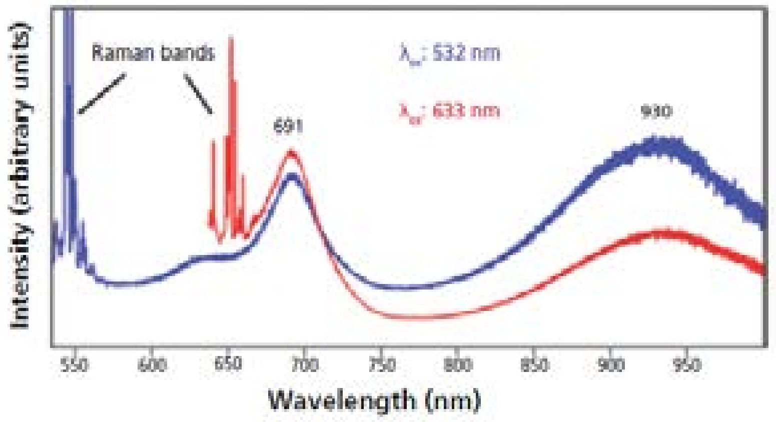

Figure 6: Photoluminescence and Raman spectra of few-layer MoS_2 flake taken at the same location with different excitation wavelengths.

The spectra were acquired at the same location on the flake, and are plotted on arbitrary intensity scales to better show the differences in relative strengths of both the photoluminescence and Raman signals. There are several differences to observe that relate to the electronic transitions and their coupling to the few-layer MoS_2 flake phonons. The photoluminescence excited at 532 nm is substantially weaker relative to the Raman scattering when compared to the photoluminescence/Raman strength ratio of the 632.8 nm-excited spectrum. Furthermore, the relative strengths of the 691 and 930 nm emissions are inverted for the 532 and 632.8 nm excitation wavelengths. An important aspect of this measurement is that one can simultaneously obtain a Raman spectrum and a photoluminescence spectrum from the same location. That fact holds important implications for the ability to simultaneously perform photoluminescence and Raman spectroscopy and imaging of few-layer MoS_2 and other TMD 2D crystals, thereby supporting the research and development of these materials to the level of electro-optic devices.

Conclusion

The high spectral resolution of a Raman spectrometer allows one to resolve narrow and closely spaced emissions from electronic transitions. Consequently, using a Raman spectrometer designed to resolve bands arising from vibrational modes and separated by wavenumbers in units of cm^{-1} is ideal for the detection of narrow band photoluminescence. Such spectral resolution may not be necessary for typical molecular fluorescence work; however, spectral resolution can be extremely important when working with solid-state materials. The free spectral range for photoluminescence when using a Raman spectrometer and CCD detector can extend from 400 nm to 1000 nm. Having the capability to perform photoluminescence and Raman spectroscopies simultaneously with the same instrument is advantageous, especially when studying 2D crystals.

When used to perform photoluminescence spectroscopy, the Raman spectrometer becomes two instruments in one.

References

(1) D. Tuschel, Spectroscopy 31(3), 14–23 (2016).
(2) K. Nassau, The Physics and Chemistry of Color: The Fifteen Causes of Color (Wiley-Interscience, New York, 1983), pp. 79–87.
(3) Q. Ma and D.R. Clarke, J.Am. Ceram. Soc .77, 298–302 (1994).
(4) H. Mahiou, A. Beakou, and R.J. Young, J. Mat. Sci. 34, 6069–6080 (1999).
(5) W. Zhu and G. Pezzotti, Phys. Status Solidi A 208, 1141–1150 (2011).
(6) W. Zhu and G. Pezzotti, J. Raman Spectrosc. 42, 2015–2025 (2011).
(7) G. Blasse and B.C. Grabmaier, Luminescent Materials (Springer-Verlag, New York, 1994), pp. 112–132.
(8) W.T. Carnall, G.L. Goodman, K. Rajnak, and R.S. Rana, J. Chem. Phys. 90, 3443–3457 (1989).
(9) G. Blasse and B.C. Grabmaier, Luminescent Materials (Springer-Verlag, New York, 1994), p. 26.
(10) J.R. Ferraro, Appl. Spec. 29, 418–421 (1975).
(11) S. Jimenez Sandoval, D. Yang, R.F. Frindt, and J.C. Irwin, Phys. Rev. B 44, 3955–3962 (1991).
(12) T.J. Wieting and J.L. Verble, Phys. Rev. B 3, 4286–4292 (1971).
(13) J.M. Chen and C.S. Wang, Solid State Commun. 14, 857–860 (1974).
(14) S. Sugai and T. Ueda, Phys. Rev. B 26, 6554–6558 (1982).
(15) D.O. Dumcenco, K.Y. Chen, Y.P. Wang, Y.S. Huang, and K.K. Tiong, J. Alloys Compounds 506, 940–943 (2010).
(16) B.C. Windom, W.G. Sawyer, and D.W. Hahn, Tribol. Lett. 42, 301–310 (2011).
(17) Y. Zhao, X. Luo, H. Li, J. Zhang, P.T. Araujo, C.K. Gan, J. Wu, H. Zhang, S.Y. Quek, M.S. Dresselhaus, and Q. Xiong, Nano Lett. 13, 1007–1015 (2013).

« PREVIOUS

Graphene is probably the most well-known of the emerging class of materials known as two-dimensional crystals.

Combined Raman and PL imaging of 2D WS_2

David Tuschel, Raman Applications Scientist - HORIBA Instruments Incorporated, 20 Knightsbridge Road, Piscataway, New Jersey, USA 08854

Abstract

Raman and photoluminescence spectroscopy and imaging are used to examine the spatial variation of the solid state structure and electronic character of two dimensional (2D) WS_2 crystals. Simultaneous acquisition of photoluminescence spectra with the Raman scattering provides complementary ways of rendering Raman and photoluminescence spectral images of thin film WS_2.

Keywords

Raman and photoluminescence spectroscopy, 2D materials, WS_2

Raman and Photoluminescence Imaging of 2D WS_2

Graphene is probably the most well-known of the emerging class of materials known as two-dimensional crystals. These materials are constituted by monolayer to few-layered structures. In recent years, new inorganic two dimensional materials have emerged including MoS_2, $MoSe_2$, WS_2, WSe_2 among others. These materials have attracted significant interest because of special electronic, optical and opto-electronic properties in the monolayer to few-layer forms that are different from those manifest by the bulk form (1, 2). One of the most significant differences of the two-dimensional crystals is the transformation from an indirect band gap semiconductor in the bulk to a direct band gap semiconductor in the monolayer to few-layer crystals. Thus, the fabrication of opto-electronic devices in addition to familiar integrated electronic circuitry is envisioned for these materials. These opto-electronic characteristics have prompted substantial research to discover the means of fabrication and the physical characteristics of two-dimensional crystals to produce integrated electronic and opto-electronic devices (3).

You may have observed the spatially varying colors in reflected white light images of 2D crystals, and so there have been developments to use optical microscopy to rapidly identify the number of molecular layers that make up the two-dimensional crystal (4). Previously, we reported on the use of resonance Raman and photoluminescence spectroscopy and imaging of few-layer MoS_2 to identify spatial variation in the number of layers and strain (5). In this Application Note, we focus on Raman and photoluminescence (PL) imaging for the characterization of 2D WS_2 crystals.

Experiment

The Raman and PL data were acquired with a LabRAM HR Evolution using 532 nm excitation in conjunction with a 300 gr/mm grating and a 50X Olympus objective, and by moving the stage in 1.5 µm increments over an area of approximately 100 µm x 100 µm. The combined Raman and photoluminescence image is actually a rendering of signal strength for the Raman band at 349 cm^{-1} and the photoluminescence band centered at 630 nm as a function of position on the sample.

The triangular crystal consists primarily of a single layer of WS_2 with a three-pronged two-layer formation growing out from the center. The two-layer formation appears as the darker purple structure in the white light image and appears brighter green in the combined Raman and PL spectral image.

Results

Here, we apply Raman and photoluminescence imaging to compare the spectral and structural differences revealed through spectroscopy to the contrast observed when viewing the crystals with reflected white light microscopy. A collection of hyperspectral data from a 2D WS_2 crystal is shown in Figure 1.

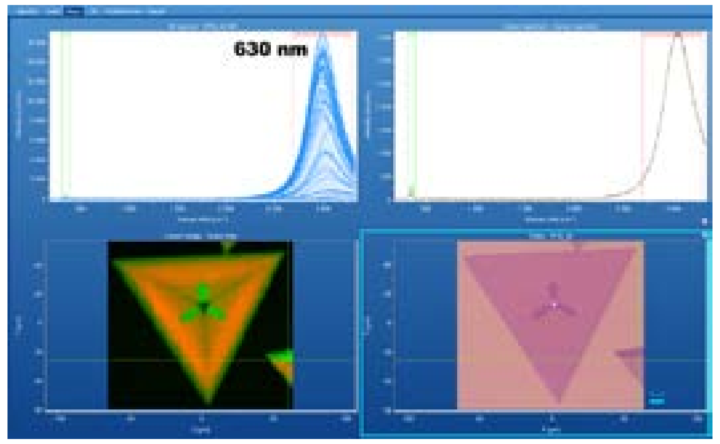

Figure 1: Combined Raman and photoluminescence image (lower left), reflected white light image (lower right), hyperspectral data set (upper left) and cursor spectrum (upper right) of 2D WS_2 crystal.

NEXT »

Combined Raman and PL imaging of 2D WS_2, cont.

A reflected white light image of the crystal appears in the lower right hand corner and a combined Raman and photoluminescence image corresponding to the reflected light image appears to its left. The plot on the upper left consists of all of the Raman and photoluminescence spectra acquired over the image area and the upper right hand plot is of the single spectrum associated with the cross hair location in the Raman and reflected light images.

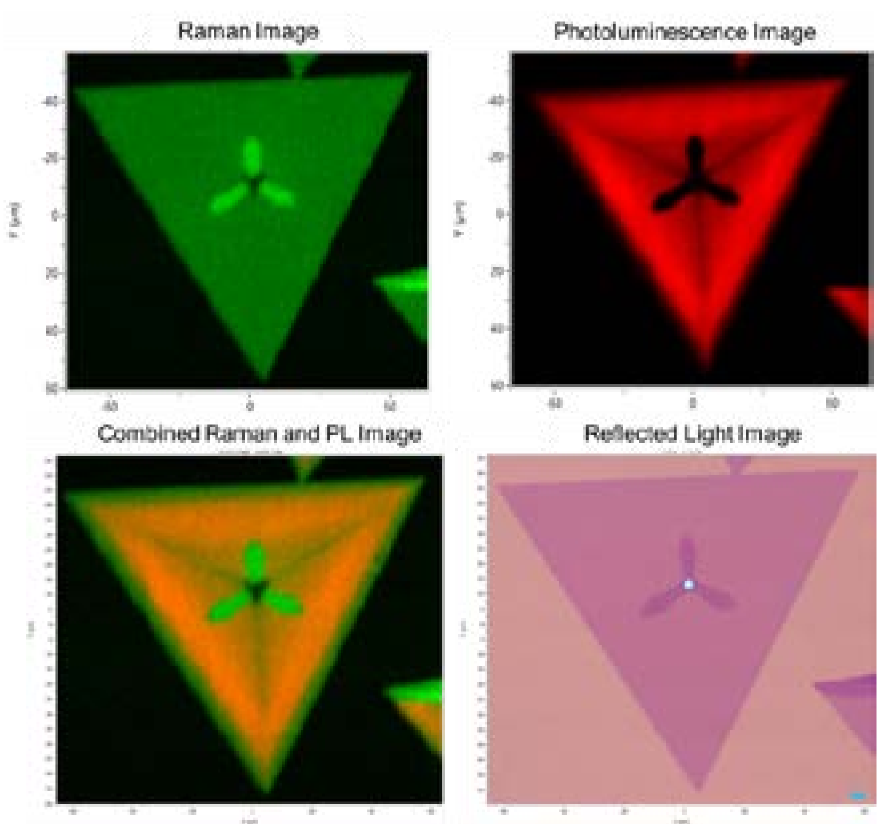

Figure 2: Raman (upper left) and photoluminescence (upper right) images of 2D WS_2. Combined Raman and photoluminescence image (lower left) and reflected white light image of 2D WS_2 (lower right).

In Figure 2, the combined spectral image is rendered through a color coded plot of Raman (green) and photoluminescence (red) signal strength over the corresponding color bracketed Raman shift positions shown in the upper traces. The perimeter of the crystal appears green because of the absence of photoluminescence at that location. The separate Raman and photoluminescence images in Figure 2 show the spatially varying differences in solid state structure, as revealed through vibrational and electronic spectroscopies.

Conclusion

Raman and photoluminescence spectroscopy reveal different aspects of the solid state structure of 2D materials. Raman and photoluminescence imaging performed simultaneously with one instrument reveals the spatial variation of the solid state structure and electronic properties of 2D crystals that is not revealed in reflected white light imaging. That ability should allow materials scientists to better design and fabricate electronic and opto-electronic devices based upon 2D crystals.

The two-layer formation appears brighter in the Raman image and the rest of the crystal appears fairly uniform. However, the photoluminescence image consists of a dark three-fold axis with diminished photoluminescence in the surrounding area. The two-layer formation yields very weak emission. These structural variations are revealed in the combined Raman and photoluminescence of other crystals as shown in Figure 3.

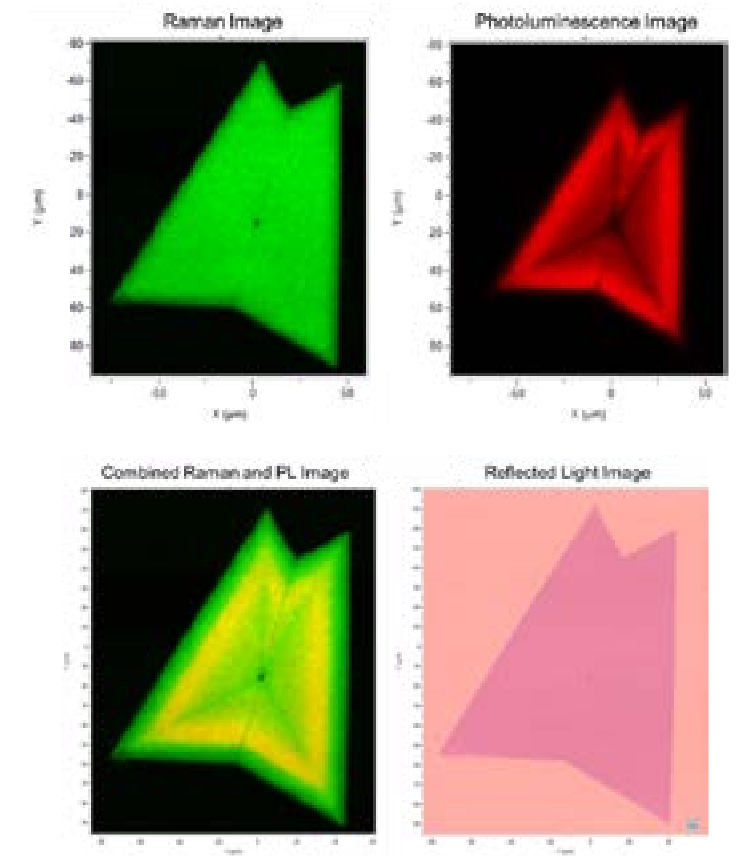

Figure 3: Raman (upper left) and photoluminescence (upper right) images of 2D WS_2. Combined Raman and photoluminescence image (lower left) and reflected white light image of 2D WS_2 (lower right).

References

[1] D. Jariwala, V.K. Sangwan, L.J Lauhon, T.J. Marks and M.C. Hersam, ACS Nano 8, 1102-1120 (2014).
[2] G. Eda and S.A. Maier, ACS Nano 7, 5660-5665 (2013).
[3] R. Ganatra and Q. Zhang, ACS Nano 8, 4074-4099 (2014).
[4] H. Li, J. Wu, X. Huang, G. Lu, J. Yang, X. Lu, Q. Xiong and H. Zhang, ACS Nano 7 10344-10353 (2013).
[5] D. Tuschel, Spectroscopy 30(3), 14-29 (2015).

Ackowledgement

This work was performed in collaboration with Prof. Davood Shahrjerdi and Abdullah Sanad M. Alharbi of New York University.

2D materials combine the strong covalent in-plane bonding with weak van der Waals (vdW) out-of-plane interactions.

Structural characterization of WS_2 flakes by PL and ULF Raman spectroscopy on a unique multimode platform

Thibault Brulé and Céline Eypert - HORIBA FRANCE SAS, Palaiseau, France.

Abstract
2D materials are state-of-the-art in nano- and opto-electronics. Characterizing their structural properties with a non-destructive approach at the micron scale is very important. We demonstrate in this paper how LabRAM Soleil™ confocal Raman multimode microscope is the perfect tool for these materials characterization.

Keywords
Raman microscopy, Ultra-low frequency, Photoluminescence microscopy, Multimode platform, WS_2 flakes.

Introduction

2D materials combine the strong covalent in-plane bonding with weak van der Waals (vdW) out-of-plane interactions. These materials exhibit remarkable thermoelectric, conductive, superconductive, optical, and photovoltaic characteristics, and hold potential for applications in nanoelectronics and opto-electronics devices. Various 2D materials have been explored, including insulators (h-BN), semiconductors (MoS_2, $MoSe_2$, WSe_2), and others.

The characterization of materials is important to identify and explore their structure. Raman spectroscopy is a powerful and non-destructive characterization tool to study 2D materials. It has the capability to characterize the structural properties of 2D materials, as well as detecting the layer thickness, band structures, strain effects, doping type, concentration, electron–phonon coupling, and interlayer coupling.

In this paper, we present an application of hyperspectral micro-spectroscopy for WS_2 nanostructures characterization by both photoluminescence and ultra-low frequency Raman analyses.

Instruments and methods:

Our HORIBA **LabRAM Soleil™** is a Raman multimode microscope offering the highest throughput in the market with no compromise on resolution. This is a consequence of the unique optical design of this microscope based on dielectric mirrors, with very low signal loss, coupled with high quality gratings, our main expertise. These outstanding characteristics are required to obtain the best quality spectra needed for both photoluminescence and ultra-low frequency Raman analyses.

By definition, photoluminescence is the most appropriate technique for band structures characterization at the micron scale. Indeed, the luminescence band of a semiconductor informs directly about the bandgap energy. Furthermore, the Raman analysis very close to the laser line allows a precise characterization of the number of layers of a 2D material. Indeed, specific interlayer vibration modes are excited in this spectral range. Being able to have both spectroscopy techniques, photoluminescence and ultra-low frequency Raman on the same instrument, is an important feature to characterize these materials as much as possible. Thanks to the fully automated modules for photoluminescence (PL) and ultra-low frequency (ULF) available on LabRAM Soleil™, it becomes easy to reach alternatively 5 cm^{-1} frequency and high wavelength range.

NEXT »

Structural characterization of WS_2 flakes by PL and ULF Raman spectroscopy on a unique multimode platform

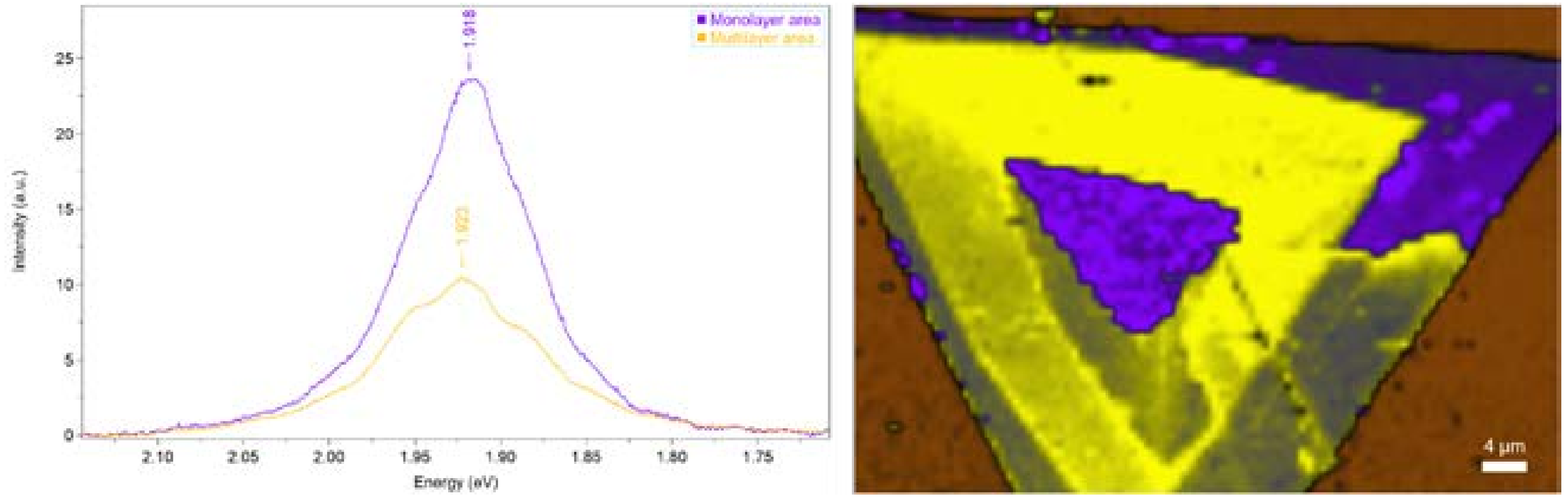

Figure 2: Photoluminescence characterization of the WS_2 flake. (Left) PL reference spectra. (Right) 2D PL map based on decomposition on reference spectra.

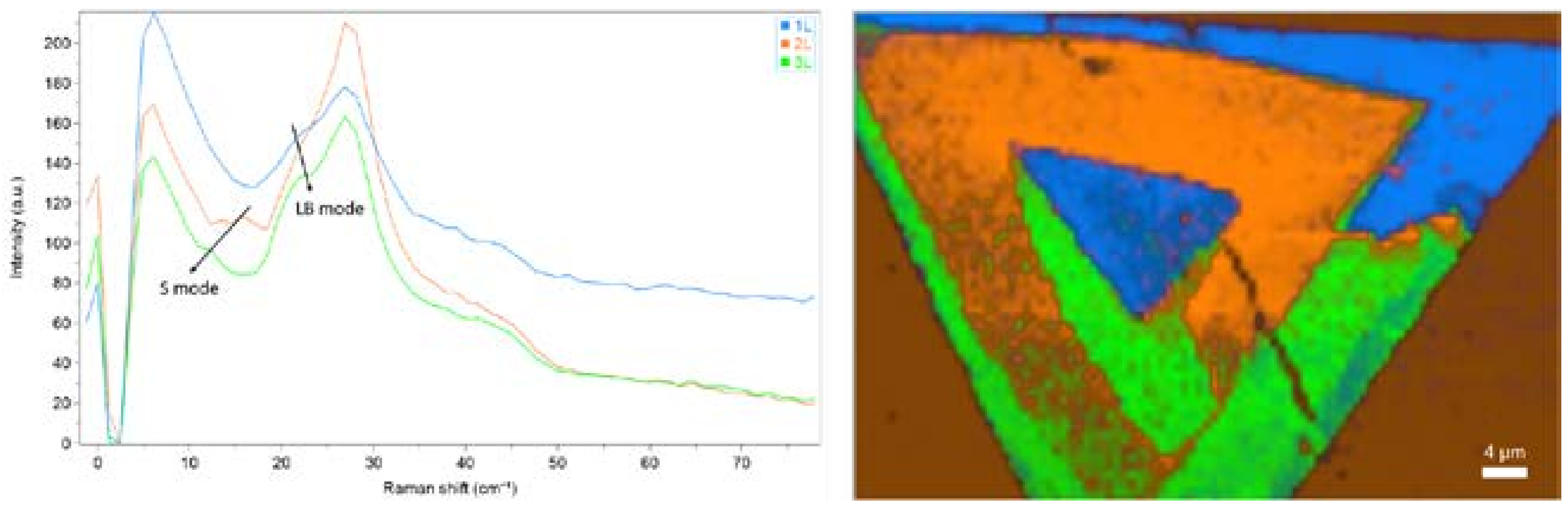

Figure 3: Ultra-low frequency Raman characterization of the WS_2 flake. (Left) ULF reference spectra. (Right) 2D ULF map based on MCR analysis.

Results

First of all, we characterized the band structure of the chosen flake acquiring its PL map. The resulting distribution is presented in Figure 2. Two main areas are observed. They are differentiated by their exciton band positions and intensities. The characteristic spectra shown on Figure 2 for the 2 main areas suggest a monolayer area (purple) and a multilayer area **(yellow)**. Each of them have a specific bandgap energy of respectively 1.918 eV and 1.923 eV.

In order to characterize the exact number of layers and their distribution over the flake, we directly investigated the ULF range of the Raman spectrum. This spectral range is known to present the interlayer modes, expressing the coupling between layers. We acquired a Raman map of the flake focusing on the ULF region, presented in Figure 3. Two interlayer modes are so highlighted. The first one (12-15 cm^{-1}) shifts from higher to lower frequencies, increasing the number of layers. It corresponds to a stretching mode (S mode). The second mode, a lateral bending mode (LB mode), (20-22 cm^{-1}) goes on the other way. Based on these changes of position of modes, we can easily differentiate the number of layers applying a multivariate analysis of all spectra (MCR tool of MVAPlus LabSpec 6 software suite). It results in the colors of the ULF Raman map of the flake (Figure 3). The number of layers are so easily differentiated and localized on the sample at the micro-scale. Comparing with PL map, it confirms that the photoluminescence effect is quenched on multilayer areas, and adds the counting step on the number of layers.

Conclusion

Correlated PL and ULF microscopies enable a precise structural characterization of 2D materials, as demonstrated on this WS_2 sample. Being able to switch from one spectroscopy technique to the other in a mouse click, is a very important point to consider for such an application.

« PREVIOUS

2D materials are defined as crystalline materials consisting of a single unit cell layer of that material.

Correlated TERS, TEPL and SPM measurements of 2D materials

Agnès Tempez[1], Ophélie Lancry[1], Andrey Krayev[2] & Marc Chaigneau - [1]HORIBA France SAS, Palaiseau, France, [2]HORIBA Instruments, Inc. Irvine, CA, USA

Abstract

This application note reports on nano-characterization of 2D transition metal dichalcogenides (TMDCs) materials which are considered of very high potential semiconductors for future nanosized electronic and opto-electronic devices. Scanning probe microscopy (SPM) giving access to the critical topographic and electronic properties at the nanoscale is coupled to photoluminescence (PL) and Raman spectroscopies by means of plasmon enhancement to yield correlated electrical and chemical information down to the nanoscale.

Keywords

AFM-Raman – 2D materials – Transition metal dichalcogenides (TMDCs) – TERS – TEPL – Heterogeneities – Nanomaterials – Opto-electronics – Heterojunctions

Context and issues

2D materials are defined as crystalline materials consisting of a single unit cell layer of that material. Among the large number of potentially stable 2D materials (more than 700), graphene and the family of transition metal dichalcogenides (TMDCs) are under thorough study as candidates for tomorrow's nanoelectronics building blocks. Monolayer TMDCs are tunable band gap semiconductors and complement zero gap graphene. A myriad of nanoelectronics applications are foreseen, ranging from transistors to photodetectors, as well as in the energy field (nanogenerators, green electronics, electrocatalytic hydrogen generation and energy storage).

Many challenges remain before the promise of 2D materials is realized in the form of practical nano-devices, e.g.: (i) understanding growth mechanism of these crystals, to be able to fabricate defect-free large area film; (ii) controlling transfer processes from growth substrates to other substrates; (iii) controlling their vertical or lateral integration. An information-rich, nanoscale characterization technique is required to qualify these materials and assist in the deployment of 2D material-based applications.

Raman and photoluminescence spectroscopies are the techniques of choice to characterize monolayer crystalline materials in terms of electronic behavior (band gap, carrier concentration) and structural quality (defect location and density). Because these conventional spectroscopies are far-field optical techniques (the spot size is diffraction-limited), their applications are restricted to the micro- and macro-worlds. Plasmon-enhanced optical spectroscopies (TEPL: Tip-Enhanced Photoluminescence, TERS: Tip-Enhanced Raman Spectroscopy) bridge the gap to NanoPL and NanoRaman and offer optical nanometric spatial resolution. These new spectroscopic techniques can now be combined with other SPM modes for multi-parameter analysis of 2D materials [1,2]. The work presented in this article opens up new possibilities for the characterization of chemical, opto-electronic, topographic and electronic properties of 2D materials.

Correlated TEPL and SPM of MoS_2 flakes on Au/Si substrate

Molybdenum disulfide (MoS_2) is a promising semiconducting transition metal dichalcogenide 2D material for next generation photovoltaic solar cells, optoelectronic circuits and sensors due to its great excitonic recombination property, high carrier mobility and low leakage current. One of the advantages of two dimensional TMDCs, e.g. with respect to graphene, comes from quantum confinement, enabling the indirect-to-direct band gap transition as a function of number of individual layers. Nano-scale characterization is needed to provide the understanding necessary to engineer nanodevices integrating monolayer MoS_2.

NEXT »

Correlated TERS, TEPL and SPM measurements of 2D materials, cont.

Monolayer MoS_2 has a band gap about 1.8 eV, as revealed by photoluminescence (PL) spectroscopic analysis. The PL spectrum is decomposed in two peaks due to excitonic features: the A_0 mode derived from an exciton consisting of one electron and one hole bound by Coulomb interaction and the A^- mode derived from a trion, a charged three-body exciton consisting of an exciton combined with another electron. It has been reported that the PL intensity decreases with an increasing number of MoS_2 layers and that the PL intensity to Raman intensity ratio is related to the number of layers [3].

Tip-enhanced optical spectroscopies based on the amplification of signal from the nano-region under the SPM tip will allow for actual nano-characterization. In the case of TMDCs, Tip-Enhanced Photoluminescence (TEPL) is capable of revealing variation in emission within a submicron size flake. Complementary morphological, chemical, and electronic structure information may be acquired simultaneously – and with nanometer spatial resolution – through AFM imaging.

TEPL measurements are performed on MoS_2 flakes transferred to a gold-on-silicon substrate using a NanoRaman™ system from HORIBA Scientific integrating an Atomic Force Microscope (AFM) (OmegaScope, based on SmartSPM) and a Raman microscope (XploRA) with a 100× WD objective tilted by 60° with respect to the sample plane. A 638 nm p-polarized laser is focused onto the cantilever-based silver coated TERS tip (OMNI TERS-FM probe). An AFM topography map is first recorded to locate MoS_2 flakes, as well as to provide electrical analysis with KPFM (Kelvin Probe Force Microscopy) giving the contact potential difference (CPD) and capacitance using a silver coated tip in frequency modulation mode (15 nm lift in dual pass setup) (Figure 1).

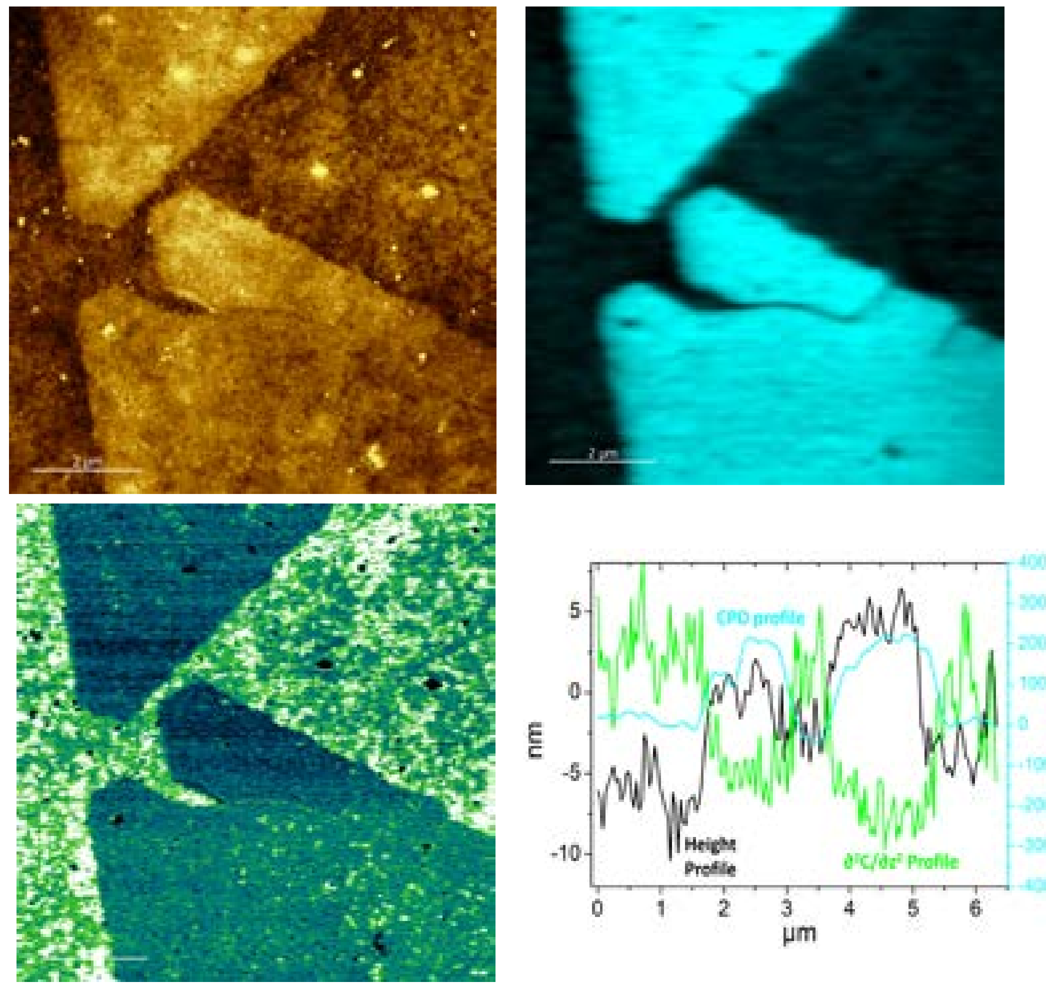

Figure 1: AFM topography, CPD and capacitance measurements on MoS_2 flakes on Au/Si substrate. The lower right graph shows section analysis (topography, CPD and capacitance) along the white arrows displayed on the different AFM images.

Here, as with other 2D materials, it is key to correlate electronic characteristics with nanoscale excitonic and chemical properties provided respectively by TEPL and TERS measurements [3-6]. A PL map of the same two flake apexes (6 × 9 µm (60 × 90 pixels)) is collected with a 100 ms integration time spectrum (640-840 nm) at each pixel (100 nm step). Two PL maps are actually recorded together with topography in a special mode called "Spec-Top™" mode with "dual spec" option: for each pixel (i) one spectrum (sum of the near-field and far-field signals) is acquired with a tip in direct contact with the surface with a typical interaction force of 2-10 nN and (ii) another spectrum is acquired with tip in tapping mode (a few nm away from the sample surface, considered to be the far-field contribution). In between two pixels of the map, the sample moves in semi-contact mode to preserve the sharpness and plasmonic enhancement of the tip.

Two PL maps are shown in Figure 2, the as-acquired far-field PL map ("tip up") and the near-field or true NanoPL map (TEPL) generated upon subtracting the far-field spectrum ("tip up") from the spectrum in contact (far-field + near-field or "tip down") for each pixel.

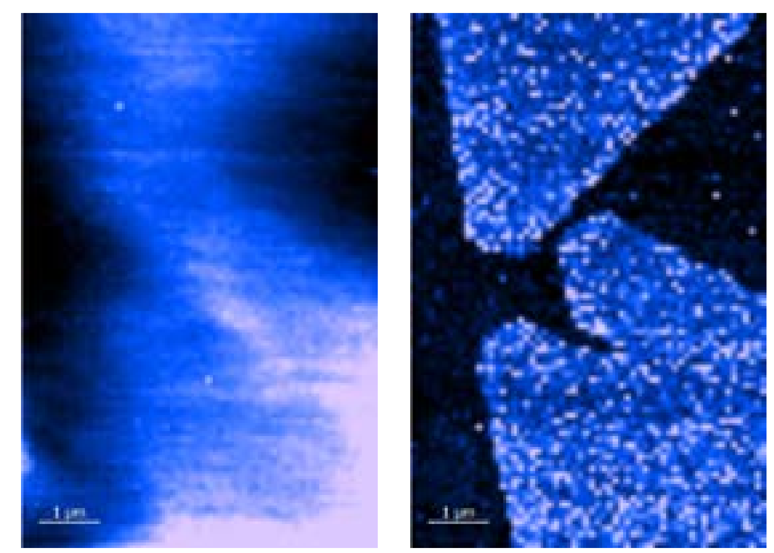

Figure 2: (left) Conventional far-field Photoluminescence map and (right) NanoPL (or TEPL) map of the same MoS_2 flake.

« PREVIOUS

NEXT »

HORIBA Scientific

Correlated TERS, TEPL and SPM measurements of 2D materials, cont.

Both PL images are generated from the integration of a PL band from 640 to 740 nm. The improved spatial resolution in the TEPL image (right) compared with the far-field PL image can be clearly seen: The edges of the flake, indistinguishable in the conventional far-field microPL image, are perfectly defined in the TEPL image. In addition, as shown in the overlay with the topography (Figure 3), edges perfectly match those of the AFM height image. Two spectra are plotted in the graph of Figure 3 from averaging 4-pixels, one from interior of the flake **(red)** and from the substrate **(blue)**. A Gaussian fit gives a peak at 660 nm (1.88 eV) which corresponds to the band gap of monolayer MoS_2. The topography profile indicates an apparent thickness that is much higher (~4-6 nm) than the expected monolayer thickness (0.8 nm), which is likely due to the roughness of the gold surface (RMS = 3 nm) onto which the flake was transferred.

This first example of TEPL on MoS_2 shows that the TEPL method, not limited by diffraction, provides a drastic improvement of the optical resolution compared to far-field photoluminescence (microPL) and is also more accurate than AFM topographic imaging to confirm the presence of monolayer flakes. The next sections of this article will demonstrate how TEPL and TERS are capable of revealing nanoscale heterogeneities impossible to access with conventional optical techniques.

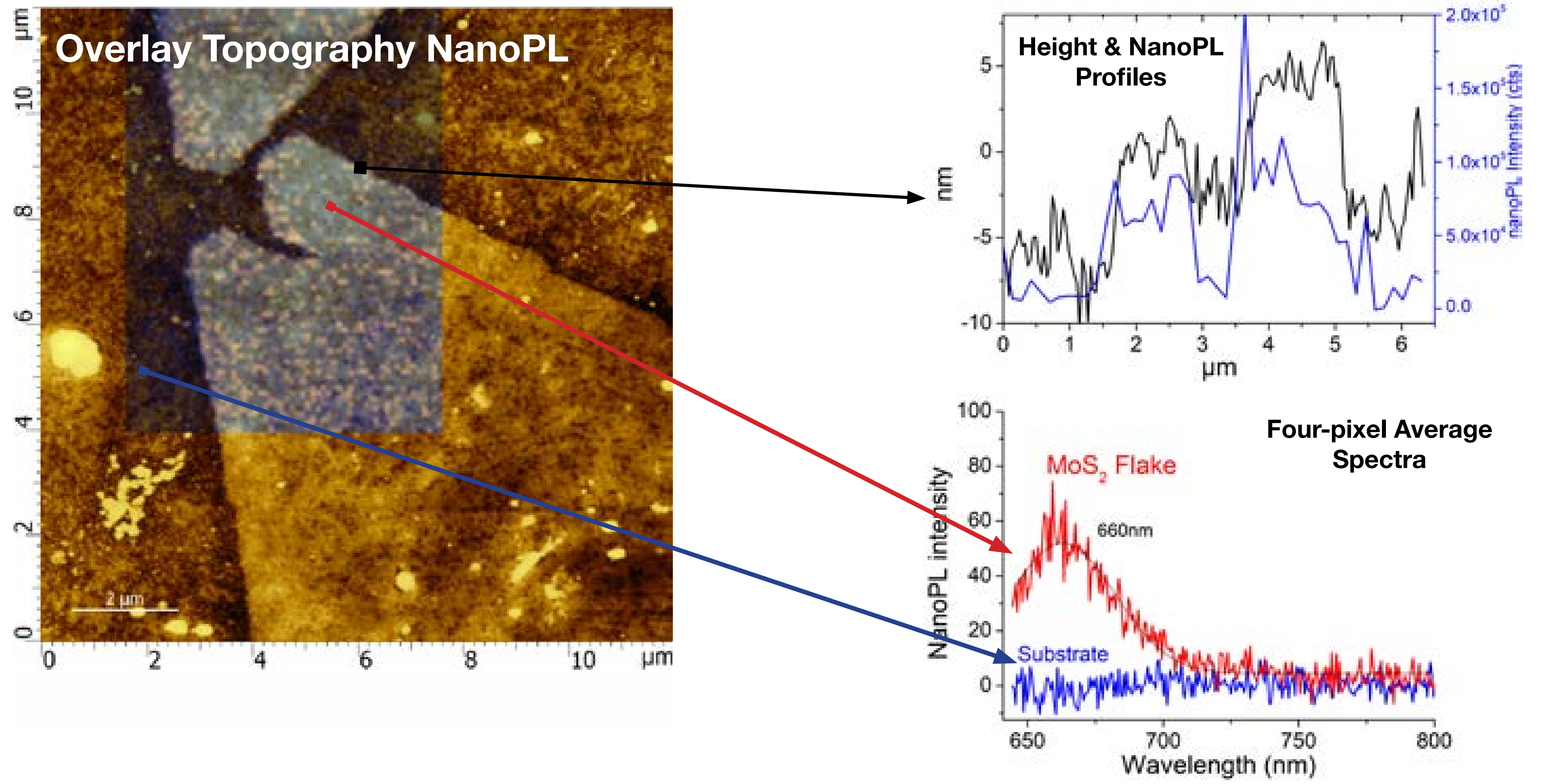

Figure 3: (left) Overlay of the AFM topography and TEPL images of MoS_2 flakes, (top right) AFM height and TEPL section analysis and (lower right) TEPL spectrum from interior of the flake and from the substrate.

Correlated TERS, TEPL and SPM measurements of 2D materials, cont.

TEPL measurements of WS_2 flakes on SiO_2/Si

Tungsten is the largest and heaviest transition metal in the family of common transition metals and in contrast with molybdenum, is more abundant in the Earth's crust, cheaper, and less toxic. Monolayer tungsten disulfide (WS_2) is a direct-gap semiconductor with an energy gap close to 2 eV and high photoluminescence quantum yield (≈ 6%) (higher compared to other 2D semiconductors, e.g. ≈ 0.1% in monolayer MoS_2). It has also exceptional properties such as large spin–orbit coupling (≈ 420 meV), large exciton/trion binding energy, and nonblinking photon emission. The most common stacking structure of WS_2 is 2H, in which the W atoms of a given layer are sitting exactly on top of the S atoms of its neighboring layer.

In this section, correlated AFM and TEPL measurements are performed on WS_2 flakes grown pseudo-epitaxially on a silica on silicon (SiO_2/Si) substrate using a NanoRaman™ system integrating an Atomic Force Microscope (OmegaScope) with a confocal Raman LabRAM HR Evolution microscope. A 532 nm p-polarized laser is focused onto the cantilever-based silver coated TERS tip.

Figure 4. shows AFM topography of a 14 µm triangular flake with 512 lines resolution. Far-field (FF) and near-field + far-field (NF+FF) maps are acquired with 500 ms integration time spectra and steps of 93 nm. PL images are generated from the integration of PL tail from 640 nm to 690 nm. Fig. 4 shows two PL images: The as-acquired far-field, and the near-field or TEPL calculated from subtraction of FF map from NF+FF map. One can observe the higher resolution of the TEPL image with respect to the far-field image.

(i) The contour of the triangular single crystalline flake as well as that of the thicker inner center triangle are much more well defined in the TEPL map than in the far-field image.
(ii) Dark spots of size ranging from 100 nm to 200 nm can clearly be seen in the TEPL map. They are likely to be nanocrystallites visible as bright features of few tens of nm of height in the AFM topography image.
(iii) The PL response non-uniformity on the outer monolayer part of the flake is resolved at the nanoscale, which reveals a lot of inhomogeneities.

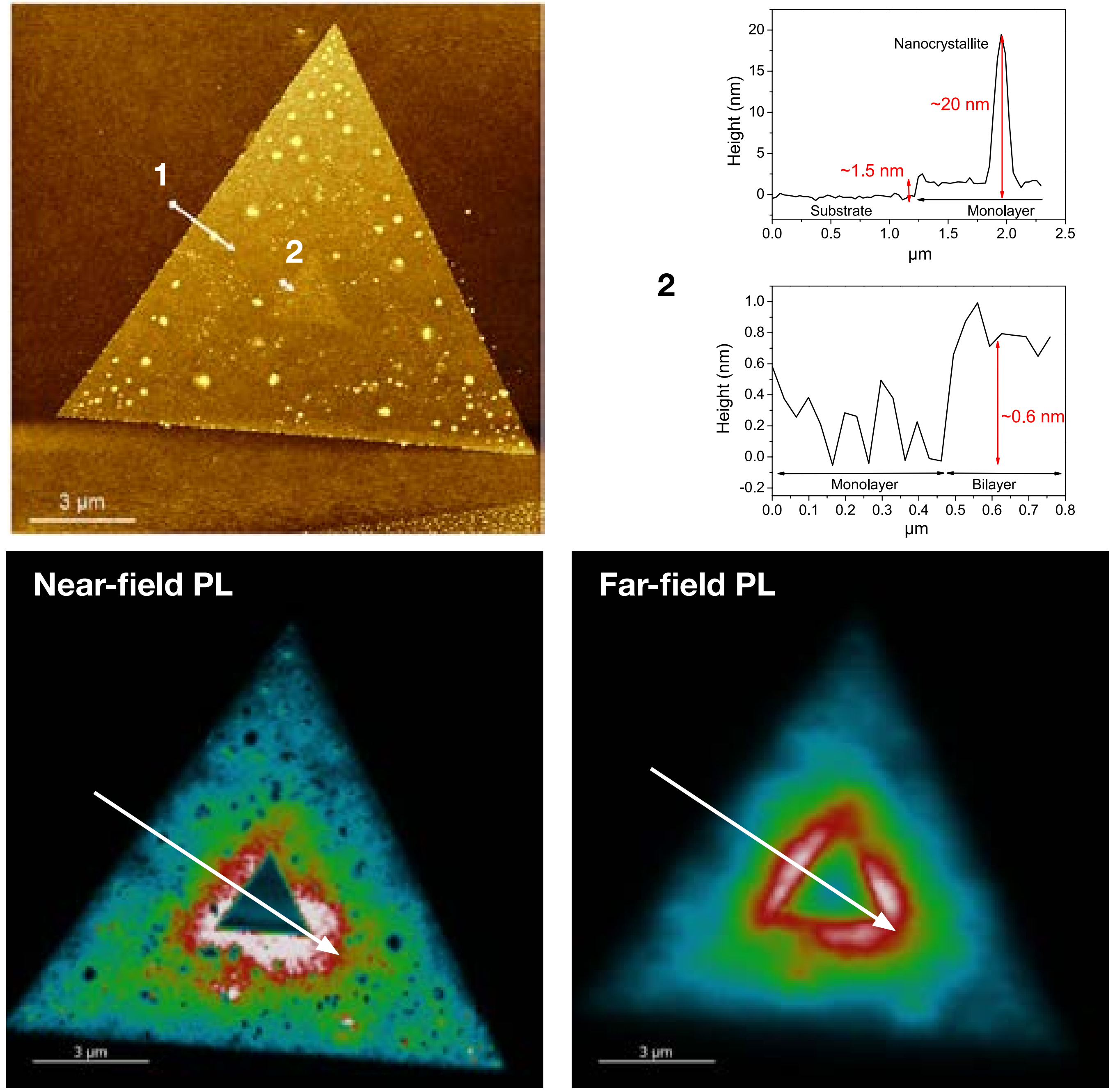

Figure 4: Topography, near-field and far-field PL images of WS_2 flake on SiO_2/Si. The upper right graphs show two section analysis done along the arrows 1 and 2 shown on the AFM topographic image.

Correlated TERS, TEPL and SPM measurements of 2D materials, cont.

This higher resolution is also demonstrated through the comparison of the PL intensity profiles crossing the flake through the inner center triangle showing (Figure 5):

(i) Abrupt rise going from substrate onto the monolayer WS_2 flake in the near-field profile compared to slow rise in the far-field.

(ii) More pronounced dip in the near-field profile when crossing the ~20 nm high nanocrystallite (height profile "1" in Fig. 4) than in the far-field profile.

(iii) More abrupt decrease (higher than one order of magnitude) going from monolayer to bilayer (height profile "2" in Fig. 4 shows a 0.6 nm difference) in the near-field than in the far-field profile.

(iv) A tremendous gain in signal to noise ratio: The dynamics go from 1.5 decades in far-field to more than 5 orders of magnitude in near-field PL.

TEPL reveals deep sub-diffraction limit details within the 2D WS_2 flake that are not resolved in conventional PL measurements [7,8]. Edge effects, nanocrystallites, grain boundaries etc. are seen in the TEPL image with improved signal to noise ratio and vastly improved resolution.

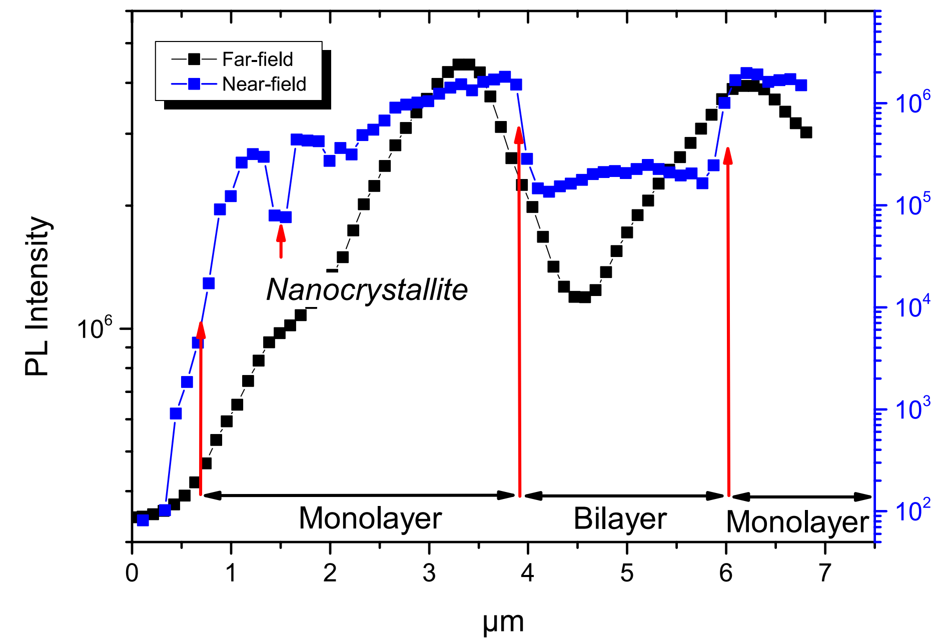

Figure 5: Section analysis of the PL signal in far-field (black) and in near-field (blue) along the arrows represented in Figure 4.

Correlated TEPL and SPM of WSe_2 flakes on SiO_2/Si

As a 2D material, WSe_2 consists in a layer of tungsten atoms sandwiched between two layers of selenium atoms. When the thickness of a WSe_2 crystal is reduced from bulk to monolayer (1L), its energy band transitions from indirect (band gap ~ 1.2 eV) to direct (band gap ~ 1.7 eV). 1L WSe_2 possesses a high exciton binding energy (~790 meV), high PL quantum yield (QY, 10%) and long photoluminescence (PL) lifetime (up to nanoseconds), which are superior to 1L MoS_2 and WS_2. Furthermore, 1L WSe_2 exhibits natural p-type doping, ultra-low thermal conductivity (0.05 W $m^{-1}K^{-1}$) and high carrier mobility (>100 cm^2 $V^{-1}S^{-1}$). This combination of properties makes 1L WSe_2 a promising candidate for novel opto-electronic devices, such as high QY light emitting diodes and quantum light sources. The development and implementation of WSe_2 2D applications require an optical characterization technique on the order of tens of nanometers. Correlated TEPL and SPM provide substantial information related to the nanoscale optical properties of WSe_2 with a resolution down to a few nanometers [9].

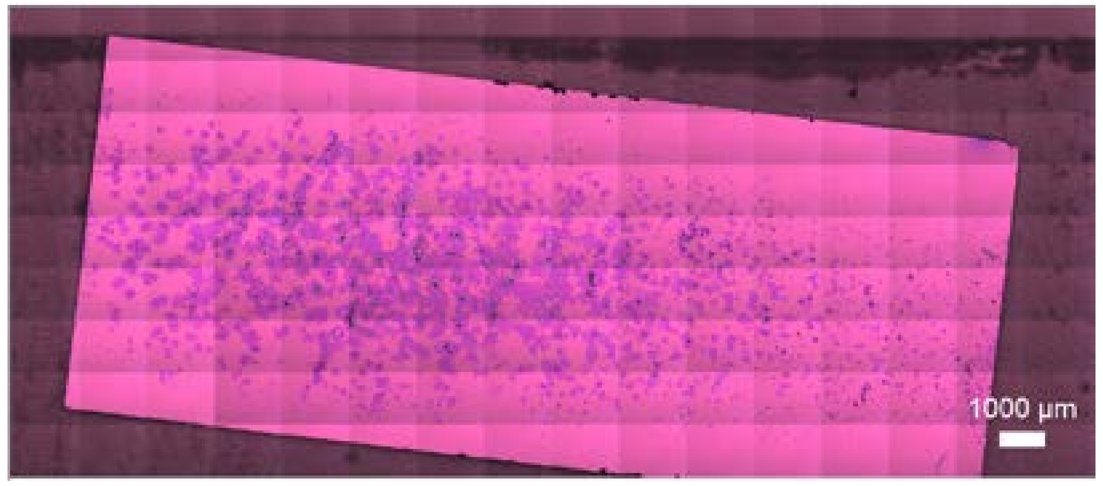

Figure 6a: Optical image of entire sample of WSe_2 on SiO_2/Si obtained with Raman microscope using Mosaic mode.

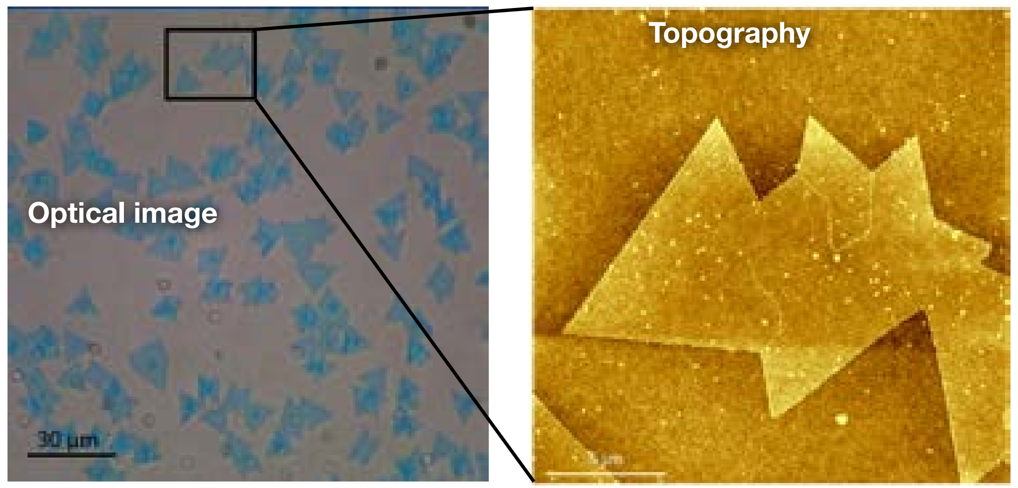

Figure 6b: Optical and AFM topographic images of WSe_2 flake on SiO_2/Si.

Correlated TERS, TEPL and SPM measurements of 2D materials, cont.

The OmegaScope top-view image shows a region of interest, which is then selected for detailed analysis: Several monolayer triangular flakes (clearly observed in a light blue color) that have merged. The corresponding AFM topography image (20×20 μm, 512 lines) shows a fraction of a large polygon flake consisting of several merged triangular flakes with different orientations. The bright spots on the flake are overlying nanocrystallites. On this high-resolution topography AFM image, some grain boundaries (GB) are also discerned.

Two PL maps are acquired corresponding to “near-field + far-field” (NF+FF) and “far-field” (FF) using “Spec-Top^{TM}” mode with “dual spec” option. The acquisition time of each spectrum was 50 ms and pixel size 116 nm. The "dual spec" option gives access to the true TEPL map upon subtraction of FF map from the NF+FF map.

Figure 6c shows the far-field and near-field PL images generated from integration of the PL band from 700 to 800 nm.

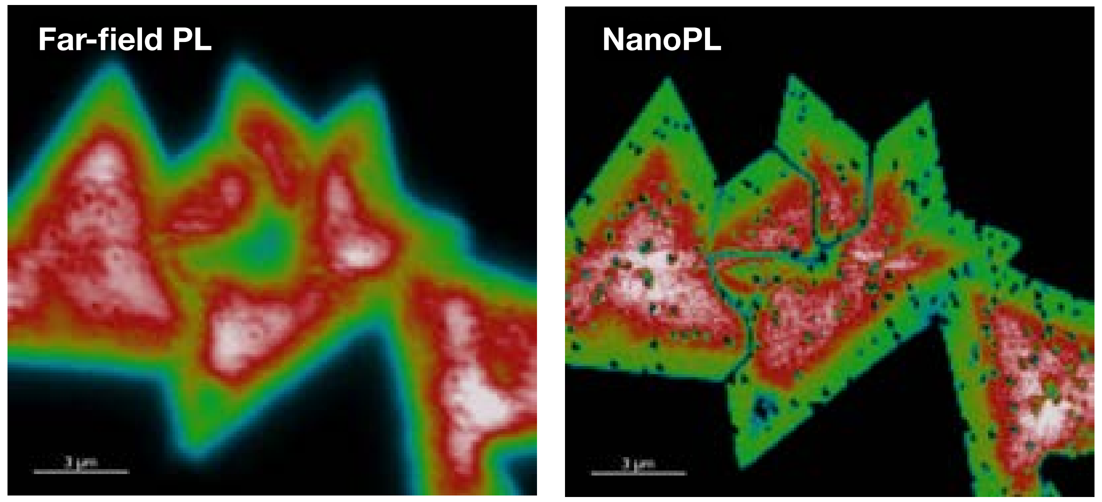

Figure 6c: Conventional far-field PL and TEPL images of WSe_2 flake on SiO_2/Si.

The far-field image with an optical resolution of 550 nm shows some variation of PL intensity over the large 20 μm size polygonal flake with lower PL along the edges and GB than in the center of the flakes. However, this far-field image cannot render nanoscale excitonic variations due to the optical diffraction limit; the higher resolution pure near-field TEPL image reveals much more details (Figure 6c):

(i) Much sharper edges.
(ii) A distinct 800 nm wide lower PL (30% quenching) edge all around the flakes.
(iii) Clearly defined grain boundaries but appearing with different contrast (PL is quenched with different ratio, depending on tilting angle between two merging flakes).
(iv) Dark spots (10% of center flake PL intensity) of size less than 200 nm corresponding to overlying nanocrystallites also observed in the topography image.

Average spectra taken from center and edge areas show TEPL quenching and slight red shift of edge with respect to center (Δ = 17 meV) (see graph in Figure 7). TEPL spectra taken from several nanocrystallites and along a GB exhibit much lower intensity and broader peaks. This TEPL measurement, showing different spectral signatures, reveals a nanoscale excitonic heterogeneity. These opto-electronic properties of WSe_2 can be further studied using the combination of TEPL and Kelvin Probe Force Microscopy (KPFM).

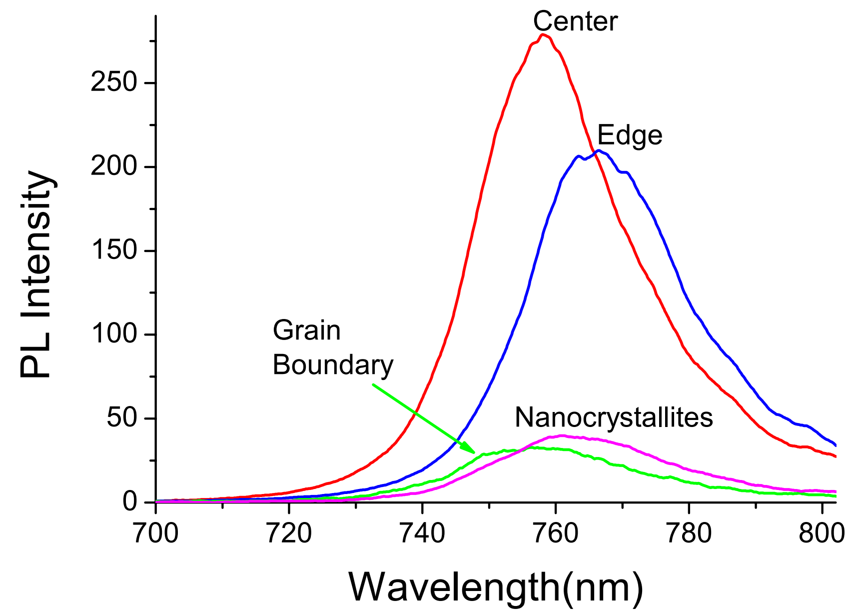

Figure 7: Tip-Enhanced Photoluminescence (TEPL) spectra taken from different locations of the WSe_2 flakes.

In the present example of several WSe_2 flakes merging at different angles, the dependence of the phonon and excitonic processes at the grain boundaries can be observed as a function of tilting angle at the nanoscale, as well as their sensitivity to light.

Frequency modulated Kelvin probe measurements (FM-KPFM) are therefore conducted with the same silver coated tip as the TEPL measurements with the 633 nm laser illumination OFF and ON (Figure 8). The contact potential difference (CPD) and the second derivative of capacitance ($\partial^2C/\partial z^2$) with respect to the tip-sample distance (relative change of capacitance) signals are collected both with and without illumination. In the images, the GB show different CPD and $\partial^2C/\partial z^2$ contrast depending on the angle of intersection.

Correlated TERS, TEPL and SPM measurements of 2D materials, cont.

With no laser illumination, some GB show higher CPD signal than basal plane, while the GB between two flakes rotated by 180° (indicated as twin GB in Figure 8) show lower CPD than basal plane. Under laser illumination, the higher CPD-GB feature even higher CPD while twin GB show slightly higher CPD signal than basal plane. As for the $\partial^2C/\partial z^2$ maps, there is also clear contrast in GB signals depending on the tilting angles.

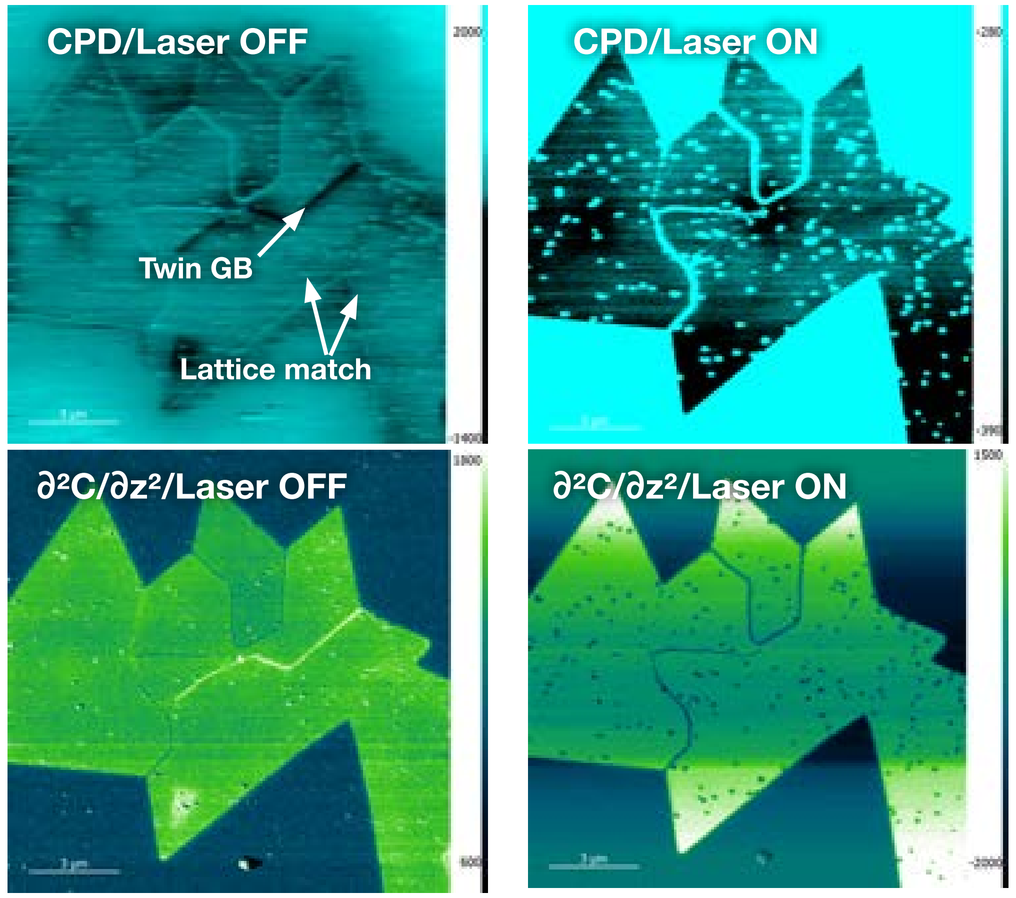

Figure 8: FM-KPFM measurements on the same WSe_2 flake showing contact potential difference (CPD) and the second derivative of capacitance ($\partial^2C/\partial z^2$) under 633 nm laser illumination and without illumination.

The capacitance of twin GB is found to be more sensitive to light than other orientation as they appear clearly under illumination but are not visible in the laser OFF map. These two distinct types of contrast observed in CPD and $\partial^2C/\partial z^2$ maps corresponding to "families" of tilting angles are consistent with the TEPL map also exhibiting GB with different contrast (Figure 6c). This could be linked to different defects density and type, as well as stoichiometry variation. In addition, it is important to note that the absence of GB between the flake in the bottom right of the map and the upper one corresponds to perfect lattice match and coincides with no contrast in CPD, $\partial^2C/\partial z^2$, and PL maps.

Correlated TERS and SPM of WS_2 flakes on template stripped silver

WS_2 flakes are exfoliated on template stripped silver. Topography, phase shift, contact potential difference (CPD), and $\partial^2C/\partial z^2$ are measured with a NanoRaman™ system (HORIBA Scientific) in the dark for 5.5 x 5.5 µm images with 400 lines resolution (Figure 9). Surface potential (CPD) image presented in Figure 9 shows significant inhomogeneities of both the silver substrate and the WS_2 flake. TERS measurements are performed using a 638 nm p-polarized laser focused onto the vicinity of a cantilever-based silver coated TERS tip.

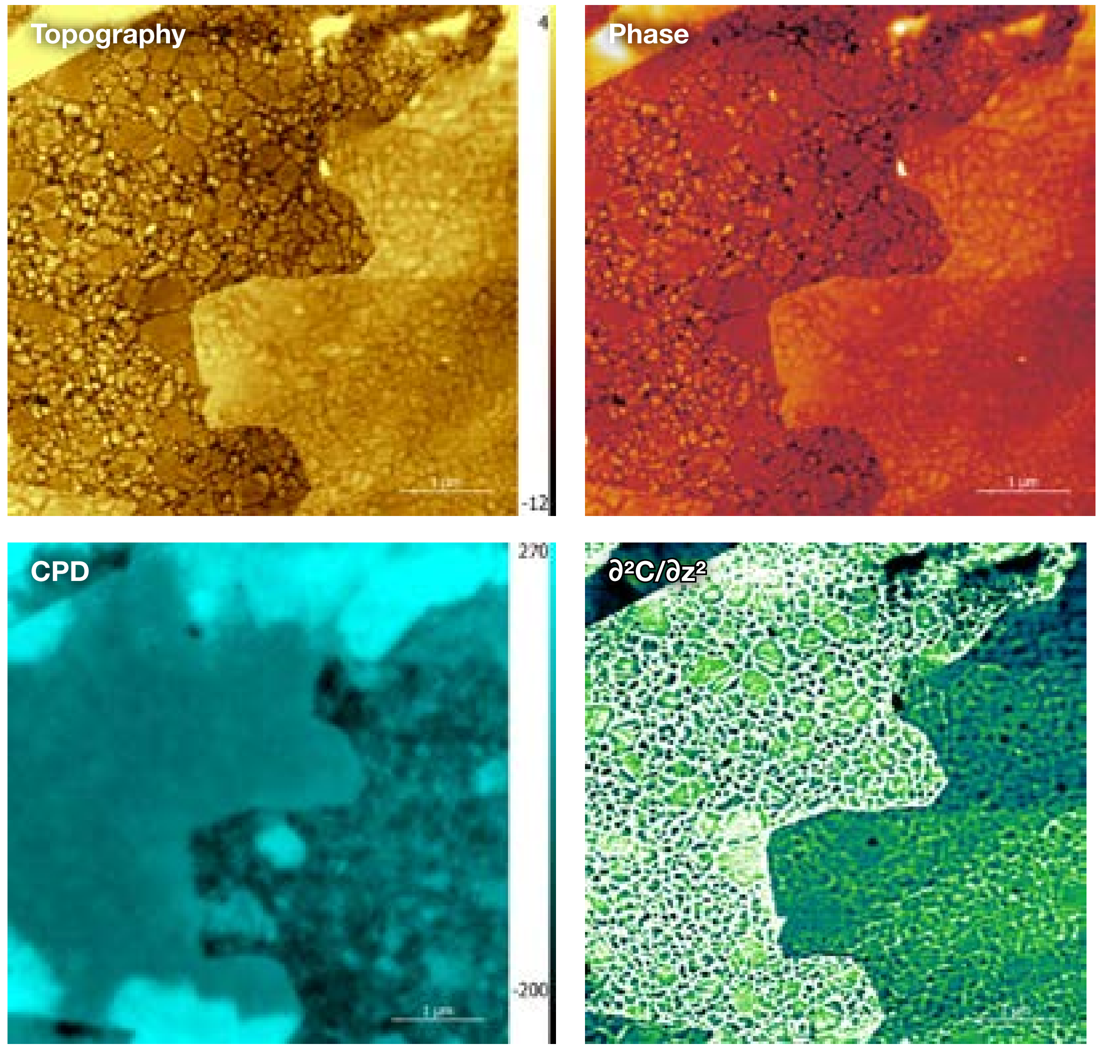

Figure 9: Topography, phase shift, CPD and $\partial^2C/\partial z^2$ measurements of WS_2 flake exfoliated on template stripped silver.

Two Raman maps are acquired corresponding to "near-field + far-field" (NF+FF) and "far-field" (FF) using "Spec-Top™" mode with "dual spec" option. The acquisition time of each spectrum is 150 ms and pixel size is 44 nm.

Correlated TERS, TEPL and SPM measurements of 2D materials, cont.

Two Raman maps are acquired corresponding to "near-field + far-field" (NF+FF) and "far-field" (FF) using "Spec-Top™" mode with "dual spec" option. The acquisition time of each spectrum is 150 ms and pixel size is 44 nm. Figure 10 shows the far-field (conventional µRaman) and near-field (TERS) images generated from the integration of 418 cm^{-1} peak (**in blue**), and the 347 cm^{-1} peak **(in green)** corresponding to the A_{1g} and 2LA(M) bands, respectively. The µRaman image with a diffraction-limited optical resolution features the flake but with blurred contours and a homogeneous distribution of both Raman signal intensities.

In contrast, the higher resolution TERS image reveals much more detail (Figure 10):

(i) Much sharper edges of the flake.
(ii) Inhomogeneities of the Raman signals, in particular of the A_{1g} peak (in blue) with the presence of dark nanodomains.

There are apparent correlations between the features in CPD and TERS images (Figure 9 and Figure 10). This is clearly illustrated with average spectra taken from 3 different areas with **positive** CPD (~ 50 meV **in red**), **negative** CPD (~ -100 meV **in green**), and highly negative CPD (~ -160 meV in blue) which exhibit **low and equal 2LA (M) and A_{1g} peaks**, **high 2LA (M)**, and high A_{1g} peak, respectively. In the areas with lower CPD, locally formed metallic phases suppress the TERS response. These correlations between surface potential (CPD) and TERS signatures indicates the presence of inhomogeneities within interfacial electronic properties, which are attributed to variations in the local doping of the WS_2 flakes [8].

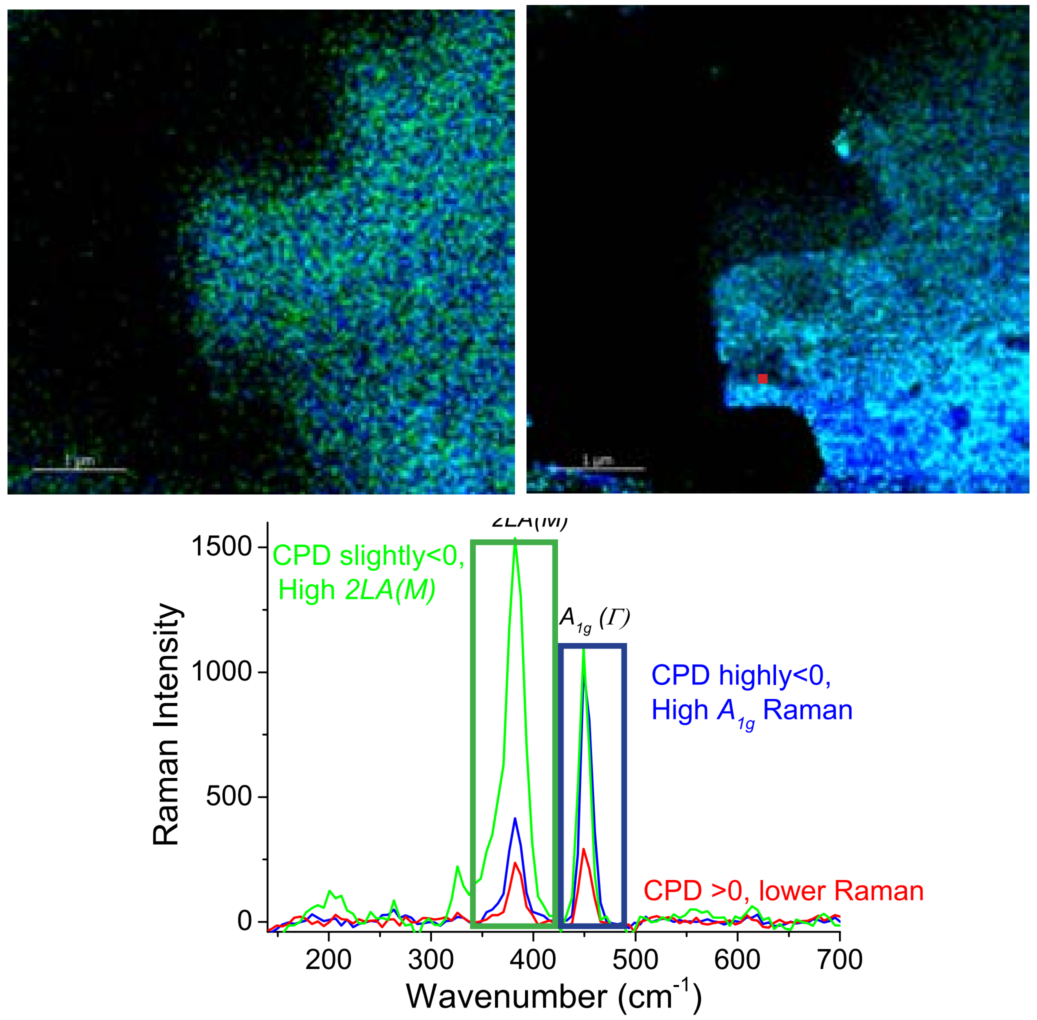

Figure 10: (Top) Conventional µRaman and TERS images of the same of WS_2 flake. (Bottom) Typical TER spectra taken from the square areas in the TERS image.

Correlated TERS and SPM of WSe_2 flakes on Au thin film

The understanding of charge transport and optimization of transistor mobility and current density in the fabrication of TMDCs-based semiconductor devices requires study of semiconductor-insulator interfaces such as with SiO_2/Si. Equally important is the interface between the semiconducting TMDC and the contact metal, as it is the locus of charge carrier injection and collection.

In this case the interface between WSe_2 and gold is probed using scanning probe microscopy (SPM) and TERS. The sample is prepared by mechanical exfoliation of WSe_2 on 120 nm thick gold.

A combination of topography, contact potential difference (CPD), TERS, and photocurrents maps is collected for nanoscale cross-correlations with a NanoRaman™ system (HORIBA Scientific) in a previously described configuration. In the AFM topography image (Figure 11a), flakes with thicknesses in the range of 0.8-3 nm range can be seen, corresponding to 1-4 layers of WSe_2.

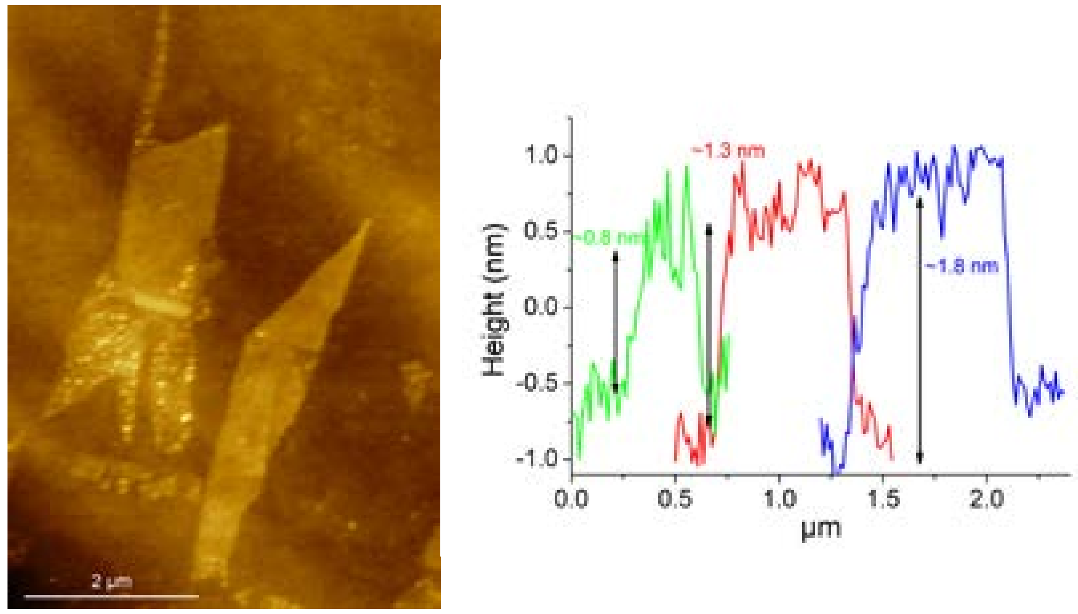

Figure 11a: AFM topography and height profiles of WSe_2 flakes on Au. The different colored profiles correspond to the arrows in the image.

Kelvin probe measurements in frequency modulation (FMKPFM) mode are conducted in the same area. The contact potential difference (CPD) map (Fig. 11b) which gives the distribution of the surface potential across the sample tells us about the change in electronic properties of the material and about the presence of contamination layers. As shown in CPD image, variations in surface can be as high as 150 meV within a flake between adjacent domains.

« PREVIOUS

NEXT »

HORIBA Scientific

Correlated TERS, TEPL and SPM measurements of 2D materials, cont.

The TERS map is also acquired on the same area of the sample in "Spec-Top™" mode. The blue-color map shown here is the intensity response of the large [217-262 cm^{-1}] band centered at 240 cm^{-1}. A striking observation occurs immediately when looking at the CPD and TERS map side by side (Figure 11b, top). The TERS intensity map correlates extremely well with the CPD with high Raman intensity coinciding with higher surface potential, and domains exhibiting low Raman intensity are also areas with lower surface potential. This is nicely illustrated by the graph plotting CPD and Raman intensity profiles on a line with variation of CPD as high as 150 meV and of Raman intensity of a factor 100 (Figure 11b, bottom). Plotting two average TERS spectra from both high (**blue**) and low (**red**) CPD value areas evidences, in the high intensity area (**blue**) the presence of additional Raman peaks (LA(M) at 135 cm^{-1}, A(M) at 240 cm^{-1}, 2LA(M) at 260 cm^{-1} as well as complex peaks at around 375 cm^{-1} and 390 cm^{-1}) as a result of Raman resonant conditions met with the 638 nm excitation laser which overlaps with a broad shoulder on the high energy side of A exciton (1.74 eV; 712 nm). The lower CPD value areas exhibit non-resonant Raman with the single $A_{1g}+E_{2g}$ peak. This correlation featuring nanoscale heterogeneities of the surface potential with matching Raman response is not feasible using conventional confocal Raman microscopy, for which the spatial resolution is limited by diffraction to approximately 400-500 nm at the 638 nm pump wavelength used in our experiments; clearly insufficient to resolve domains 10 nm-100 nm in lateral size.

Complementary measurements of WSe_2 exfoliated on another metal, namely template stripped silver, has shown nanoscale inhomogeneities with similar correlation between Raman and surface potential [9]. In addition, photocurrent measurements at the same nano-resolution confirm the semi-conducting nature of WSe_2 and that surface potential variation most likely results from intrinsic non-uniformity of the WSe_2 crystalline structure. Nanodomains with higher CPD have negative photocurrent and low CPD regions exhibit photocurrent of opposite sign, which can be interpreted as due to nanodomains having complementary doping type.

TEPL of $WS_2/WS_xSe_{1-x}/WSe_2$ heterostructure on SiO_2/Si

Building up nanodevices from 2D layered materials requires heterostructures. The electrical and optical properties of such heterojunctions will depend on the alignment of the energy bands at the interface. Using alloys of transition metal dichalcogenides allows for band gap engineering which is likely to lead to sharp and well controlled interfaces.

TEPL has already been applied to the $MoSe_2$-WSe_2 heterojunction for the study of quantum plasmonic injection and aging effect [10, 11], here we present TEPL data obtained on a lateral single layer $WS_2/WS_xSe_{1-x}/WSe_2$ heterostructure grown on SiO_2/Si.

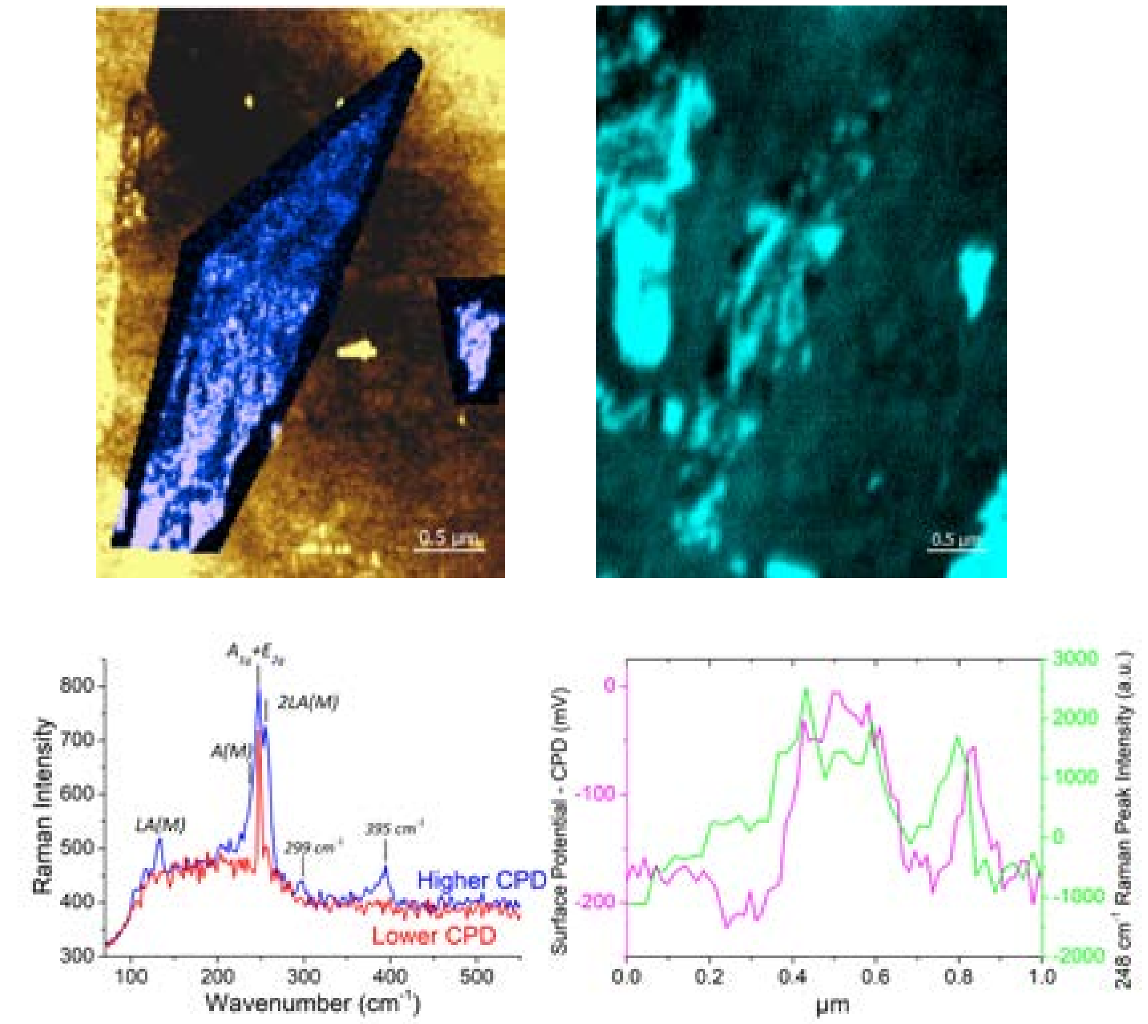

Figure 11b: Contact potential difference (CPD) and TERS images of the same WSe_2 flakes on Au. The different colored profiles correspond to the arrows in the images.

Correlated TERS, TEPL and SPM measurements of 2D materials, cont.

The 10×10 µm AFM topography and phase shift images (512 lines) show the apex of a 60 µm triangular flake with a contrast allowing to distinguish the presence of both binary and ternary alloys (Figure 12). The nicely defined interfaces seen on both images allow the width of the ternary WS_xSe_{1-x} layer to be measured: 700 nm on one side of the flake apex and 350 nm on the other side. The height profile (not shown) across the three materials shows a rise of 0.6 nm from WS_2 to the ternary alloy, no measurable height change from the ternary alloy to the peripheral WSe_2, and a WSe_2 thickness of about 2.5 nm.

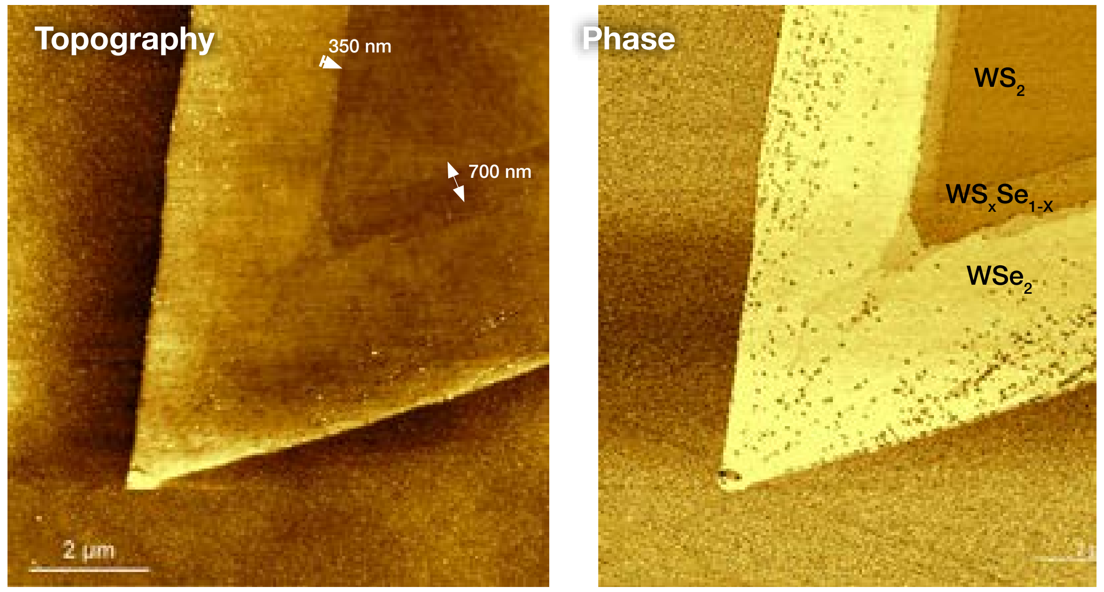

Figure 12: AFM topography and phase images of the 2D heterostructure.

Tip-Enhanced Photoluminescence (TEPL) is performed using a NanoRaman™ system, 532 nm excitation laser and cantilever-based silver coated TERS tips. Two PL maps are acquired on the same run using "Spec-Top™" mode with "dual spec" option. The acquisition time of each spectrum is 50 ms and pixel size is 100 nm. A three color map (Figure 13) including the TEPL response from **WS_2 (peak centered at 625 nm)**, **WS_xSe_{1-x} (peak centered at 665 nm)**, **WSe_2 (peak centered at 765 nm)** confirms the presence of the three single layer compounds, as well as a difference in the WS_xSe_{1-x} PL signal quenched on the left side of the apex (appearing narrower on the height and phase shift images). The graph showing average spectra from the three regions indicates the integration PL response intervals (Figure 13, right).

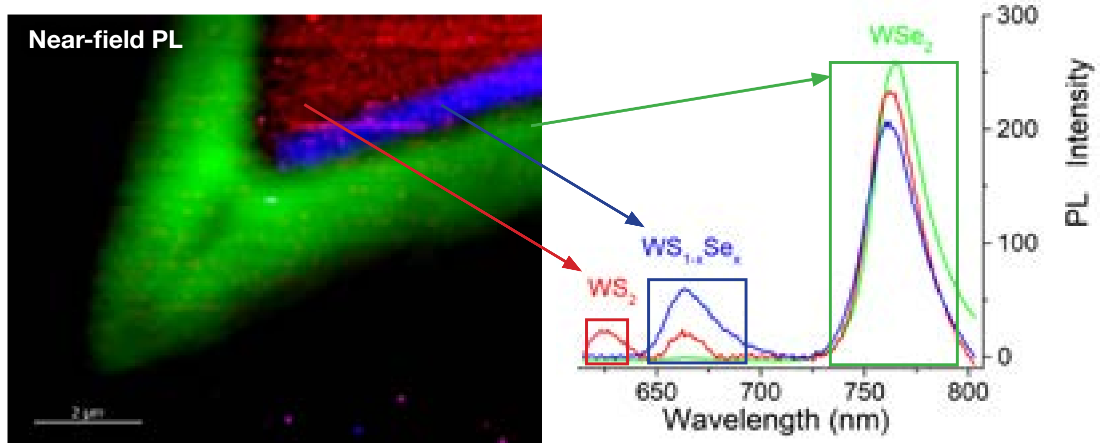

Figure 13: (left) TEPL (aka near-field PL) of the WS_2/WS_xSe_{1-x}/WSe_2 heterostructure on SiO_2/Si, (right) TEPL spectra from different regions of the heterojunction.

Two true TEPL maps (far-field subtracted) are generated for the **WS_xSe_{1-x} PL** and the **WSe_2 PL** responses and are overlaid with an AFM topography map (Figure 14). The **WSe_2 TEPL** map shows some inhomogeneities due to excitonic heterogeneities at the nanoscale, as illustrated by the signal profile (insert in Figure 14). These nanoscale variations could not be seen in the topography and phase shift images. The WS_xSe_{1-x} TEPL map shows an intense ~600 nm wide stripe for the right side alloy and a much less intense and narrower stripe on the left side of the flake apex.

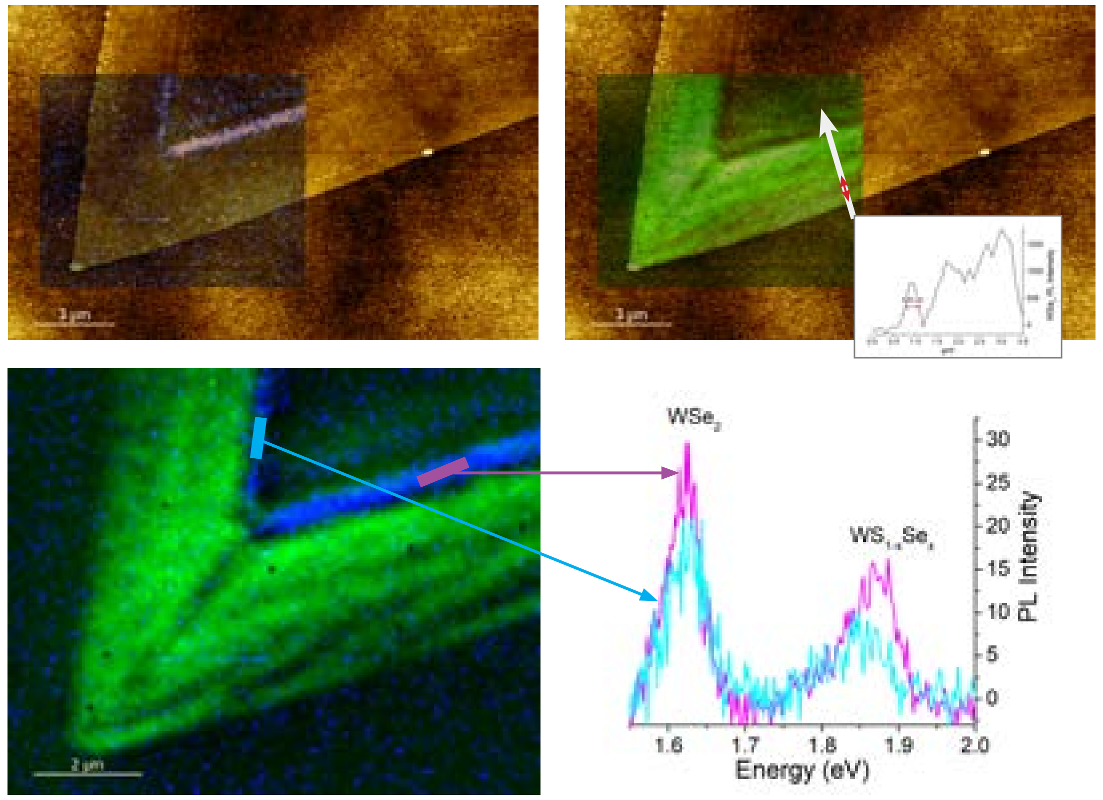

Figure 14: (Top) Overlay of AFM topography with (left) WS_xSe_{1-x} TEPL and (right) WSe_2 TEPL images. (Bottom left) Overlay of WSSe and WSe_2 PL. (Bottom right) Typical spectra from the WSSe regions.

HORIBA Scientific

Correlated TERS, TEPL and SPM measurements of 2D materials, cont.

This correlates well with the first observations from the AFM images. The graph comparing average spectra extracted from both regions gives some further insight with PL response for the left side being shifted to lower energy (1.84 eV versus 1.87 eV for the right side). The observed PL peak shift is associated with the alloying across the interfaces, the observed peak shift can be directly linked to the change in alloy composition.

XploRA Nano

Conclusions

In this application note, we have presented new nano-imaging capabilities with correlated TERS, TEPL and SPM measurements of different 2D materials and heterojunction. We have demonstrated that TEPL, not limited by diffraction, provides a drastic improvement of the optical resolution compared to conventional far-field photoluminescence (microPL) and is also more accurate than AFM topographic imaging to confirm the presence of transferred MoS_2 monolayer flakes. Single crystal WS_2 and WSe_2 flakes directly grown on SiO_2/Si have been also analyzed with TEPL: NanoPL response maps nicely overlay on topography images (monolayer, bilayer, nanocrystallites). Moreover, we have shown the sensitivity of electronic properties (contact potential and capacitance related to Fermi level and charge accumulation) upon light illumination. Beside these semiconductor/dielectric (SiO_2) interfaces, results from probing TMCD/metal interfaces, namely WS_2 on silver and WSe_2 on gold have been also shown. TERS and Kelvin probe measurements revealed nanoscale inhomogeneities both observed in CPD and Raman maps. Finally, NanoPL, together with AFM topography data on a lateral single layer WS_2/$WSxSe_{1-x}$/WSe_2 heterostructure grown on SiO_2/Si, have been presented and revealed nanoscale PL response variations beyond the smooth nano-resolution topography.

References

[1] Nature Communications 9, 2891 (2018).
[2] ACS Appl. Nano Mater. 1 (2), 572 (2018).
[3] Nanoscale 10, 14055 (2018).
[4] Nanoscale 10, 2755 (2018).
[5] Nano Lett.17 (10), 6027 (2017).
[6] Phys. Rev. B 97, 085305 (2018).
[7] 2D Mater. 4, 021024 (2017).
[8] Sci. Adv. 5:eaau8763 (2019).
[9] 2D Mater. 5 035003 (2018).
[10] Phys. Rev. B 98, 041402(R) (2018).
[11] Opt. Mater. Express 9, 1620 (2019).

Acknowledgments

We thank Eddy Robinson for the manuscript correction. We thank Thomas Carlier for help in data processing. We thank all the R&D team (Alexey Belyayev, Dmitry Evplov, Vasily Gavrilyuk, Sergey Katsur, Alexander Yagovkin, Yury Turlapov, Maxim Eremin, Sergey Kostromin, Patrick Hsia, Philippe de Bettignies) for the development and the support.

Laser Raman microspectroscopy is a standard analytical technique in many gemmological laboratories.

Raman Diffusion and Photoluminescence Analysis for Coloured Diamond Investigation

Laser Raman microspectroscopy is a standard analytical technique in many gemmological laboratories. Such spectrometers can also be used to investigate luminescence emissions.

The set of analyzed diamonds consists of gemstones naturally coloured or colour enhanced by means of a specific treatment (heating, irradiation…). The aim of the following investigation is to determine if the photoluminescence (PL) generated by a UV excitation of these diamonds leads to significant differences depending on the technique used to colour the gemstones. Indeed, routine characterizations based on photoluminescence analysis already allow us to determine if the diamond is originally colourless or has undergone a decolourisation treatment (High Pressure High Temperature –HPHT- treatment) [1].

Photoluminescence analyses may also help to confirm that the colour of a diamond has been enhanced by an appropriate processing. The study initiated here tries to evidence the treatments (irradiation, annealing [3]) that the diamond could have undergone to look more intensely coloured.

Experimental and technical aspects

1. Experimental Set-Up

The LabRAM HR UV-Vis is an integrated and compact 800 mm focal length Raman system equipped with an internal He-Ne laser of 17mW at 632.8 nm. An external entry is also available to provide the system - in the present case - with the 325 nm line of an Helium-Cadmium laser.

The spectral range investigated in those experiments covers a wide domain from 388 nm to 780 nm to collect both Raman diffusion and Photoluminescence emission.

2. Measurement Conditions

Measurements were undertaken at room temperature and at -100°C for each diamond. Indeed, luminescence bands are significantly sharpened when cooling at -100°C. Therefore the structure of the luminescence emission and its intensity are easier to determine and tendencies can be pointed out that can be assigned to colour centers in diamond crystallographic structure.

The colour centers in the diamond structure are due to vacancies and Nitrogen atoms and are classified under diamond type (Ib, IaA, IaB) and defect centers (N3, H3, H4, N-V) [2]. The samples are easily cooled down thanks to a temperature-monitored stage.

Results

PL spectra of native brown and yellow diamonds were recorded and compared to PL spectra of corresponding colour-enhanced diamonds. PL spectra of artificial violet and green diamonds were also investigated.

1. Temperature effect on photoluminescence (PL) spectra

The first spectrum reported (Figure 1) includes the Diamond Raman band located at 340 nm (1332 cm^{-1}) and luminescence bands between 400 nm and 650 nm.

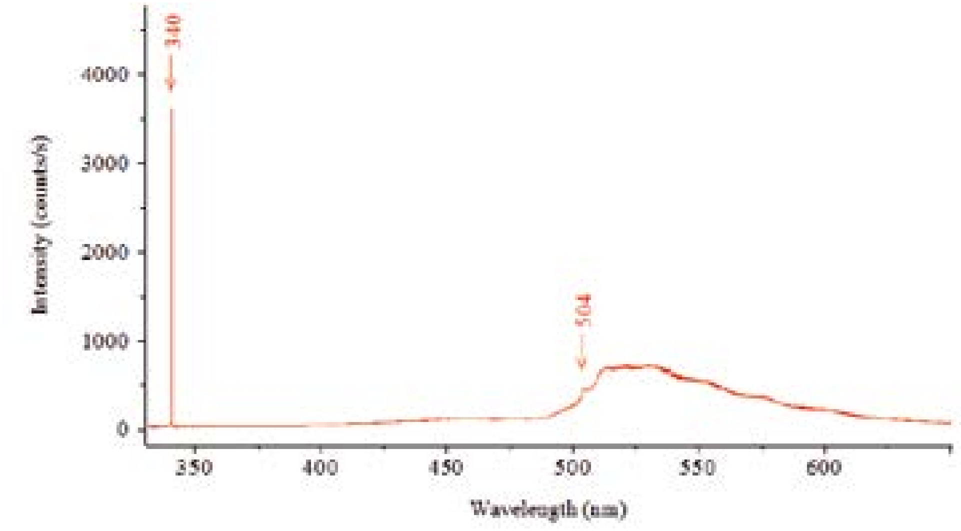

Figure 1: Full spectrum of the natural brown diamond.

NEXT »

Raman Diffusion and Photoluminescence Analysis for Coloured Diamond Investigation, cont.

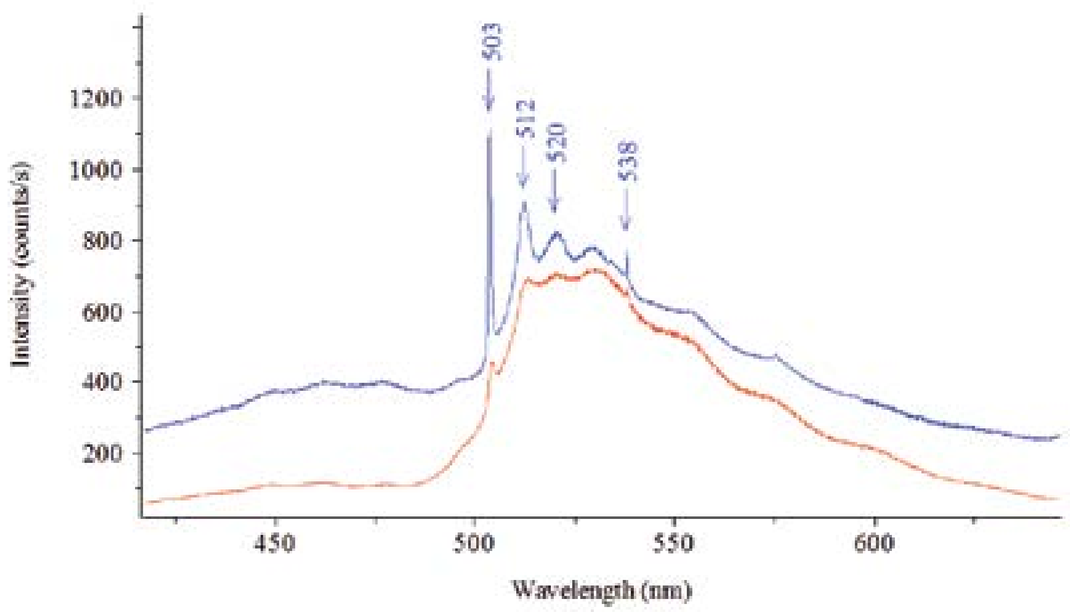

Figure 2: Photoluminescence bands of the natural brown diamond at room temperature (a) and at -100°C (b).

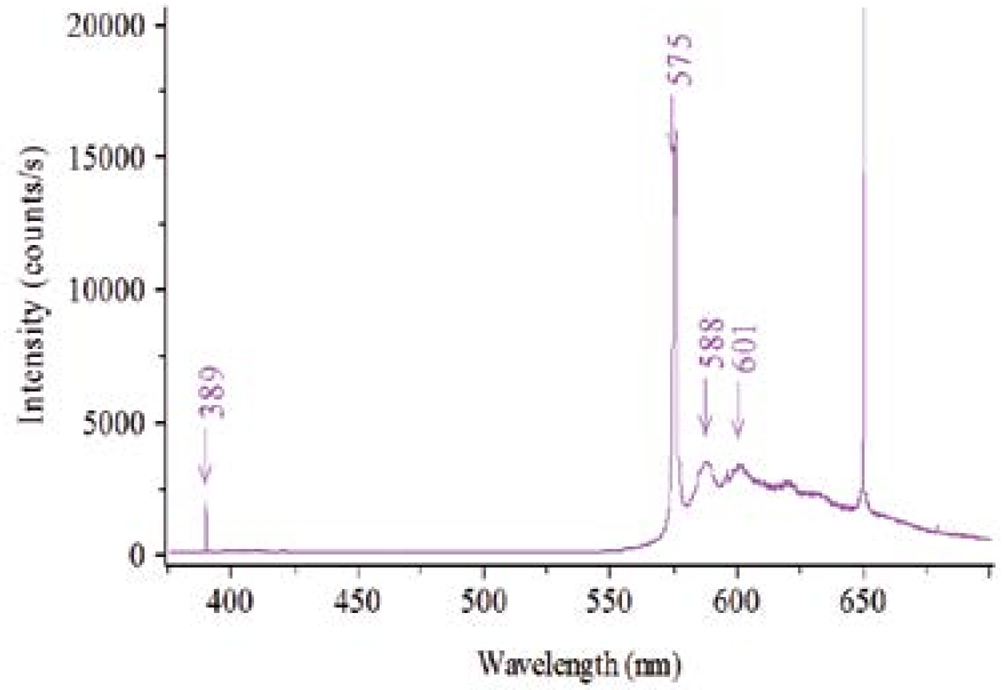

Figure 3: Spectra of the natural and treated brown diamonds at -100°C.

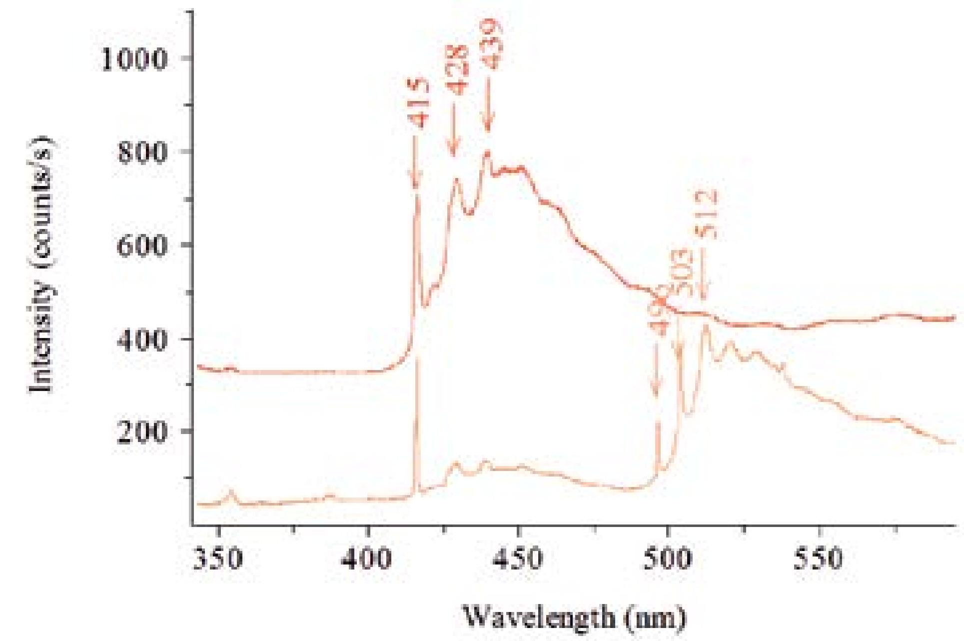

Figure 4: Photoluminescence bands of the natural and irradiated yellow diamonds at -100°C.

We can clearly see in Figure 2 that lowering the temperature sharpena and intensifies luminescence emission.

2. Untreated / treated & annealed brown diamond

The photoluminescence spectrum of the treated and annealed brown diamond shows new bands at 415 nm, 496 nm and 503 nm that are assigned respectively to N3, H3 and H4 systems. Those systems may be generated by the treatment and annealing of the natural brown diamond. In the range 400 nm-450 nm, the spectrum is modified with a new peak at 415 nm.

So, the photoluminescence, emitted around 400-450 nm, is able to give a characteristic signature of the specific treatment to turn the diamond browner.

3. Untreated / irradiated & annealed yellow diamonds

Usually native yellow diamonds owe their colour to the presence of the N3 system. And so we observe that the luminescence emission spectrum of the native yellow diamond exhibits a band at 415 nm, characteristic of the N3 system.

The PL emission spectrum of the irradiated and annealed yellow diamond displays other features at 496 nm (H3) and at 503 nm (H4). With these latter PL bands, the specific treatment to enhance the colouration of a yellow diamond is proved to be identifiable, thanks to a Raman spectrometer.

Raman Diffusion and Photoluminescence Analysis for Coloured Diamond Investigation, cont.

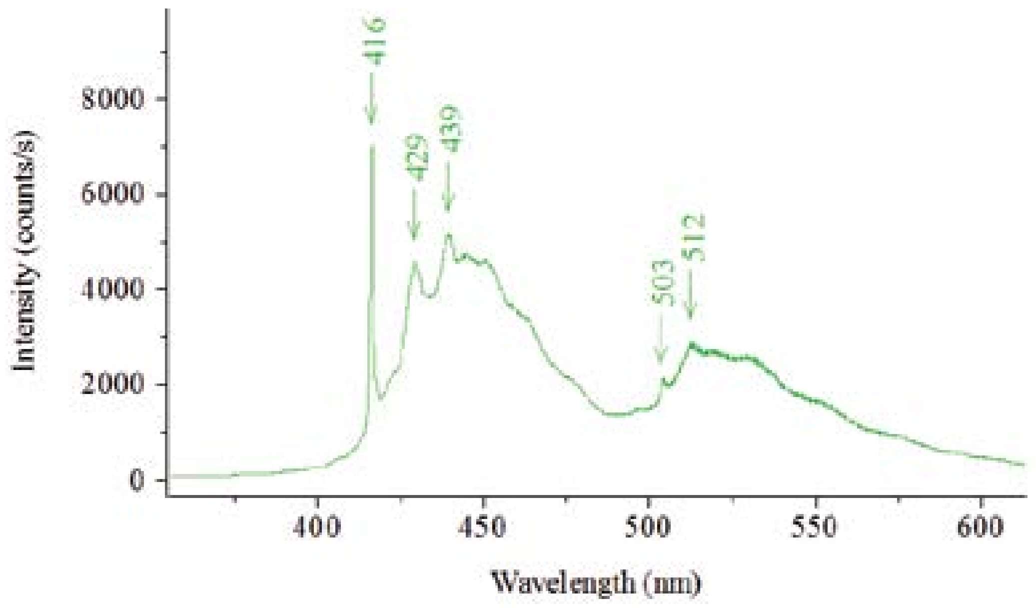

Figure 5: Photoluminescence bands of the treated green diamond at room temperature.

4. Treated green diamond

The treated green gemstone exhibits features relative to H3, N3 systems.

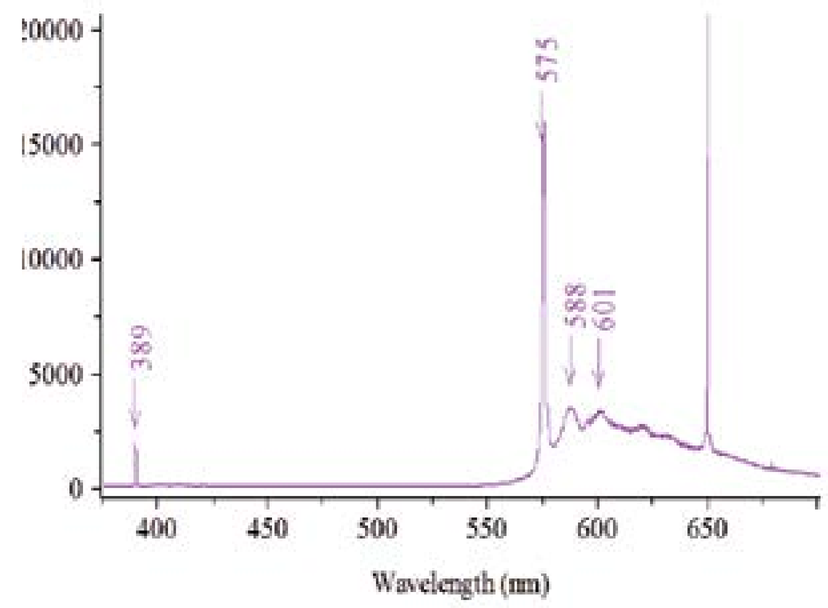

Figure 6: Photoluminescence bands of the irradiated violet diamond at -100°C.

5. Irradiated violet diamond

The irradiated violet diamond PL spectrum exhibits very particular features at high wavelengths. These are characteristic of N-V centers [2].

Conclusion

The colour enhancement treatment on native brown and yellow diamonds can be highlighted by photoluminescence analyses performed with the Raman spectrometer, LabRAM HR. The PL signature of green and violet diamonds has also been recorded. The defect centers responsible of the colour of the diamonds have all been detected and assigned. This proves the Raman spectrometer to be a very good tool to investigate the fine defects in the diamond structure by photoluminescence analysis.

References

1- Spectroscopic evidence of the GE POL HPHT-Treated Natural Type IIa Diamonds. David Fisher and Raymond A. Spits, Gem & Gemology. pp 42-49, Spring 2000.

2- GE POL Diamonds: Before and After. Christopher O. Smith, George Bosshart, Johann Ponahlo, Vera M.F. Hammer, Helmut Klapper and Karl Schmetzer. Gem & Gemology. pp 192-205, Fall 2000.

3- Des Diamants Bien Traités, Emmanuel Fritsch, James Shigley, Pour la Science (French edition of Scientific American) pp 78-83, special issue April-June 2002.

The MicOS is a specially-built instrument that places an emphasis on spectroscopy in its design considerations.

The MicOS microscope spectrometer

HORIBA Scientific's MicOS (Figure 1) microscope spectrometer is a versatile instrument designed and optimized specifically for spectroscopy using a direct-coupled microscope. Such streamlining is required because this field traditionally has been served by a coupling between a standard imaging microscope and a spectrometer. This combination, in many cases, has proven to be sub-optimal for spectroscopy. For one, the design considerations that often make a microscope very good for imaging (aberration-correction using glass optics) often prove to be a hindrance for spectroscopy, especially in the UV and IR regions of the spectrum. This hindrance is not only undesirable from a spectroscopic point of view, but also can be expensive. Furthermore, the coupling between the microscope and the spectrometer is often implemented using optical fibers, which is not optimal, for fibers can have significant losses in transmission and coupling for some regions of the spectrum. Not least is the fact that many traditional microscopes do not offer an easy method to couple an excitation laser while maintaining a port for vision, or the flexibility to accommodate different configurations for measuring samples.

The MicOS is a specially-built instrument that places an emphasis on spectroscopy in its design considerations. It offers a direct-coupled microscope with more than a ten-fold improvement in optical throughput compared to some fiber-coupled systems. It offers the flexibility to couple different laser excitation wavelengths without the need for factory- or field-servicing. The MicOS also provides the flexibility to measure the sample in different configurations: down-looking for flat samples such as wafers, and side-looking for such samples such as facet-emitting diodes or samples in upright cryostats.

In this application note, we provide examples of how the MicOS can advance your micro-luminescence research.

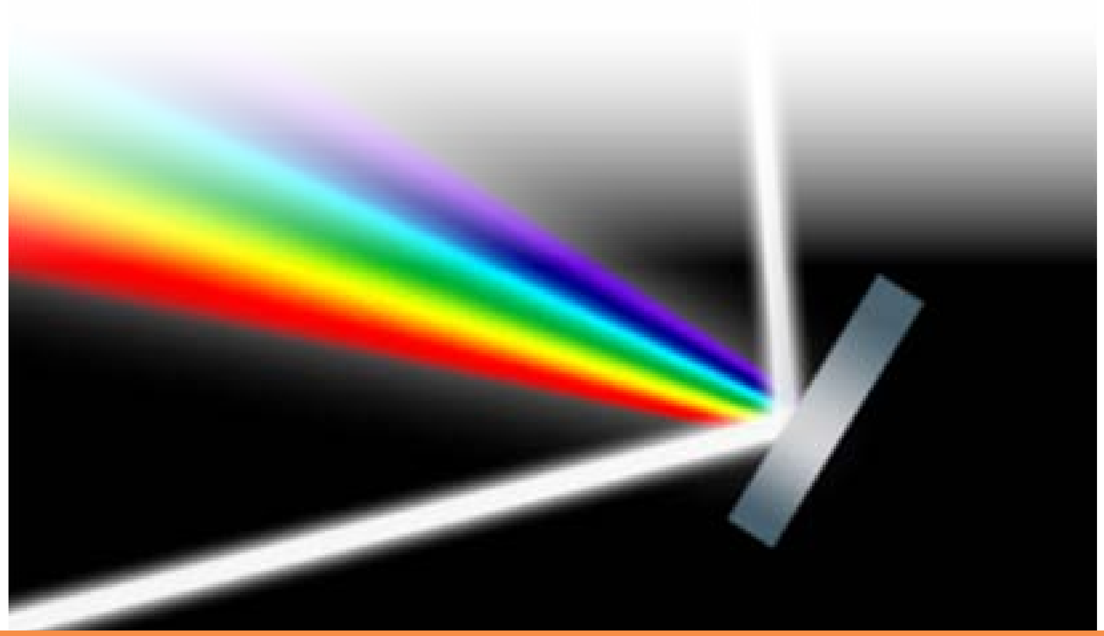

Figure 1: MicOS microscope spectrometer from HORIBA Scientific.

The MicOS microscope spectrometer, cont.

Examples

The first example shows how the MicOS may be used to study luminescence of III-V semiconductor materials. GaN and related alloys are important materials used to build short-wavelength light sources (lasers and LEDs). Room- and low-temperature photoluminescence (PL) are used to characterize these materials, as well as device performance. These samples usually consist of micrometer-sized structures requiring selective laser-excitation in order to observe the PL emission. Selective excitation means fine control of laser-excitation beam size and positioning, as well as ability to see the sample under measurement.[1] In addition, for many such measurements, important electronic structure information can only be revealed at low temperatures. Therefore a PL measurement system must also be compatible with a cryostat. Figure 2 shows a typical configuration of a HORIBA MicOS measurement system, and Figure 3, the resultant PL spectra.[2] The MicOS also has the flexibility to accommodate different user-selectable excitation laser wavelengths for III-V material excitation, and includes vision so that the user can readily see excitation position and areas of interest on the sample.

References
1. J. Korean Phys. Soc., 58(6) June 2011, 1660–1663.
2. Proprietary—semiconductor manufacturer.

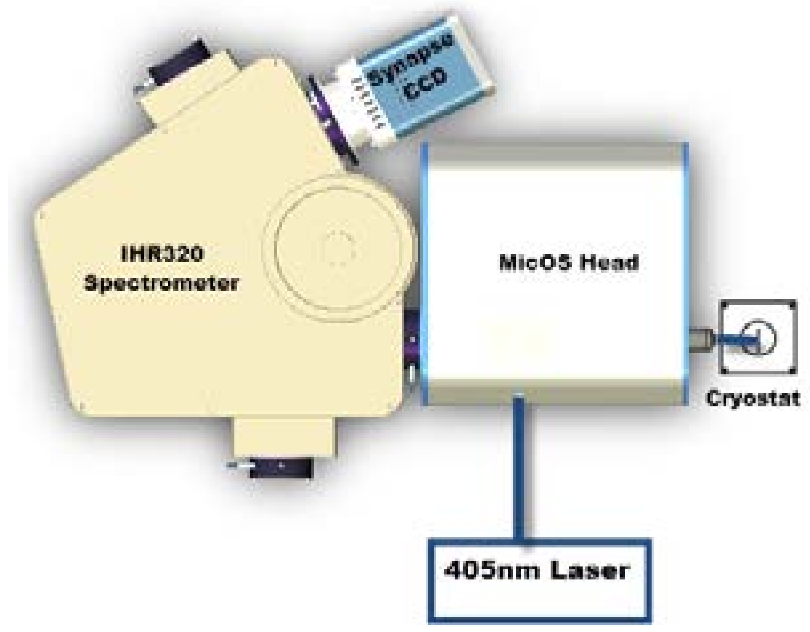

Figure 2: Typical low-temperature, direct-coupled micro-PL setup. Direct coupling of the microscope's front end increases throughput to the spectrometer (for low-light samples). The system also has flexibility to measure a sample via the side window of an upright cryostat or in a down-looking configuration.

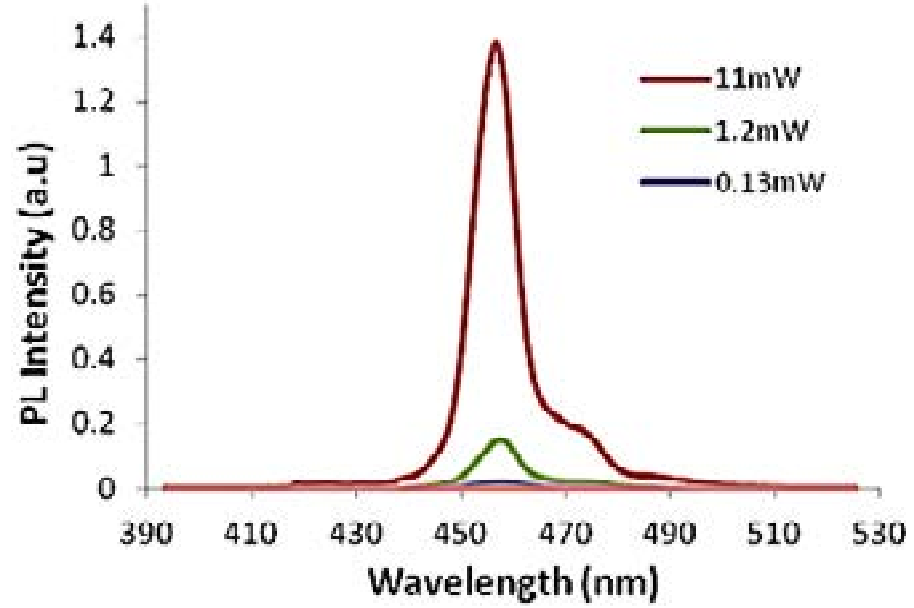

Figure 3: GaInN PL spectrum taken at 10 K after 405 nm laser-excitation at different excitation power-levels.

For the second example, we use the MicOS to observe electroluminescence from a micro-LED (Fig. 4). The MicOS is particularly well-suited to this type of measurement because it allows measurement in a down-looking configuration with long working distance objectives, for samples such as VCSELs, in which the user may need to introduce probe pins under the objective, as well as a side-looking configuration for planar waveguide structures, such as SiGe integrated IR waveguide sources. These latter structures are facet-emitting and suited to measuring in a side-looking configuration.[3,4]

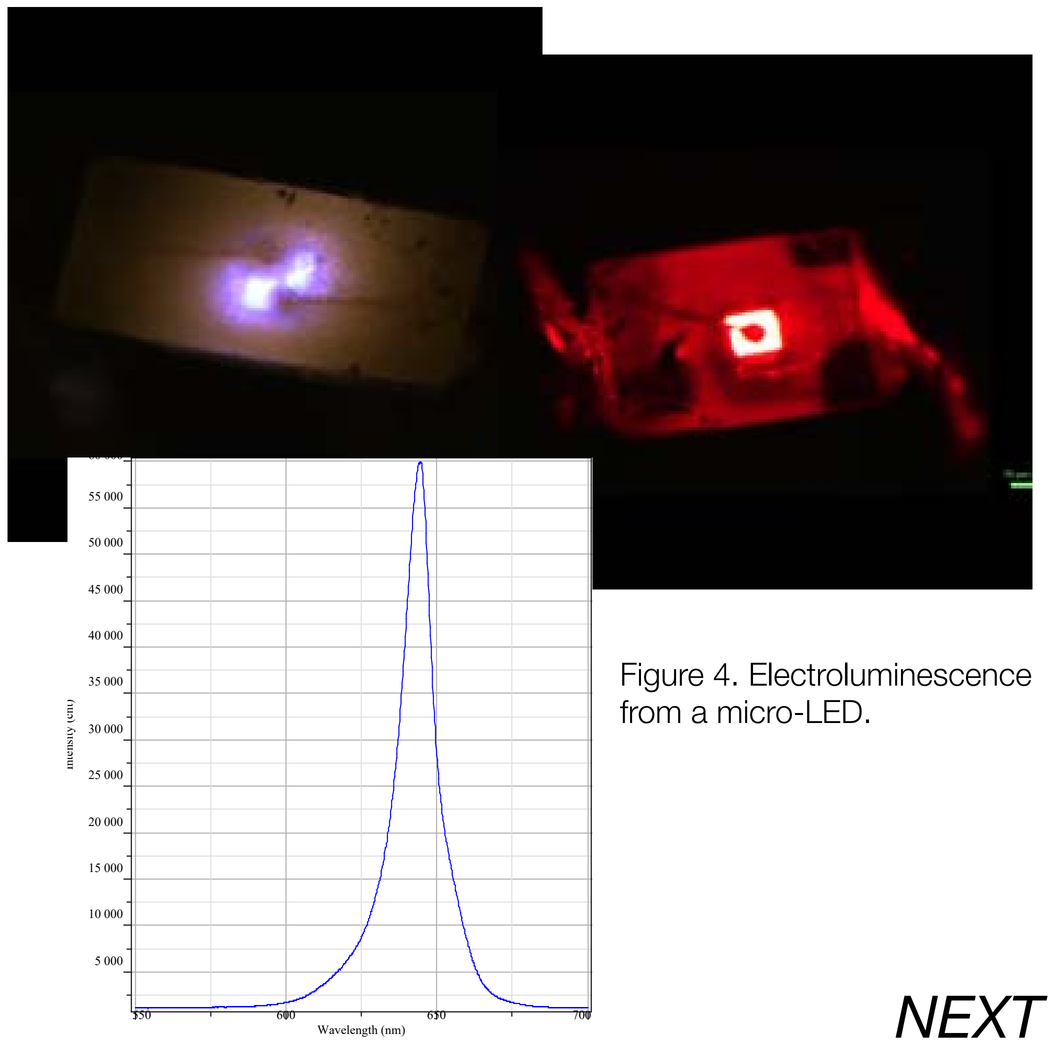

Figure 4. Electroluminescence from a micro-LED.

« PREVIOUS

NEXT »

The MicOS microscope spectrometer, cont.

Finally, the MicOS also comes with an optional motorized stage for photoluminescence mapping, in which the user is not only interested in the measured spectra, but also in the spatial distribution of emitting centers on the sample. The map information is generated by a two-dimensional translation of the mapping stage so that PL data is collected at an array of points coincident with the tightly focused excitation beam (Figure 5).

This spatial distribution information is relevant in diverse applications such as in isolating biological species (Figure 6), as well as maps of wafer homogeneity in quality control in the semiconductor industry (Figure. 7).

Figure 5: Tightly focused excitation laser spot on the sample. This spot excitation is scanned across a region of interest in a raster fashion to generate a 2D map.

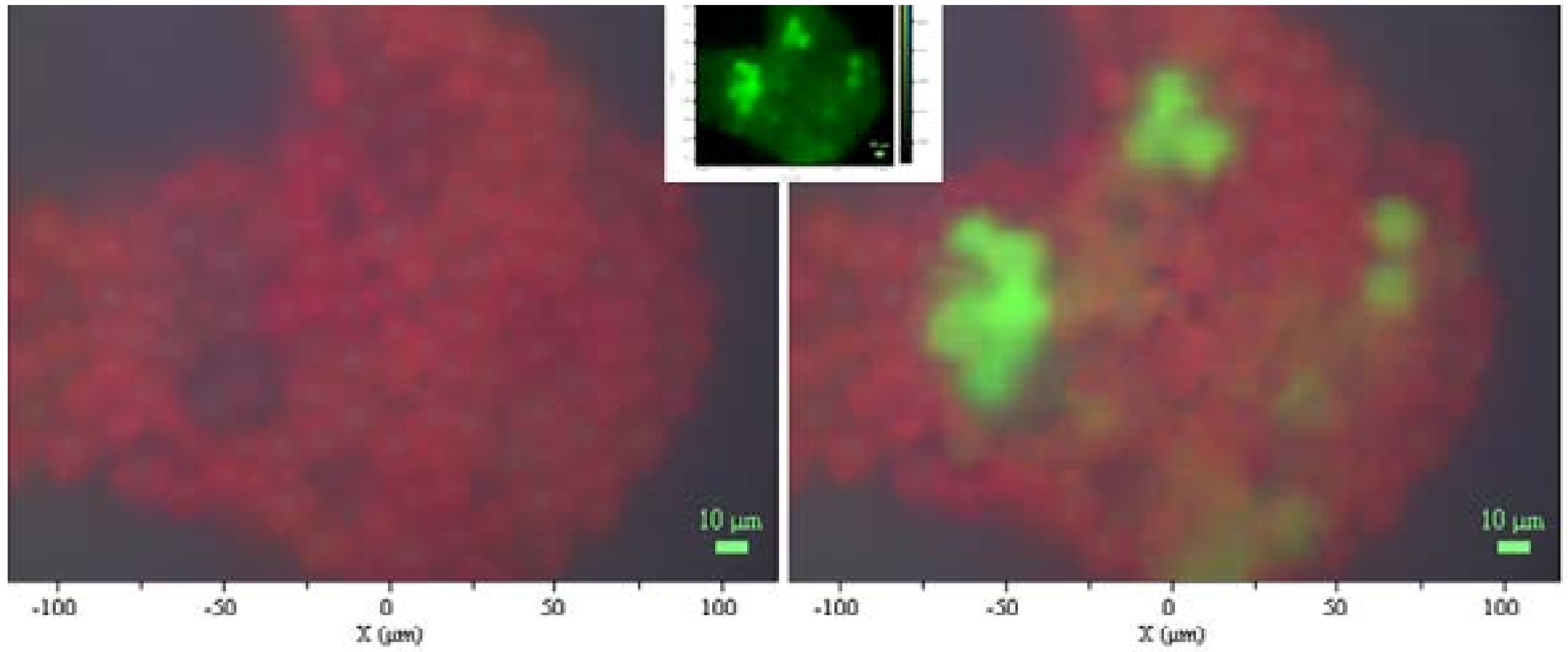

Figure 6: (left) 50× image of a distribution of fluorescent beads; (inset) Fluorescence map at 737 nm; (right) Overlay of the fluorescence map upon the visual image, showing regions of sample responsible for fluorescence.

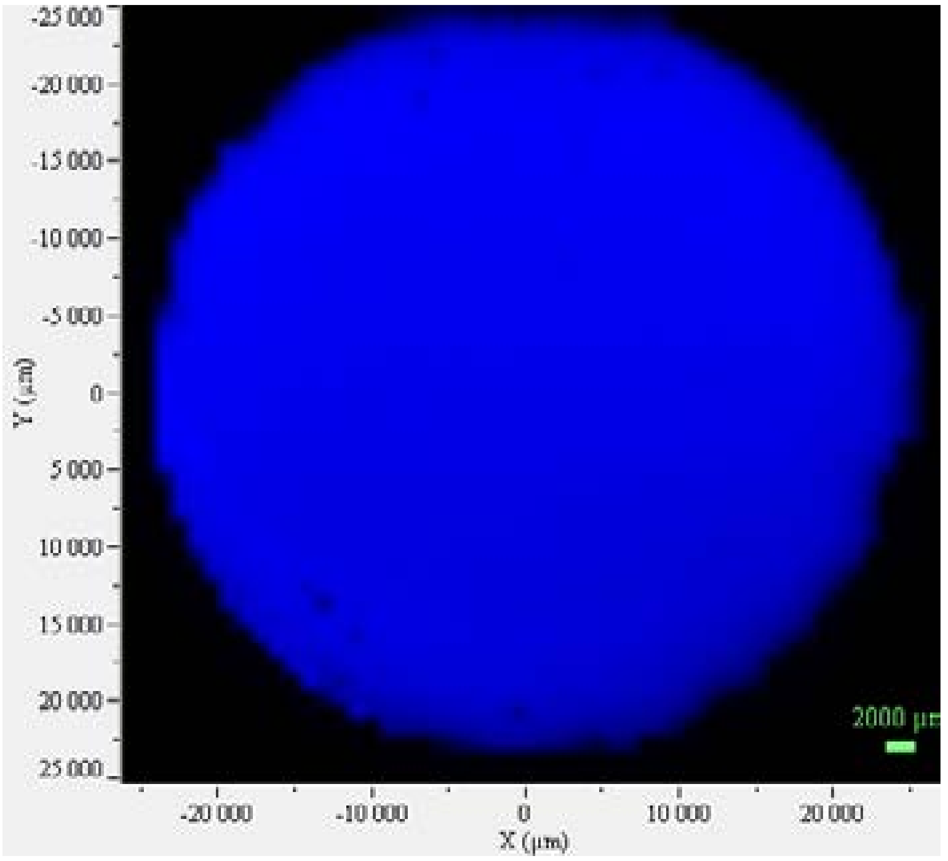

Figure 7: 2D map at an array of points over a wafer.

The MicOS microscope spectrometer, cont.

MicOS Specifications

Spectrometers		iHR320		iHR550
Spectral range[1]		200 nm to 1600 nm		
Spectral resolution[2]		0.18 nm		0.1 nm
Detector	Type	CCD 1024 × 256 OE[3]	IGA 512 × 25	Single-channel
	Range	200–1050 nm	800–1600 nm	190–1600 nm[4]
Excitation Laser Wavelength[5]		325 nm, 355 nm, 405 nm, 532 nm, 633 nm, 785 nm		
Microscope Objectives	Magnification	10x	50x	100x
	Spot Size	100 µm	<20 µm	<20 µm
Sample Stage		XYZ (manual or motorized)		

[1]Depends on choice of objective, filters, and detectors.
[2]For 1200 gr/mm grating and open-electrode CCD
[3]BIUV, BIVS, and BIDD formats available for specific quantum-efficiency requirements.
[4]Needs two detectors to cover entire range.
[5]Other options are available upon request.
*Specifications are subject to change without notice.

The MicOS-based system...uses a versatile platform for performing micro- as well as macro-photoluminescence (PL) measurements.

Integrated micro and macro photoluminescence

MicOS for photoluminescence research - The system

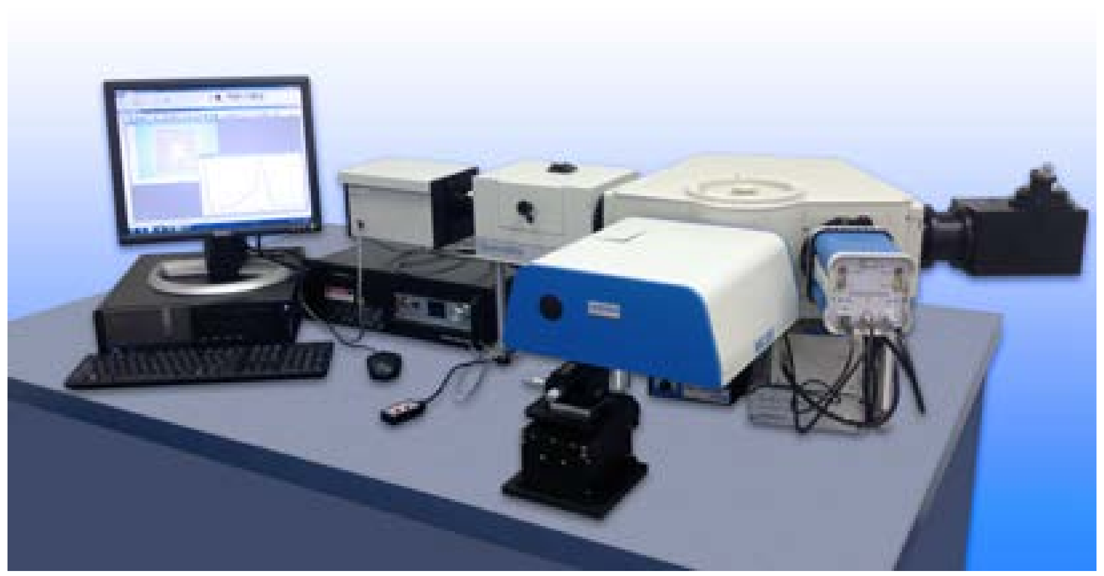

Figure 1

The MicOS-based system (Figure 1) described in this Technical Note uses a versatile platform for performing micro- as well as macro-photoluminescence (PL) measurements, and which can take transmittance and absorbance measurements, at an affordable price.

The core of the system is a HORIBA Scientific triple-grating spectrometer with two entrance ports and two exit ports. The MicOS head—the Micro-PL accessory—is coupled to the front entrance port, while the transmission accessory (sample chamber and tunable light source) is coupled to the side entrance port.

Direct coupling of these accessories ensures the highest throughput of light through the spectrometer to the detectors, which are attached the two exit ports. The exit ports can accommodate up to three different detectors (one port can accept two detectors) to cover a wide spectral range (200 nm–40 µm). HORIBA Scientific's LabSpec software controls all components, and also collects and analyzes the data.

Micro-PL measurements

Figures 2a and b are photoluminescence spectra of InP and GaAs wafers collected using the Micro-PL accessory on the platform. The inserts in the graphs are the samples themselves with the bright circular laser spot at the center. The samples were excited at 532 nm.

The InP data were collected using an InGaAs single channel detector on the side exit port, while the GaAs PL spectrum was collected using a CCD array detector on the front exit port. The spectral range spans 200–1600 nm.

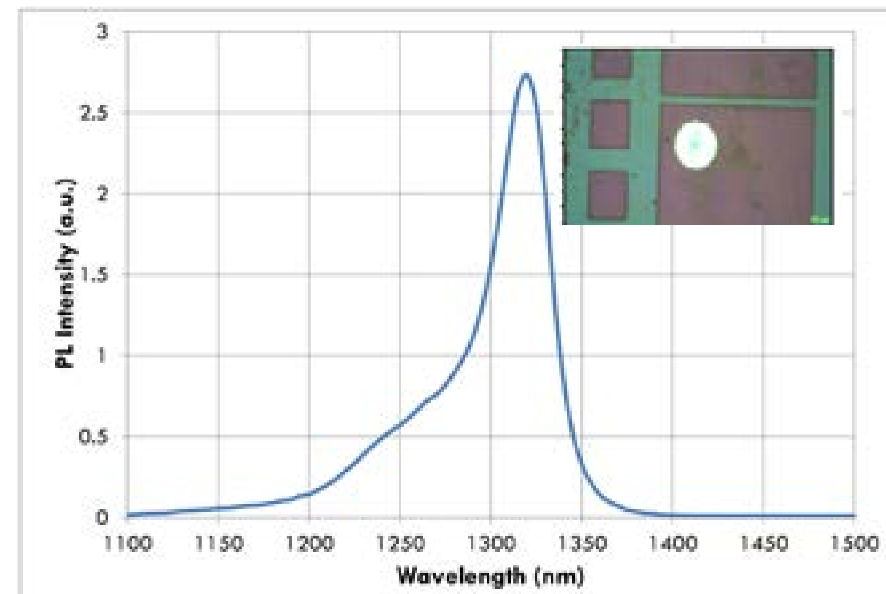

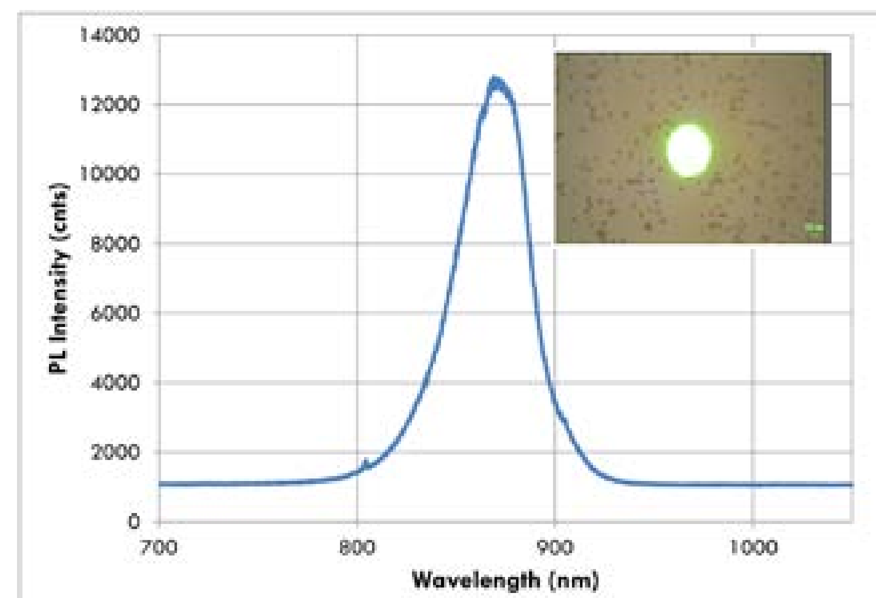

Figure 2: PL spectra of (a) InP and of (b) GaAs wafer.

NEXT »

HORIBA Scientific

Integrated micro- and macro-photoluminescence, cont.

Macro-PL measurements

Figure 3 shows the configuration of the system for macro-PL measurements. An optional monochromator (not shown) may be added between the light source and sample chamber for tunability in the excitation wavelength. A 250 W tungsten-halogen lamp was used, but an optional 450 W Xe light source is available, as well. For these measurements, a bandpass filter was used inside the sample chamber to select the excitation wavelength. The sample was a cuvette of aqueous coumarin. Figure 4 shows the fluorescence spectrum following UV excitation of the sample.

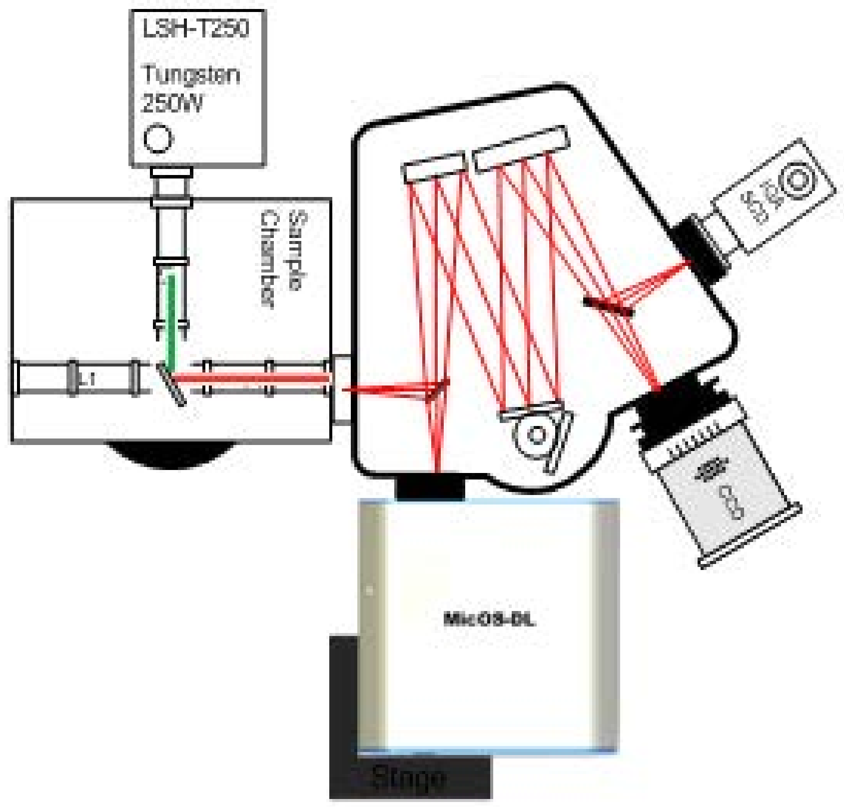

Figure 3: Macro luminescence setup.

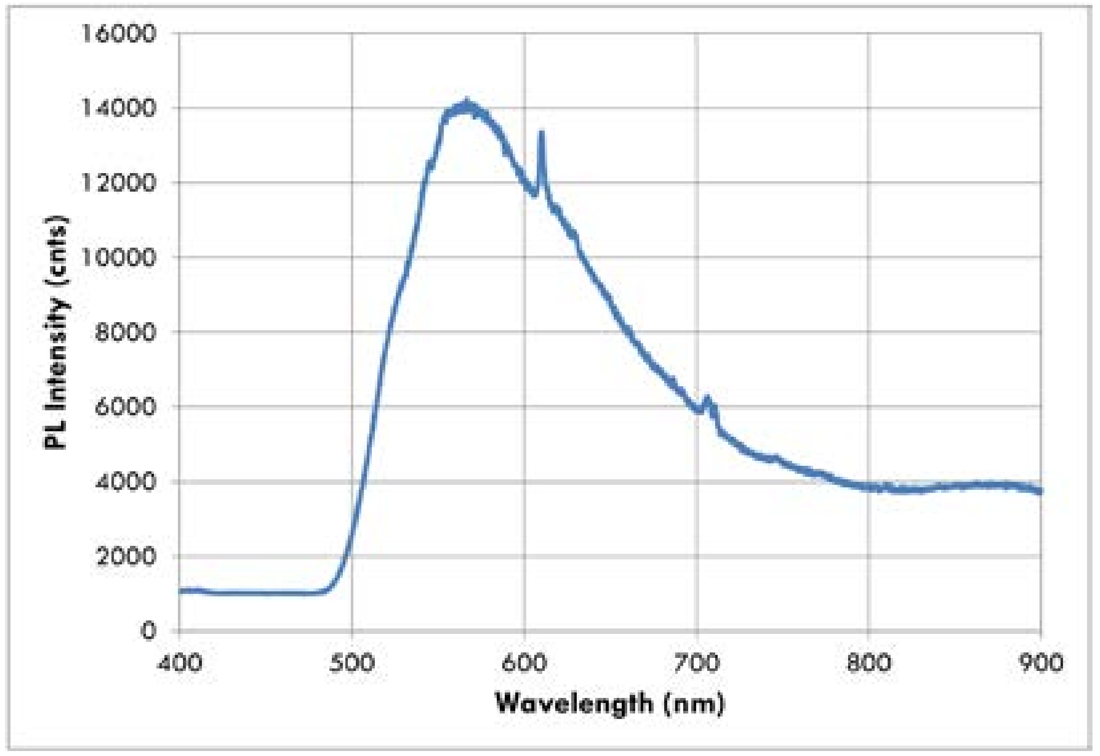

Figure 4: Luminescence spectrum of aqueous coumarin excited at approximately 325 nm

Macro-transmission measurements

Figure 5 shows the system configuration for macro-transmission measurements. A collimated white-light beam was directed through the sample in the sample chamber; lenses collected and imaged the transmitted light onto the input slit of the spectrometer. Figure 6 is the transmission spectrum of a long-pass glass filter, normalized to a reference measurement without the sample.

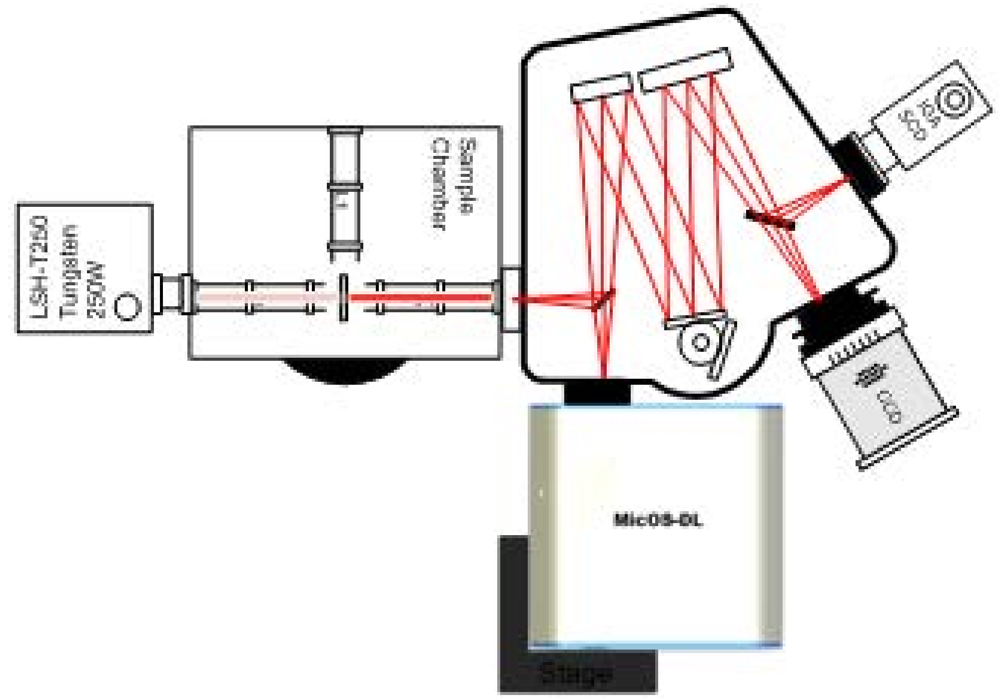

Figure 5: Micro-PL measurement setup.

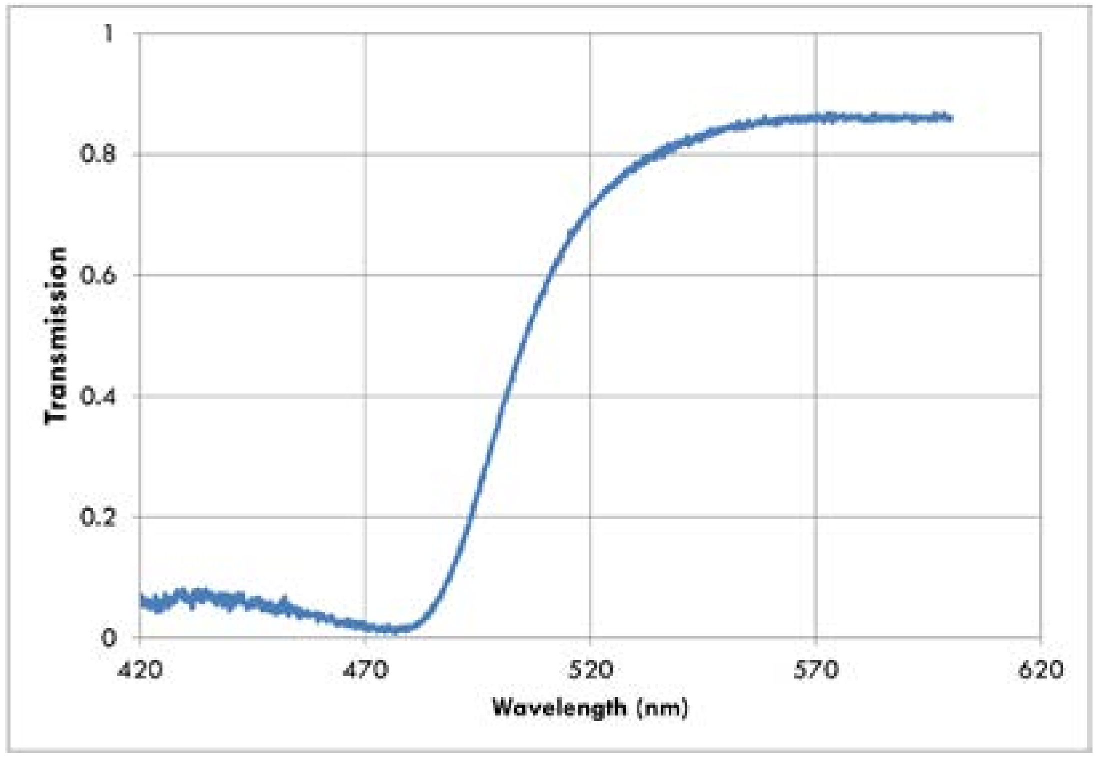

Figure 6: Normalized transmission spectrum of glass long-pass filter.

« PREVIOUS

Videos

MicOS Hybrid PL Micro Optical Spectrometer: Complete solution for steady state and time resolved photoluminescence

MicOS: Microscope Optical Spectrometer

Contact

horiba.com/scientific

Phone: 732-494-8660

HORIBA Scientific